Mechanism and structure sensitivity of electrocatalytic reactions of inorganic nitrogen compounds on platinum

Mechanism and Structure Sensitivity of Electrocatalytic Reactions of Inorganic Nitrogen Compounds on Platinum

PROEFSCHRIFT

ter verkrijging van de graad van doctor aan de Technische Universiteit Eindhoven, op gezag van de Rector Magnificus, prof.dr.ir. C.J. van Duijn, voor een commissie aangewezen door het College voor Promoties in het openbaar te verdedigen op woensdag 15 februari 2006 om 16 uur

door

Victor Rosca

geboren te Chisinau, Moldavië

Dit proefschrift is goedgekeurd door de promotoren

prof.dr. M.T.M. Koper
en
prof.dr. R.A. van Santen

Copromotor:
Dr. G.L. Beltramo

The work described in this thesis has been carried out at Schuit Institute of Catalysis, Laboratory of Inorganic Chemistry and Catalysis, Eindhoven University of Technology. Financial support was provided by the Netherlands Foundation for Scientific Research (NWO).

CIP-DATA LIBRARY TECHNISCHE UNIVERSITEIT EINDHOVEN

Rosca, V.

Mechanism and structure sensitivity of electrocatalytic reactions of inorganic nitrogen compounds on platinum / by Victor Rosca. – Eindhoven : Technische Universiteit Eindhoven, 2006.
Proefschrift. – ISBN 90-386-3027-1. – ISBN 978-90-386-3027-4
NUR 913
Trefwoorden: elektrochemie / heterogene katalyse / eenkristal
platina oppervlakken / adsorptie / elektrokatalytische reductie ; stikstofmonoxide / hydroxylamine / elektrokatalytische oxidatie ; ammoniak / reactiekinetiek / infraroodspectroscopie
Subject headings: electrochemistry / heterogeneous catalysis / single-crystal platinum surfaces / adsorption / electrocatalytic reduction ; nitric oxide / hydroxylamine / electrocatalytic oxidation ; ammonia / reaction kinetics / infrared spectroscopy

Printed at the *Universiteitsdrukkerij*, Eindhoven University of Technology.

To Katia and Alex

Table of Contents

Chapter 1. Introduction **1**

Chapter 2. Electrocatalytic reduction of NO adlayers on Pt(110) and Pt(111) in acidic media: evidence for adsorption site – specific reduction **17**

Chapter 3. Rate laws for reductive stripping of NO adlayers at single-crystal platinum electrodes as deduced from transient experiments **37**

Chapter 4. Mechanism of electrocatalytic reduction of nitric oxide on Pt(100) surface **55**

Chapter 5. Electrocatalytic reactions of hydroxylamine at low-index single crystal platinum surfaces in acidic media **73**

Chapter 6. Electrocatalytic oxidation of ammonia on Pt(111) and Pt(100) surfaces **99**

Summary **123**

Samenvatting **125**

Rezumat **127**

Резюме **129**

List of Publications **132**

Acknowledgements **133**

Curriculum Vitæ **134**

1

Introduction

The electrocatalytic reactions of nitrogen compounds on transition metals is a classic topic in electrochemical research, determined by the technological importance as well as by the complexity of the redox chemistry of nitrogen compounds. The present thesis concerns the adsorption and electrocatalytic reactions of selected inorganic nitrogen compounds, namely, nitric oxide, hydroxylamine, and ammonia, on platinum electrocatalyst. Although understanding the reactivity of the above compounds is of considerable practical interest (see sections 1.1 to 1.3.), the main motivation for the research described herein is a fundamental understanding of the mechanism and structure sensitivity of the electrocatalytic processes involved.

Electrocatalysis can be defined as catalysis of electrode reactions (Trasatti 1995).[1] If the catalytic effect is determined by the action of the electrode material, then one is dealing with a heterogeneous electrocatalyst. The most important and extensively studied electrocatalysts are metals (electronic conductor), as well as their oxides or alloys, in contact with an electrolyte solution (ionic conductor).[2-9] Although any electrode surface, at which an electrode reaction occurs and involves adsorbed intermediates, can be viewed as a catalyst, the term electrocatalyst is commonly applied to the electrode materials at which the electrochemical reaction rates are considerably higher, as compared to those at other electrode materials. The rate of an electrocatalytic process depends exponentially on the applied potential, provided the rate of the electrode reaction is limited by an electron-transfer step.

A (supported) metal catalyst in contact with an electrolyte solution is essentially an electrochemical system. The polarization of the metal–electrolyte interface, also affected by the composition of the solution and the interaction of the components of the solution with the metal surface, is a factor to be taken into consideration, whatever the exact mechanism of the reaction.[10] Moreover, many

liquid-phase catalytic hydrogenation and oxidation reactions involve electron transfer (often combined with proton transfer) to or from the metal.[11,12] Therefore, the electrochemical studies are highly relevant, and often more convenient, for understanding catalysis at the metal-electrolyte interface.

Similar to heterogeneous catalysis, bonding is in many respects the decisive factor in electrocatalysis.[3,8] Electronic factors – related to the effect of the surface structure on the local electronic properties – and the closely related geometric factors – for instance, manifested in a site preference for a given adsorbate (or, in simple terms, coordination) – should also influence the rate of an electrocatalytic process. Therefore, the structure sensitivity of electrocatalytic reactions has been receiving increasing attention in recent years.[3,9] The electrode potential is a parameter that may significantly affect the bonding and, therefore, the reactivity of participants of a reaction, but also modulate the interaction of the electrode surface with other components of the electrolyte, thus affecting the rate of the electrocatalytic process in a complex manner. This thesis provides many examples in this respect.

Fundamental understanding of the mechanism of complex electrocatalytic processes can be achieved through studies on structurally and chemically well-defined (model) systems.[9] The use of single crystal electrodes, the development of (in situ) surface-sensitive techniques, and an increase of the theoretical activity resulted in significant advances in the molecular-level understanding of electrochemical processes.[9,13] At the same time, the above advances brought about an increasing overlap with surface science.[13] Indeed, electrochemistry and surface science have similar goals and share a number of techniques.[9,14]

The research described in the present thesis is an illustration to the above observations. The low-index single-crystal surfaces were used to investigate the structure sensitivity of selected reactions, allowing a better resolution of complex electrode processes, as compared to studies on polycrystalline electrodes. Electrochemical techniques can be very insightful, in mechanistic studies in particular, but they are still macroscopic probes. Therefore, a molecular-level probe, namely, in situ infrared spectroscopy,[15] was employed to identify the (adsorbed) products or stable intermediates of the electrocatalytic reactions under investigation. On-line electrochemical mass spectrometry[16] is a very useful tool for (real-time) detection of volatile products in solution and, therefore, was employed to acquire the information on the product distribution with the applied potential.

Platinum, an important hydrogenation and oxidation (electro)catalyst, is in many respects an ideal model (electro)catalyst. As an important factor in fundamental studies, the electrochemistry of the single-crystal platinum surfaces is fairly well understood.[4,9] Furthermore, the voltammetry of the single-crystal platinum surfaces provides straightforward criteria for assessing the order and

cleanliness of a surface, which are of paramount importance in model electrochemical studies. As a comparison, the voltammetry of palladium and rhodium, two metals with very similar properties, is much less informative in assessing the surface order and the cleanliness of the system, which is a drawback indeed.

The remainder of this chapter contains an introduction into adsorption and reactions of nitric oxide, hydroxylamine, and ammonia on platinum under electrochemical conditions, although a detailed review is beyond the scope. Rather, the most significant literature data are presented, along with indicating the gaps in the current knowledge. The chapter is concluded with an outline of the present thesis.

1.1. Adsorption and reactions of nitric oxide on platinum under electrochemical conditions

In this section a summary of the adsorption and reactions of nitric oxide (NO) on platinum is given, with an emphasis on the mechanistic aspects of NO reduction in acidic media, as well as on the closely related nitrite reduction.

The adsorption and reactivity of NO on transition metal surfaces in an electrochemical environment are of considerable technological and scientific interest. Nitric oxide is a key intermediate or reagent in a series of environmentally and industrially important processes, such as nitrate and nitrite reduction[17,18] or the liquid-phase catalytic hydrogenation of nitric oxide or nitrate to hydroxylamine.[19,20] Electrochemical sensing[21] of nitric oxide requires a thorough understanding of the electrochemistry of NO. Furthermore, NO reduction and oxidation are relatively simple reactions,[22] which are in many respects attractive for investigating the activity and selectivity issues in electrocatalysis and also for comparison of reactions at solid–gas and solid–liquid interfaces.

Nitric oxide adsorbs strongly on transition metal surfaces.[23] As for platinum, NO adsorbs molecularly on Pt(111) and Pt(110) surfaces under ultra-high vacuum (UHV) conditions at low to near-room temperatures.[24-28] Adsorption of NO on Pt(100) seems to be (at least partially) dissociative even at near-room temperatures.[29] Breaking of the N–O bond strongly depends on the surface structure and is often the rate-determining step in NO reduction on platinum in UHV.[24] This step is believed to occur prior to hydrogenation and requires free neighboring site(s).[24] Nevertheless, several UHV studies of NO reduction on Pt(111) at near-room temperature suggested the formation of HNO intermediate.[30,31] The site occupation, coverage, and the structure of the NO adlayer depend on the surface structure. Generally, multifold coordination is preferred at

low to moderate coverage.[23] At high coverages linearly-bonded NO may coexist with multifold-coordinated NO, as for NO adsorption on Pt(111),[32-34] or a site switch to a lower coordination site may occur, as for NO adsorption on Pt(110).[27] On Pt(100), NO occupies a site between the atop and bridge site,[35] the "side-on" configuration being a possible stable configuration at low coverage values.[36]

The electrochemistry of NO on polycrystalline platinum and on other metals has been receiving considerable attention,[37-47] also in relation with the work on nitrate and nitrite reduction.[37,48-52] In acidic solutions, inorganic nitrogen-oxygen compounds are involved in complex redox equilibria,[52,53] which often complicate the analysis. As such, nitrous acid is in equilibrium with NO^+ species:

$$HNO_2 + H_3O^+ \leftrightarrows NO^+ + 2H_2O \qquad (1.1)$$

This equilibrium is shifted to the right with increasing acidity. Therefore, NO^+ species are present in considerable concentration and are assumed to be the electrochemically active species in nitrite reduction in strongly acidic solutions.[49,51,54] In diluted acids, however, nitrite is in electrochemical equilibrium with (adsorbed) NO, as shown in recent studies on single-crystal platinum surfaces:[55-57]

$$HNO_{2\,(ads)} + H_3O^+ + e^- \leftrightarrows NO_{ads} + 2H_2O \qquad (1.2)$$

Accordingly, NO adlayers can be formed by exposing the electrode surface to a diluted acidic solution of nitrite;[58] these layers being (electro)chemically stable in a wide potential window. With this in mind, it is quite surprising that adsorbed NO, which is a thermodynamically stable and strongly adsorbed species on transition metals, was largely disregarded as a possible intermediate in the electrochemical reactions of nitrogen compounds on platinum or other transition metals. In more recent studies, nitric oxide was shown to be a stable intermediate in nitrate reduction[18] and hydroxylamine oxidation[59] on platinum.

It is important to make a clear distinction between continuous NO reduction, (i.e. with NO present in solution) and the reduction of adsorbed NO (without NO in solution). The continuous NO reduction results in the formation of nitrous oxide (and some dinitrogen) at low reductive potentials (typically 0.6-0.3 V vs. RHE), and hydroxylamine and ammonia at potentials corresponding to the hydrogen underpotential deposition (H_{upd}) region (between ca. 0.4-0 V vs RHE).[37,38,40-42,45,46] In contrast, the reductive stripping of NO adlayers does not result in the formation of nitrous oxide, ammonia being shown to be the dominant (if not the only) product, as indicated in recent studies on polycrystalline[45,46] as well as on single-crystal platinum[58,60,61] electrodes.

As repeatedly suggested in early studies on polycrystalline platinum,[38,40,41,51] the formation of the N–N bond could result from dimerization of NOH (or HNO) adsorbed intermediates followed by a decay of the resulting dimer to N_2O. In a recent detailed mechanistic analysis of NO reduction on polycrystalline platinum, de Vooys et al.[46] proposed the following mechanism for N_2O formation:

$$NO_{ads} + NO + H_3O^+ + e^- \rightarrow HN_2O_{2\,(ads)} + H_2O \qquad \text{(rds)} \qquad (1.3)$$
$$HN_2O_{2\,(ads)} + H_3O^+ + e^- \rightarrow N_2O + 2H_2O \qquad \text{fast} \qquad (1.4)$$

The formation of a (protonated) NO dimer as a precursor to N_2O formation is the key feature of this mechanism. The dimer is formed only when NO is present in solution, suggesting that the second NO molecule is weakly adsorbed. The formation of NO dimers on metal surfaces in vacuum or in the gas phase has been recently indicated and discussed.[23,62]

The electrochemical reduction of NO to hydroxylamine and ammonia is commonly perceived as a stepwise hydrogenation process, involving the formation of NOH (or HNO), HNOH, and H_2N intermediates.[38,40,43,51,63] De Vooys et al.[46] combined on-line differential electrochemical mass spectrometry (DEMS) and the rotating-disk electrode (RDE) technique and proposed the following EC mechanism for NO electroreduction to ammonia on polycrystalline platinum:

$$NO_{ads} + H_3O^+ + e^- \leftrightarrows HNO_{ads} + H_2O \qquad \text{equilibrium} \qquad (1.5)$$
$$HNO_{ads} + \ldots \rightarrow \text{Unknown Intermediate} \qquad \text{(rds)} \qquad (1.6)$$
$$\text{Unknown Intermediate} \ldots \rightarrow NH_4^+ \qquad \text{fast} \qquad (1.7)$$

The authors suggested that the rate-determining step is likely to be a (potential-independent) chemical step. In a recent detailed voltammetric study of the reduction of adsorbed NO on stepped Pt[n(111)×(111)] surfaces, Beltramo and Koper[60] proposed an EE mechanism for NO_{ads} reduction to ammonia:

$$NO_{ads} + H_3O^+ + e^- \leftrightarrows HNO_{ads} + H_2O \qquad \text{equilibrium} \qquad (1.8)$$
$$HNO_{ads} + H_3O^+ + e^- \rightarrow H_2NO_{ads} + H_2O \qquad \text{(rds)} \qquad (1.9)$$
$$H_2NO_{ads} + 4H_3O^+ + 3e^- \rightarrow NH_4^+ + 5H_2O \qquad \text{fast} \qquad (1.10)$$

The first two steps of the reaction are assumed to be combined proton-electron transfers, involving hydronium ions from solution. In agreement with the latter assumption, NO_{ads} reduction on Pt(110) (and partly on Pt(111)) occurs at potentials at which the hydrogen coverage is negligible.[60] Additionally, the reductive stripping of NO adlayers on polycrystalline platinum shows a pH

dependence, which agrees with the electrochemical mechanism of NO_{ads} hydrogenation.[46] The HNO and H_2NO intermediates are suggested on the basis of their lower energy in vacuum compared to NOH and HNOH species.[46,60] Note that in mechanism 1.8-1.10, the breaking of the N–O bond occurs after the rate-determining step.

Recent work on single-crystal electrodes provided important information on the adsorption of nitric oxide, which is the first step in understanding the structure sensitivity of reactions of NO. Most importantly, the NO adsorption on platinum under electrochemical conditions, as well as on other platinum-group metals, is very similar to NO adsorption on platinum in UHV, as deduced from the in situ Fourier transform reflection-absorption infrared spectroscopy (FTIRRAS) studies.[58,64] Furthermore, the charge analysis of the reductive stripping of NO adlayers on the low-index platinum surfaces gave the coverage values comparable to those under UHV conditions. Accordingly, the saturation NO coverage on Pt(111), Pt(100), and Pt(110) electrodes is 0.4-0.5 monolayers (ML),[58,60] 0.5 ML,[58,61] and 0.7 to 1 ML,[60] respectively. The measured value of the coverage seems to be somewhat affected by the nature of electrolyte. On Pt(110), for instance, the saturation NO coverage is ca. 1 ML in perchloric acid and 0.7 ML in sulfuric acid.[60] The above observations suggest that the structure of NO adlayers on platinum surfaces under electrochemical conditions is very similar to that under UHV conditions. This conclusion is further supported and exploited in the mechanistic studies of NO_{ads} reduction described in this work (Chapters 2 to 4).

Despite a fairly detailed picture of NO adsorption and reactions on platinum, and to some extent on other metal surfaces, knowledge of a detailed mechanism and of the structure sensitivity of NO reduction is still lacking. It is important to understand the mechanism of breaking the N–O bond, which is crucial for steering the selectivity towards the formation of hydroxylamine. Also, the structure sensitivity of NO reduction is still to be resolved. Beltramo et al.[60] noticed that all the stepped Pt[n(111)×(111)] surfaces examined showed comparable activity in NO_{ads} reduction, and only the details of the voltammetric profile for the reductive stripping were clearly structure-sensitive. Explaining the nature of the features (peaks) observed in the stripping voltammetry could be an important piece of information in resolving the reaction mechanism. Furthermore, it would be interesting to see whether the similarities in adsorption under UHV and electrochemical conditions result in similar NO reactivity patterns. Specifically, under UHV conditions, breaking of the N–O bond is a structure sensitive process, which requires a neighboring free site.

1.2. Adsorption and reactions of hydroxylamine on platinum under electrochemical conditions

Knowledge of the reactivity of hydroxylamine under electrochemical conditions is important from a fundamental point of view – in the context of redox chemistry of inorganic nitrogen compounds – as well as from a technological point of view, mostly in relation to its industrial synthesis. In industry, hydroxylamine (HAM), a key intermediate in the production of ε-caprolactam and a compound with various applications in technology, is obtained by the liquid-phase catalytic hydrogenation of nitric oxide or nitrate at carbon-supported platinum or palladium catalysts.[19,20] The relevance of the electrochemical studies on similar systems for understanding the processes practiced in industry is well accepted.[19,65]

An important aim of the applied electrochemical research is the identification of the factors controlling the selectivity of nitric oxide or nitrate reduction to hydroxylamine. However, the investigation of these factors is hampered by a lack of data on HAM electrochemistry itself. This is particularly true for HAM reduction on platinum electrodes in acidic media, which are the conditions of interest from a practical point of view.

The electrochemical reactions of HAM on platinum appear complex,[53] and only few detailed mechanistic studies have been reported so far. In a series of studies, Möller and Heckner[66,67] addressed the reduction of HAM on bright Pt, using voltammetry and the rotating disc electrode (RDE) technique. The adsorption of HAM was shown to be the first step in HAM reduction. The electroreduction of HAM on Pt proved difficult to study, as it is strongly masked by the hydrogen adsorption and hydrogen evolution reaction (HER). Möller and Heckner[66] interpreted their preliminary results on HAM reduction at a platinum RDE in acidic media (pH<3) by the HAM involvement in the hydrogen adsorption reaction:

$$NH_3OH^+_{ads} + e^- \rightarrow NH_2OH + H_{ads} \qquad (1.11)$$

In alkaline media, HAM was found to be much more reactive and reduction to ammonia was postulated, although with no reference to the nature of the adsorbed intermediates. In a later, more detailed, study,[67] the authors argued for the possibility of breaking the N–O bond in acidic media as well. The rate-determining step was formulated as follows:

$$NH_3OH^+_{ads} + e^- \rightarrow NH_{3\,(ads)} + OH_{ads} \qquad (1.12)$$

The low reduction activity of hydroxylamine was explained by the blocking effect of $(NH_3)_{ads}$.

Möller and Heckner extensively studied the electrooxidation of HAM on bright Pt.[68-71] Both NH_2OH and NH_3OH^+ were perceived as reactive species, depending on pH. The oxidation of HAM was described in terms of successive dehydrogenation steps, accompanied by chemical side reactions involving the reaction intermediates. In acidic solution, the first two reaction steps were formulated as follows:

$$NH_3OH^+_{ads} \rightarrow HNOH + e^- + 2H^+ \quad (1.13)$$

$$HNOH \rightarrow NOH + e^- + H^+ \quad (1.14)$$

Both intermediates (presumably adsorbed) were assumed to form dinitrogen, either by dimerization of HNOH and further disproportionation of the resulting dimer, or as a result of a reaction between NOH and HAM. Furthermore, by referring to the homogeneous association-dissociation of the $HNO/H_2N_2O_2$ couple and the decomposition of $H_2N_2O_2$ to N_2O, the authors considered the experimentally observed N_2O evolution as a proof for NOH formation. Finally, it was suggested that nitrate is the final product of HAM oxidation in acidic media and neutral media, while nitrite is perceived as a stable intermediate, particularly in alkaline media.

More recently, Karabinas et al.[72] presented a detailed study of HAM electrooxidation on polycrystalline Pt in neutral (buffered) and acidic solutions by combining voltammetry and on-line DEMS. In their mechanism, the authors accepted the previously proposed dehydrogenation scenario, resulting in the formation of NOH species. The dimerization of NOH to hyponitrous acid ($H_2N_2O_2$) and its subsequent decomposition to N_2O and water were also supported. At potentials up to 0.7 V vs. RHE (pH 6.5, phosphate buffer) NOH is partially oxidized to NO. Nevertheless, NOH species was considered as precursor in nitrite formation: the authors argued that as soon as Pt-OH species become available at the surface, NOH species are oxidized directly to HNO_2. The reaction of HNO_2 with HAM was held responsible for the formation of N_2O at potentials around 1 V. Above ca. 1.1 V nitrite is oxidized to nitrate. Oxidation via Pt-OH species was perceived as the main reaction pathway in neutral solutions, while in acidic media the reaction can also proceed via formation of NO_2.

Piela and Wrona studied HAM oxidation at rotating disk electrodes, namely, platinum, gold, and glassy carbon in acidic media.[73] Only Pt showed noticeable activity for HAM oxidation, which was explained by HAM adsorption on platinum and weak interaction of HAM with the other two materials. The reaction was assumed to proceed via NHOH, NOH, and nitrite as intermediates, nitrate being the final oxidation product. The observed kinetic hindrance was explained by an affect

of the platinum oxide layer. The electrochemical transformations of HAM were shown to be accompanied by various homogeneous chemical reactions. As such, the reaction of nitrite, a product of HAM oxidation, and HAM itself was shown to be an important source of N_2O accumulation in solution.

Recently, in this laboratory HAM electrochemistry on polycrystalline platinum in acidic media was studied using voltammetry, on-line DEMS, and in situ FTIRRAS.[59] It was shown that the adsorption and reactions of HAM are essentially controlled by other species that interact strongly with the electrode surface (e.g., hydrogen, anions, strongly-adsorbed intermediates). This explains quite moderate current densities, both in oxidation and reduction, observed between ca. 0 and 1 V vs. RHE. Hydroxylamine is slowly reduced to ammonia in the H_{upd} region, somewhat inhibited at high hydrogen coverages. The HAM electrooxidation is strongly influenced by the absorption of its products, as well as by their transformations in solution. In disagreement with previous studies, the adsorbed nitric oxide was shown to be the key intermediate of HAM oxidation, as deduced from both voltammetry and in situ infrared measurements. On the basis of a Tafel slope analysis, the following EE (electrochemical–electrochemical) mechanism was proposed for HAM oxidation to NO_{ads}:

$$H_3NOH^+ \leftrightarrows H_3NOH^+_{ads} \qquad (1.15)$$

$$H_3NOH^+_{ads} \leftrightarrows H_2NO_{ads} + 2H^+ + e^- \qquad (1.16)$$

$$H_2NO_{ads} \rightarrow HNO_{ads} + H^+ + e^- \quad \text{(rds)} \qquad (1.17)$$

$$HNO_{ads} \rightarrow NO_{ads} + H^+ + e^- \qquad (1.18)$$

Nitric oxide forms an adlayer that is (electro)chemically stable in a wide potential window, thus acting as a poison in HAM oxidation. At potentials corresponding to the oxidation of the platinum surface (above ca. 0.75 V), NO_{ads} is oxidized to (adsorbed) nitrite. Finally, N_2O formation between ca. 0.4 and 1 V was shown to have multiple sources. The most important source of N_2O is likely a reaction between nitrite and HAM.

Previous studies indicated HAM adsorption as the primary step of HAM transformations.[59,67,72,73] At the same time, HAM reactions are strongly masked by adsorption and reaction of species like hydrogen, nitric oxide, sulfate, which adsorb strongly on platinum and, thus, block the sites for HAM adsorption and transformations.[59] At single-crystal platinum surfaces, the interfering processes are much better defined, which may allow their separation and, therefore, a better chance to "unmask" the reactivity of HAM on platinum. Therefore, the investigation of HAM reactions on single-crystal surfaces is a logical step.

1.3. Adsorption and reactions of ammonia on platinum under electrochemical conditions

The electrochemical oxidation of ammonia on transition metals has been receiving considerable attention, particularly in connection with the possibility of using ammonia in the electrochemical fuel cells.[74-77] Furthermore, an adequate knowledge of ammonia electrochemistry is important for application in environmental (electro)catalysis[78,79] and in the electrochemical detection of ammonia.[80,81] From a scientific point of view, ammonia electrooxidation on platinum, as well as on other metal surfaces, is an attractive model electrocatalytic system. Achieving a molecular level understanding of the electrocatalytic reactions of ammonia obviously requires studies of chemically and structurally well-defined systems, i.e. single-crystal surfaces.

Ammonia interacts weakly with platinum surfaces in UHV, showing predominantly molecular adsorption at near-room temperatures, largely regardless the surface structure.[82-85] Dehydrogenation of ammonia (and further oxidation to NO) requires high temperatures (typically over 500K) and the presence of coadsorbed oxygen.[83,85,86] With this in mind, the appreciable activity of platinum in ammonia electrooxidation at room temperature is quite a remarkable phenomenon. This activity may be related to an activating role of the hydroxyl or water, either coadsorbed or in solution. At the same time, the polarization of the metal–electrolyte interface may have a direct activation effect. Assuming that ammonia interacts with the surface through its unpaired electrons, increase of the electrode potential, and the associated lowering of the Fermi level in the metal, brings about increasing deficiency of charge density on nitrogen and, therefore, a polarization of the Pt–N bond and, therefore, an activation of the N–H bond.

In early studies on polycrystalline platinum, ammonia oxidation in alkaline media was commonly viewed as a stepwise electrocatalytic dehydrogenation process, resulting in the formation of NH_x adsorbed species (x=1,2) and ultimately the formation of the adsorbed atomic nitrogen:[78,87,88]

$NH_3 \leftrightarrows NH_{3\,(ads)}$	equilibrium	(1.19)
$NH_{3\,(ads)} + HO^- \rightarrow NH_{2\,(ads)} + e^- + H_2O$		(1.20)
$NH_{2\,(ads)} + HO^- \rightarrow NH_{(ads)} + e^- + H_2O$	(rds)	(1.21)
$NH_{(ads)} + HO^- \rightarrow N_{(ads)} + e^- + H_2O$		(1.22)
$2N_{(ads)} \rightarrow N_2$	slow	(1.23)

On the basis of the experimentally observed Tafel slope (39 mV decade^{-1}) and assuming the Langmuir adsorption isotherm for ammonia adsorption, Oswin

and Solomon suggested that the transformation $NH_{2\ (ads)} \rightarrow NH_{(ads)}$ is the rate-determining step at moderately oxidative potentials.[87] It was assumed that molecular nitrogen was formed by the recombination of two nitrogen adatoms (reaction 1.23), which was the rate-determining step at high overpotentials.

In a later, more detailed, mechanistic study, Gerischer and Mauerer[89] suggested that, similar to the role of oxygen (or hydroxyl) in ammonia dehydrogenation under UHV conditions, (partially) discharged surface-bonded hydroxyl plays an important role in ammonia dehydrogenation under electrochemical conditions. The dimerization of NH_x (x=1,2) fragments and the subsequent dehydrogenation of the resulting dimer was proposed as the most plausible scenario for the formation of molecular nitrogen, whereas atomic nitrogen was assumed to act as a catalyst poison. The authors performed an ex situ analysis indicating the formation of atomic nitrogen. Specifically, a platinized platinum electrode was polarized until its activity for ammonia oxidation dropped to zero. Then the electrode was removed from the electrochemical cell, dried and heated to 400-600°C, and a gas chromatographic analysis of the resulting gas mixture was performed. The gas mixture contained predominantly dinitrogen, the hydrogen content being negligible.

More recent studies provided further details on the ammonia oxidation on polycrystalline platinum, mostly extending the Gerischer-Mauerer mechanism.[90-92] Gootzen et al.[91] identified an NH adsorbate as a stable intermediate in ammonia oxidation to molecular nitrogen and also suggested atomic nitrogen as the catalyst poison. De Vooys et al.[92] examined the reactivity of a series of transition and coinage metals for ammonia oxidation. The authors pointed to the importance of the nature of the products of ammonia anodic adsorption and the overpotentials at which these adsorbates are formed. Thus, an electrode surface was active in the formation of dinitrogen, provided the NH_x species were formed at sufficiently low overpotentials, whereas atomic nitrogen was indicated as the poison. In a subsequent in situ surface-enhanced Raman spectroscopy (SERS) study, de Vooys et al.[93] demonstrated the formation of atomic nitrogen on palladium, which is a poor dinitrogen formation electrocatalyst. This result supports the Gerischer-Mauerer mechanism.

Importantly, in a number of studies (on polycrystalline platinum) the on-line DEMS technique was used,[90-92] which assured a better understanding of the product distribution with the applied potential. In a very recent rotating ring-disk electrode (RRDE) study, Endo et al.[94] could detect in situ some weakly adsorbed intermediates, both oxidizable and reducible ones. The authors suggested the oxygen-containing species (NO_x and NH_2OH) as likely candidates.

There are few studies of ammonia oxidation on single-crystal platinum electrodes. Nonetheless, these studies provided important information on the

structure sensitivity of ammonia oxidation. Gao et al.[95] reported mass spectrometry measurements of ammonia oxidation on Pt(100) and pointed to a high activity of this surface. These authors also observed the production of molecular nitrogen between ca. 0.6 and 0.9 V. More recently, Vidal-Iglesias et al.[96] reported a voltammetric study of ammonia oxidation on Pt(111), Pt(110), and Pt(100). The authors demonstrated a structure sensitivity of ammonia oxidation on platinum: Pt(100) was highly active for ammonia oxidation at potentials as low as 0.5 V, whereas Pt(111) and Pt(110) showed virtually no activity in the potential range up to ca. 0.9 V. In a subsequent paper, Vidal-Iglesias et al.[97] concluded that the activity for ammonia oxidation was quite sensitive to the width of the (100) terrace and the orientation of the step. Very recently, the same authors reported results of a DEMS study of ammonia oxidation on Pt(111), Pt(110), and Pt(100) using labeled ammonia (^{15}N).[98] The Pt(100) surface showed a very high activity and selectivity (up to ca. 0.7 V vs. RHE) in ammonia oxidation to dinitrogen. At potentials more positive than ca. 0.7 V, nitrous oxide and nitric oxide become dominant products at this surface. For a cyclic voltammogram with the upper potential limit of ca. 1.5 V, a strong deactivation of the surface was observed. Pt(111) and Pt(110) were shown to be much poorer electrocatalysts for ammonia oxidation in general and to dinitrogen in particular.

With all experimental data on ammonia oxidation available, our current understanding of the electrocatalytic oxidation of ammonia is still rather inadequate. To be more specific, there is little insight into the factors controlling the activity and selectivity of platinum for ammonia oxidation to dinitrogen. A lower energy of adsorption of atomic nitrogen on Pt(100), as compared to that on Pt(111) and Pt(110) could explain a high activity of Pt(100). At the same time, it is still to be established whether atomic nitrogen is the precursor in the formation of dinitrogen. Therefore, identification of the intermediates of the reaction is the key issue here. The Gerischer-Mauerer mechanism appears to be a useful starting model for a critical reconsideration of the mechanism of ammonia electrooxidation.

1.4. Scope and outline of the thesis

The main goal of the research described in the present thesis is a molecular-level understanding of the mechanisms and structure sensitivity of electrocatalytic reactions of nitric oxide, hydroxylamine, and ammonia at platinum electrodes. For that purpose, the adsorption and reactions of the above compounds were investigated on low-index single-crystal platinum electrodes in contact with ultrapure electrolyte solutions. Electrochemical techniques, namely, voltammetry and chronoamperometry, were combined with non-electrochemical molecular-level probes, namely, in situ Fourier transform reflection-absorption infrared

spectroscopy and on-line electrochemical mass spectrometry. Quantum chemical calculations (ab-initio density functional theory (DFT) calculations) were employed for a better understanding of the experimental results, as a complementary technique.

Mechanistic aspects of electrocatalytic reduction of nitric oxide adlayers on Pt(111), Pt(110), and Pt(100) surfaces in acidic media is the subject of Chapters 2 to 4. Chapter 2 describes a combined voltammetric and in situ infrared spectroscopy analysis of the reductive stripping of NO adlayers on Pt(111) and Pt(110) in acidic media, aimed at explaining the detailed voltammetric profile observed for NO_{ads} reduction on the two surfaces. As a result, a relationship between the NO binding site(s) and reactivity (voltammetric peaks) is established.

Chapter 3 reports the results of a chronoamperometric study of the reductive stripping of NO adlayers on Pt(111) and Pt(110), aimed at establishing the rate laws for the reduction of adsorbed NO. The experimental current transients were examined in terms of a kinetic model, which accounts for the effect of coverage and lateral interactions on the kinetics of NO_{ads} reduction under electrochemical conditions.

Chapter 4 describes the results of a detailed voltammetric, in situ infrared spectroscopy, and on-line mass spectrometry study of the reductive stripping of NO adlayers on the Pt(100) surface. The aim was to formulate a detailed mechanism of NO_{ads} reduction on Pt(100), including the effect of the surface coverage, anion (co)adsorption, and the role of the surface defects. This chapter also completes the comparison of the electrocatalytic reduction of NO adlayers on Pt(111), Pt(110), and Pt(100) surfaces.

Chapter 5 reports on the electrocatalytic reactions of hydroxylamine at Pt(111), Pt(110), and Pt(100) in acidic media, as deduced from voltammetry, on line mass spectrometry, and in situ infrared spectroscopy. The aim was to characterize the reactivity of hydroxylamine and to unravel the mechanisms of hydroxylamine reduction and oxidation on platinum. The mechanistic results are discussed in light of the mechanistic data on NO reduction on the same surfaces.

Chapter 6 describes a combined voltammetric and in situ infrared study of the electrocatalytic oxidation of ammonia on Pt(111) and Pt(100). The results obtained allow a better understanding of the initial stages of ammonia dehydrogenation and shed light on the factors controlling the activity and selectivity of ammonia oxidation to dinitrogen. A tentative mechanism of the dinitrogen production on Pt(100) is proposed and discussed.

References

(1) Trasatti, S. *Int. J. Hydrogen Energy* **1995**, *20*, 835.
(2) Appleby, A. J. Electrocatalysis. In *Compr. Treatise Electrochem.*, 1983; Vol. 7; pp 173.
(3) *Electrocatalysis*; Lipkowski, J.; Ross, P. N., Eds., 1998, pp 43.
(4) Herrero, E.; Feliu, J. M.; Aldaz, A. Electrocatalysis. In *Encyclopedia of Electrochemistry*, 2003; Vol 2; pp 443.
(5) Wendt, H.; Rausch, S.; Borucinski, T. *Adv. Catal.* **1994**, *40*, 87.
(6) Markovic, N. M.; Ross, P. N. *Surf. Sci. Rep.* **2002**, *45*, 117.
(7) *Catalysis and Electrocatalysis at Nanoparticle Surfaces*; Wieckowski, A.; Savinova, E. R.; Vayenas, C. G., Eds., 2003.
(8) Koper, M. T. M.; Van Santen, R. A.; Neurock, M. Theory and modeling of catalytic and electrocatalytic reactions. In *Catalysis and Electrocatalysis at Nanoparticle Surfaces*, 2003; pp 1.
(9) *Interfacial Electrochemistry. Theory, Experiment, and Applications*; Wieckowski, A., Ed.; Marcel Dekker, Inc.: New-York, 1999.
(10) Mallat, T.; Baiker, A. *Topics Catal.* **1999**, *8*, 115.
(11) Horanyi, G. *Catal. Today* **1994**, *19*, 285.
(12) Horanyi, G. *J. Mol. Catal. A: Chem.* **2003**, *199*, 7.
(13) Schmickler, W. *Interfacial Electrochemistry*; Oxford University Press: New-York, 1996.
(14) *Electrochemical Interfaces: Modern Techniques for In Situ Surface Characterization*; Abruna, H., Ed.; VCH: New-York, 1991.
(15) Iwasita, T.; Nart, F. C. In *Advances in Electrochemical Science and Engineering*; Gerischer, H., Tobias, C. W., Eds.; Verlag Chemie: Weiheim, 1995; Vol. 4; pp 123.
(16) Baltruschat, H. *J. Am. Soc. Mass Spectrometry* **2004**, *15*, 1693.
(17) Horold, S.; Vorlop, K.-D.; Tacke, T.; Sell, M. *Catal. Today* **1993**, *17*, 21.
(18) Dima, G. E.; de Vooys, A. C. A.; Koper, M. T. M. *J. Electroanal. Chem.* **2003**, *554-555*, 15.
(19) Tauszik, G. R.; Grocetta, P. *Appl. Ctalysis* **1985**, *17*, 1.
(20) Ritz, J.; Fuchs, H.; Perryman, H. G. Hydroxylamine. In *Ulmann's Encyclopedia of Industrial Chemistry*; 6th ed.; Wiley: Chichester, 2000.
(21) Allen, B. W.; Piantadosi, C. A.; Coury, L. A., Jr. *Nitric Oxide* **2000**, *4*, 75.
(22) de Vooys, A. C. A.; Beltramo, G. L.; van Riet, B.; van Veen, J. A. R.; Koper, M. T. M. *Electrochim. Acta* **2004**, *49*, 1307.
(23) Brown, W. A.; King, D. A. *J. Phys. Chem. B* **2000**, *104*, 2578.
(24) Masel, R. I. *Catal. Rev. -Sci. Eng.* **1986**, *28*, 335.
(25) Levoguer, C. L.; Nix, R. M. *Surf. Sci.* **1996**, *365*, 672.
(26) Gorte, R. J.; Gland, J. L. *Surf. Sci.* **1981**, *102*, 34.
(27) Brown, W. A.; Sharma, R. K.; King, D. A. *J. Phys. Chem.* **1998**, *102*, 5303.
(28) Agrawal, V. K.; Trenary, M. *Surf. Sci.* **1991**, *259*, 116.
(29) Rienks, E. D. L.; Bakker, J. W.; Baraldi, A.; Carabiniero, S. A. C.; Lizzit, S.; Weststrate, C. J.; Nieuwenhuys, B. E. *Surf. Sci.* **2002**, *516*, 109.
(30) Smirnov, M. Y.; Gorodetskii, V. V.; Cholach, A. R. In *Fundamental Aspects of Heterogeneous Catalysis Studied by Particle Beams*; Brongersma, H. H., van Santen, R. A., Eds., 1991; pp 249.
(31) Smirnov, M. Y.; Gorodetskii, V. V.; Block, J. H. *J. Mol. Catal. A: Chem.* **1996**, *107*, 359.
(32) Matsumoto, M.; Fukutani, K.; Okano, T.; Miyake, K.; Shigekawa, H.; Kato, H.; Okuyama, H.; Kawai, M. *Surf. Sci.* **2000**, *454-456*, 101.
(33) Matsumoto, M.; Tatsumi, T.; Fukutani, K.; Okano, T. *Surf. Sci.* **2002**, *513*, 485.
(34) Aizawa, H.; Morikawa, Y.; Tsuneyuki, S.; Fukutani, K.; Ohno, T. *Surf. Sci.* **2002**, *514*, 394.
(35) Gardner, P.; Tueshaus, M.; Martin, R.; Bradshaw, A. M. *Surf. Sci.* **1990**, *240*, 112.

(36) Ge, Q.; Neurock, M. *J. Am. Chem. Soc.* **2004**, *126*, 1551.
(37) Dutta, D.; Landolt, D. *J. Electrochem. Soc.* **1972**, *119*, 1320.
(38) Savodnik, N. N.; Shepelin, V. A.; Zalkind, T. I. *Elektrokhimiya* **1970**, *7*, 424.
(39) Savodnik, N. N.; Shepelin, V. A.; Zalkind, T. I. *Elektrokhimiya* **1971**, *7*, 583.
(40) Janssen, L. J. J.; Pieterse, M. M. J.; Barendrecht, E. *Electrochim. Acta* **1977**, *22*, 27.
(41) Paseka, I.; Vonkova, J. *Electrochim. Acta* **1980**, *25*, 1251.
(42) Paseka, I.; Hodinar, A. *Electrochim. Acta* **1982**, *27*, 1461.
(43) Colucci, J. A.; Foral, M. J.; Langer, S. H. *Electrochim. Acta* **1985**, *30*, 521.
(44) Colucci, J. A.; Foral, M. J.; Langer, S. H. *Electrochim. Acta* **1985**, *30*, 1675.
(45) Gootzen, J. F. E.; van Hardeveld, R. M.; Visscher, W.; van Santen, R. A.; van Veen, J. A. R. *Recl. Trav. Chim. Pays-Bas* **1996**, *115*, 480.
(46) de Vooys, A. C. A.; Koper, M. T. M.; van Santen, R. A.; van Veen, J. A. R. *Electrochim. Acta* **2001**, *46*, 923.
(47) de Vooys, A. C. A.; Koper, M. T. M.; van Santen, R. A.; van Veen, J. A. R. *J. Cat.* **2001**, *202*, 387.
(48) Schmid, G.; Lobeck, M. A. *Ber. Bunsenges. Phys. Chem.* **1969**, *73*, 189.
(49) Hecker, H. N.; Schmidt, G. *Electrochim. Acta* **1971**, *16*, 131.
(50) Gaade, R. G.; Bruckenstein, S. *J. Electroanal. Chem.* **1974**, *50*, 163.
(51) Barendrecht, E.; van der Plaas, J. F. *Recl. Trav. Chim. Pays-Bas* **1977**, *96*, 133.
(52) Snider, B. G.; Johnson, D. C. *Anal. Chim. Acta* **1979**, *105*, 9.
(53) Plieth, W. J. Encyclopedia of Electrochemistry of the Elements; Bard, A. J., Ed.; Marcel Dekker: New-York, 1978; Vol. 8.
(54) Garsia, C. T.; Calandra, A. J.; Arvia, A. J. *Electrochim. Acta* **1972**, *17*, 1281.
(55) Ye, S.; Kita, H. *J. Electroanal. Chem.* **1993**, *346*, 489.
(56) Rodes, A.; Gomez, R.; Orts, J. M.; Feliu, J. M.; Perez, A.; Aldaz, A. *J. Electroanal. Chem.* **1993**, *359*, 315.
(57) Zang, Z.-H.; Wu, Z.-L.; Yau, S.-L. *J. Phys. Chem. B* **1999**, *103*, 9624.
(58) Gomez, R.; Rodes, A.; Orts, J. M.; Feliu, J. M.; Perez, J. M. *Surf. Sci.* **1995**, *342*, L1104.
(59) Rosca, V.; Beltramo, G. L.; Koper, M. T. M. *J. Electroanal. Chem.* **2004**, *566*, 53.
(60) Beltramo, G. L.; Koper, M. T. M. *Langmuir* **2003**, *19*, 8907.
(61) Rodes, A.; Climent, V.; Orts, J. M.; Perez, J. M.; Aldaz, A. *Electrochim. Acta* **1998**, *44*, 1077.
(62) Zaera, F.; Gopinath, C. S. *Chem. Phys. Lett.* **2000**, *332*, 209.
(63) Benderski, V. A.; Krivenko, A. G.; Ponomarev, E. A. *Elektrokhimiya* **1990**, *26*, 318.
(64) Weaver, M. J.; Zou, S.; Tang, C. *J. Chem. Phys.* **1999**, *111*, 368.
(65) van de Moesdijk, C. G. M. The catalytic reduction of nitrite and nitric oxide to hydroxylamine: kinetics and mechanism. Ph.D. Thesis, Eindhoven University of Technology, 1979.
(66) Möller, D.; Heckner, K. H. *Z. Chem.* **1971**, *11*, 157.
(67) Möller, D.; Heckner, K. H. *Z. Phys. Chem.* **1974**, *255*, 33.
(68) Möller, D.; Heckner, K. H. *Z. Chem.* **1971**, *11*, 32.
(69) Möller, D.; Heckner, K. H. *Z. Chem.* **1971**, *11*, 356.
(70) Möller, D.; Heckner, K. H. *Z. Chem.* **1970**, *10*, 477.
(71) Möller, D.; Heckner, K. H. *Z. Phys. Chem.* **1972**, *251*, 81.
(72) Karabinas, P.; Wolter, O.; Heitbaum, J. *Ber. Bunsenges. Phys. Chem.* **1984**, *88*, 1191.
(73) Piela, B.; Wrona, P. K. *J. Electrochem. Soc.* **2004**, *151*, E69.
(74) Wynveen, R. A. *Fuel Cells* **1963**, *2*, 153.
(75) Simons, E. L.; Cairns, E. J.; Surd, D. J. *J. Electrochem. Soc.* **1969**, *116*, 556.
(76) Strickland, G. *J. Hydrogen Energy* **1984**, *9*, 759.
(77) Vitse, F.; Cooper, M.; Botte, G. G. *J. Power Sources* **2005**, *142*, 18.
(78) Marincic, L.; Leitz, F. B. *J. Appl. Electrochem.* **1978**, *8*, 333.

(79) Feng, C.; Sugiura, N.; Shimada, S.; Maekawa, T. *J. Hazard. Mater.* **2003**, *103*, 65.
(80) Pfennig, D.-M.; Deprez, J.; Kitzelmann, D. *Ber. Bunsenges. Phys. Chem.* **1990**, *94*, 988.
(81) Lopez de Mishima, B. A.; Lescano, D.; Molina Holgado, T.; Mishima, H. T. *Electrochim. Acta* **1997**, *43*, 395.
(82) Sexton, B. A.; Mitchell, G. E. *Surf. Sci.* **1980**, *99*, 523.
(83) Mieher, W. D.; Ho, W. *Surf. Sci.* **1995**, *322*, 151.
(84) Bradley, J. M.; Hopkinson, A.; King, D. A. *Surf. Sci.* **1997**, *371*, 255.
(85) Gohndrone, J. M.; Olsen, C. W.; Backman, A. L.; Gow, T. R.; Yagasaki, E.; Masel, R. I. *J. Vac. Sci. Technol.* **1989**, *7*, 1986.
(86) Bradley, J. M.; Hopkinson, A.; King, D. A. *J. Phys. Chem.* **1995**, *99*, 17032.
(87) Oswin, H. G.; Salomon, M. *Can. J. Chem.* **1963**, *41*, 1686.
(88) Despic, A. R.; Drazic, D. M.; Rakin, P. M. *Electrochim. Acta* **1966**, *11*, 997.
(89) Gerischer, H.; Mauerer, A. *J. Electroanal. Chem.* **1970**, *25*, 421.
(90) Wasmus, S.; Vasini, E. J.; Krausa, M.; Mishima, H. T.; Vielstich, W. *Electrochim. Acta* **1994**, *39*, 23.
(91) Gootzen, J. F. E.; Wonders, A.; Visscher, W.; van Santen, R. A.; van Veen, J. A. R. *Electrochim. Acta* **1998**, *43*, 1851.
(92) de Vooys, A. C. A.; Koper, M. T. M.; van Santen, R. A.; van Veen, J. A. R. *J. Electroanal. Chem.* **2001**, *506*, 127.
(93) de Vooys, A. C. A.; Mrozek, M. F.; Koper, M. T. M.; Van Santen, R. A.; Van Veen, J. A. R.; Weaver, M. J. *Electrochem. Comm.* **2001**, *3*, 293.
(94) Endo, K.; Katayama, Y.; Miura, T. *Electrochim. Acta* **2005**, *50*, 2181.
(95) Gao, Y.; Kita, H.; Hattori, H. *Chem. Lett.* **1994**, *11*, 2093.
(96) Vidal-Iglesias, F. J.; Garcia-Araez, N.; Montiel, V.; Feliu, J. M.; Aldaz, A. *Electrochem. Comm.* **2003**, *5*, 22.
(97) Vidal-Iglesias, F. J.; Solla-Gullon, J.; Montiel, V.; Feliu, J. M.; Aldaz, A. *J. Phys. Chem. B* **2005**, *109*, 12914.
(98) Vidal-Iglesias, F. J. PhD thesis, Universidad de Alicante, 2005.

2

Electrocatalytic reduction of NO adlayers on Pt(110) and Pt(111) in acidic media: evidence for adsorption site - specific reduction

Abstract
Described herein is a combined in situ Fourier transform infrared reflection-absorption spectroscopy (FTIRRAS) and voltammetric study of the reduction of saturated and subsaturated NO adlayers on Pt(111) and Pt(110) single–crystal surfaces in acidic media. The stripping voltammetry experiments and the associated evolution of infrared spectra indicate that different features (peaks) observed in the voltammetric profile for the electrochemical reduction of NO adlayers on the surfaces considered are related to the reduction of NO_{ads} at different adsorption sites and not to different (consecutive) processes. More specifically, reduction of high- and intermediate-coverage NO adlayers on Pt(110) (ca. 0.5–1 monolayers (ML)) is accompanied by site switching from atop to bridge position, in agreement with the ultra-high-vacuum data. On Pt(111), linearly-bonded (atop) NO and face-centered cubic 3-fold-hollow NO species coexist at high coverages (0.25–0.5 ML) and can be reduced consecutively and independently. On Pt(111), Pt(110), and Pt(100) electrodes, linearly-bonded NO species are more reactive than multifold-bonded NO species. Both spectroscopic and voltammetric data indicate that ammonia is the main product of NO_{ads} reduction on the surfaces examined.

This chapter is based on article by V. Rosca, G.L. Beltramo, and M.T.M. Koper, published in Langmuir, 21 (2005) 1448.

2.1. Introduction

The adsorption and reactions of nitric oxide (NO) on transition metal surfaces in an electrochemical environment are of considerable technological and scientific interest. NO is a key intermediate or reagent in a series of environmentally and industrially important processes, such as nitrate (nitrite) reduction and ammonia oxidation[1] or the liquid-phase catalytic hydrogenation of nitric oxide (NO) or nitrate to hydroxylamine.[2,3] Furthermore, electrochemical sensing and removal of nitric oxide[4] requires a thorough understanding of electrochemistry of NO. From a fundamental point of view, NO reduction is a relatively simple electrocatalytic process and could serve as a model system for studying activity and selectivity issues in electrocatalysis. Finally, similar to the extensively studied oxidation of carbon monoxide, NO is in many respects a suitable molecule for comparing reactions at the solid–gas and solid–liquid interface, especially when combined with work at single-crystal surfaces.

Recent studies of the electrochemical transformation of NO adlayers (NO_{ads}) on low-index single-crystal platinum electrodes[5-13] have significantly improved our understanding of the reactivity of nitric oxide, as compared to the knowledge gained from studies on polycrystalline platinum.[14] Recently, Beltramo et al.[15] reported a systematic voltammetric analysis of reduction and oxidation of NO adlayers on Pt(111), Pt(110) and a series of stepped Pt[n(111)×(111)] electrodes, aimed at establishing both the mechanism and structure sensitivity of reactions of adsorbed NO. The following tentative mechanism was proposed for the reduction of adsorbed NO:[15]

$NO_{ads} + H^+ + e^- \leftrightarrows HNO_{ads}$	equilibrium	(2.1)
$HNO_{ads} + H^+ + e^- \rightarrow H_2NO_{ads}$	rds	(2.2)
$H_2NO_{ads} + 4H^+ + 3e^- \rightarrow NH_4^+ + H_2O$	fast	(2.3)

Most importantly, the first two reaction steps are assumed to be two combined proton and electron transfers. It is difficult to elaborate on the nature and the elementary steps of the process (2.3), because they take place after the rate-determining step.

Reduction of NO_{ads} appears to be structure insensitive with regard to the kinetics of the process: the NO adlayer may be stripped off in two to three voltammetric features in the potential region between ca. 0.15 and 0.4 V vs RHE (0.5 M sulfuric or perchloric acid) at all surfaces examined. On the other hand, the voltammetric profile proved to be clearly structure sensitive. This structure sensitivity was ascribed to different NO surface configurations and coverages,

combined with structure sensitive adsorption of hydrogen and anions, rather than with a structure sensitivity of the NO reduction per se.[15]

Due to its ability to supply vibrational information and its in situ applicability to electrochemical interfaces, Fourier transform infrared reflection-absorption spectroscopy (FTIRRAS) has become an important tool for investigating electrode processes at a molecular level.[16] An important, if not critical, factor enabling FTIRRAS application in (in situ) electrochemical studies was the development of links between related metal–vacuum and metal–solution interfaces. In this sense, in addition to extensive studies on carbon monoxide (CO), adsorption of NO on platinum-group metals has been receiving increasing attention in recent years.[13,17-19]

Described herein is a combined in situ FTIRRAS and voltammetric study of the reduction of saturated and subsaturated NO adlayers on Pt(111) and Pt(110) single crystal surfaces in acidic media. We aimed particularly at the structure sensitivity of the voltammetric profile in relation to the coverage and the associated evolution of FTIRRAS spectra. Specifically, we shall demonstrate a relationship between the NO binding site(s) and the reduction peak(s) in the voltammetry of the surfaces studied.

2.2. Experimental Section

The H_2SO_4 and $HClO_4$ working solutions were prepared from their respective concentrated acids ("Suprapur", Merck) and ultrapure water (Millipore MilliQ system, 18.2 MΩ cm, 1-2 ppb total organic carbon) or triply distilled deuterium oxide ("Uvasol", Merck, deuteration degree min. 99.8%).

Two types of single-crystal platinum electrodes were used. Bead-type single-crystal platinum electrodes, prepared by Clavilier's method,[20] were used for most of the electrochemical measurements. For in situ FTIR measurements, commercial platinum disk electrodes of 10 mm diameter were used (oriented within 1°, Surface Preparation Laboratory, Zaandam, The Netherlands). Prior to each experiment, the working electrode was flame-annealed, cooled to room temperature in an $Ar:H_2$ (3:1) atmosphere and transferred to the electrochemical cell under the protection of a droplet of deoxygenated ultrapure water. To avoid the so-called missing row reconstruction, the Pt(110) electrode was cooled in an intensive stream of Ar, following the approach proposed by Markovic et al.[21]

Electrochemical measurements were performed in a single-compartment three-electrode glass cell, using a computer-controlled potentiostat (AutoLab-PGSTAT20, Eco Chemie, Utrecht, The Netherlands). The cell contained a small movable glass spoon[22] that allowed dosing of NO at open circuit potential from a diluted $NaNO_2$ solution under the argon atmosphere, thus allowing deposition of saturated and subsaturated NO adlayers without dissolving NO in the working solution. As for the in situ FTIR experiments, NO

adlayers were generated in a similar way: immersion of the working electrode in a separate solution of $NaNO_2$ was followed by a thorough washing of the electrode with pure deuterated water and subsequent transfer of the electrode to the cell. The cell and the other glassware were cleaned by boiling in a 1:1 mixture of concentrated nitric and sulfuric acid, followed by repeated boiling with ultrapure water. A coiled platinum wire served as counter electrode. In $HClO_4$ solutions, the reference electrode was an internal reversible hydrogen electrode (RHE). In H_2SO_4 solutions a saturated mercury-mercury sulfate ($Hg/Hg_2SO_4/K_2SO_4$) electrode, connected via a Luggin capillary, was used as a reference. However, all potentials are quoted versus the RHE. Prior to each experiment, all solutions were deoxygenated by purging with pure (N50) argon.

The in situ FTIRRAS measurements were performed under external reflection conditions. All the spectra reported were recorded under potential control. The Fourier transform infrared spectrometer was a Brüker IFS113V, equipped with a narrow-band MCT detector. The design of the spectroelectrochemical cell closely resembles that described elsewhere.[23] The cell featured a prismatic CaF_2 transmission window beveled at 60°. Five hundred interferograms were collected at each potential. The spectral resolution was 8 cm^{-1}. The reflectance spectra were calculated as $(R–R_0)/R_0$, where R and R_0 are the reflectance at the sample and the reference potential respectively. Consequently, the $\Delta R/R$ ratio gives negative bands for species that are formed and positive bands for species that are consumed at the sample potential, as compared to the reference potential.

The surface order and cleanliness of the electrodes were checked before each experiment by recording the blank cyclic voltammograms and their comparison to standard voltammetric profiles.[24-26] Specifically, the voltammetric profile for the Pt(110) electrode (Figure 2.1) agrees well with those reported by other groups,[21,27,28] allowing us to conclude that our electrode preparation procedure results in a well-ordered Pt(110)-(1×1) surface (for a detailed discussion, see reference 26).

2.3. Results and Data Analysis

2.3.1. Pt(110)

We shall begin with presenting the voltammetric data for the reductive stripping of NO adlayers on Pt(110). Figure 2.1 shows the stripping voltammetry of saturated and subsaturated NO adlayers on Pt(110) at low scan rates. Note that the subsaturated NO adlayers were deposited by immersion in $NaNO_2$ solution for different periods of time (see the Experimental Section for details). The voltammetric profile for the reduction of a saturated NO adlayer in sulfuric acid exhibits three characteristic peaks: E_1^{110} at ca. 0.33 V, E_2^{110} at ca. 0.23 V, and E_3^{110} at ca. 0.11 V. The third reduction peak (E_3^{110}) is assumed to correspond mainly to the hydrogen underpotential deposition (H_{upd}). Accordingly, the charge associated with this peak is similar to the charge for the H_{upd}/(bi)sulfate adsorption and desorption on clean Pt(110). Next, the position and charge of this peak are only

slightly affected by the initial coverage of NO. The shift of the position of peak E_3^{110}, as compared to that for a clean surface, and the apparent irreversibility (Tafel slope of 32 mV decade^{-1}) is most probably related to some residual NO left on the surface. The inset of Figure 2.1 shows the stripping voltammetry for the reduction of a saturated NO adlayers in perchloric acid (solid line). In perchloric acid the main reduction peak involves more charge than in sulfuric acid, whereas peaks E_1^{110} and E_2^{110} significantly overlap. Note that in perchloric acid both reduction peaks are positioned slightly more positively than those in sulfuric acid, thus indicating an effect of the (bi)sulfate coadsorption for experiments in sulfuric acid. As argued elsewhere,[15] it would be reasonable to assume that in perchloric acid practically all adsorbed NO is stripped off at ca. 0.2 V, whereas in sulfuric acid a small amount of NO may be still present at this potential.

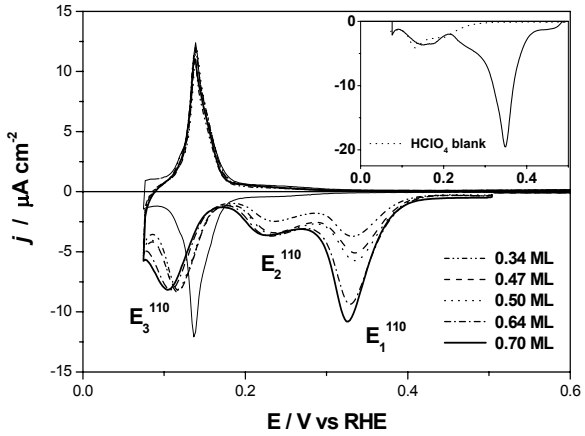

Figure 2.1. Cyclic voltammograms for the reduction of NO adlayers having different initial coverage (as indicated by the numbers in the legend) on Pt(110) in 0.5 M H_2SO_4 at 2 mV s^{-1}. The bold solid line is the voltammogram for the reduction of a saturated NO adlayer; the solid line is the Pt(110) blank voltammetry. The inset shows the voltammetry for the reduction of a saturated NO adlayer (the solid line) on Pt(110) and the blank voltammetric profile (the dotted line) in 0.5 M $HClO_4$ at 2 mV s^{-1}.

Figure 2.1 also shows that peak E_3^{110} does not exhibit a significant change in charge with the initial NO coverage, which is in agreement with assigning this feature to the H_{upd}/(bi)sulfate adsorption and desorption. Nevertheless, the peak position shifts slightly negatively with increasing NO coverage. The charge corresponding to the first two reduction peaks increases with increasing NO coverage, while their positions remain the same. Importantly, the reduction peak E_2^{110} is "saturated" at intermediate NO coverage, while the charge under the main

peak (E_1^{110}) increases until the maximum NO coverage [ca. 0.7–1 monolayers (ML)][15] is reached. This observation suggests that the two reduction features are rather due to NO reduction at different adsorption sites than due to different (consecutive) processes.

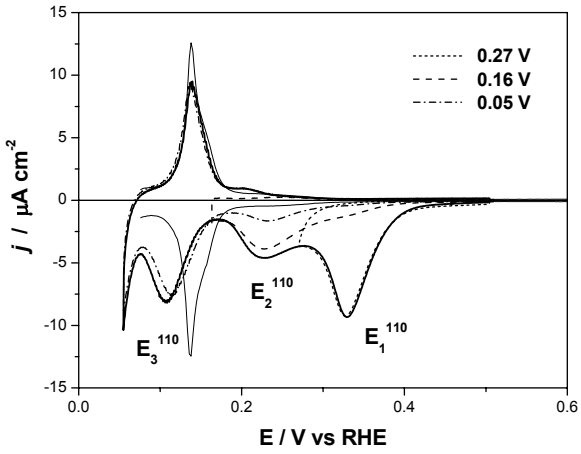

Figure 2.2. Cyclic voltammograms showing the independent removal of the voltammetric features characteristic to NO reduction on Pt(110) (see text for details). Experimental conditions: 0.5 M H_2SO_4; 2 mV s^{-1}. Numbers in the legend indicate the lower potential limit of the corresponding CVs. The bold solid line is voltammogram for the reduction of a saturated NO adlayer; the solid line is the Pt(110) blank voltammetry.

If the voltammetric peaks E_1^{110} and E_2^{110} were due to reduction of NO molecules at different adsorption sites, it would be interesting to see if those features could be removed independently. The experimental results shown in Figure 2.2 demonstrate that this is indeed the case. Three voltammetric runs were performed, starting with 0.5 V, and recorded one after another, with decreasing the lower potential limit (as indicated by the numbers in the figure). Note that the voltammetric features cannot be reduced completely independently, because they partially overlap. Significantly, the position and charge of voltammetric peak E_3^{110} is not affected by this experiment as compared to the profile for an uninterrupted stripping of a saturated NO adlayer (Figure 2.2, the bold solid line). This result is in good agreement with the above interpretation of this feature. Finally, the same experiment in perchloric acid gives the same result: the voltammetric peaks E_1^{110} and E_2^{110} can be reduced consecutively and independently, and therefore can be attributed to the reduction of adsorbed NO at different adsorption sites.

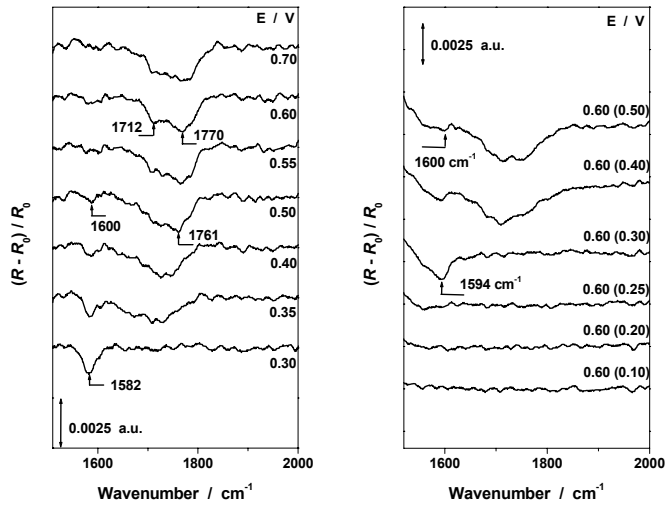

Figure 2.3. (left panel) The potential-difference infrared spectra acquired at a Pt(110) electrode covered with a preadsorbed NO adlayer. Numbers indicate the applied electrode potential on the RHE scale. Experimental conditions: 0.1 M $HClO_4$ (in D_2O), reference potential 0.1 V, p-polarized light.

Figure 2.4. (right panel) The potential-difference infrared spectra acquired at a Pt(110) electrode covered with NO adlayers at different coverage, as obtained by partial reductive stripping. All spectra were recorded at 0.60 V. Numbers in parentheses indicate the potential to which the potential was stepped prior to recording the spectrum at 0.60 V (see text for details). Experimental conditions: 0.1 M $HClO_4$ (in D_2O), reference potential 0.1 V, p-polarized light.

Turning now to the spectroscopic data on NO reduction on Pt(110), Figure 2.3 shows a series of spectra for a (initially) saturated NO adlayer on Pt(110) electrode. To obtain unipolar (better-defined) bands, the reference potential was chosen at 0.1 V, i.e. the potential where NO is stripped off completely, as deduced from the CV data (see above). In the potential region in which chemisorbed NO is stable (between ca. 0.7 and 0.45 V), the spectra show two characteristic absorption bands: a broad band between ca. 1800 and 1680 cm^{-1} with the maximum contribution around 1770 cm^{-1} and a weaker band at around 1600 cm^{-1}. The two bands are not present in spectra acquired by using s-polarized light under the same experimental conditions, thus indicating that the two bands originate from adsorbed species, namely, adsorbed NO. At the same time, the two spectroscopic features mentioned show a weak, though significant, dependence of the applied potential. Accordingly, in the potential region of NO stability the maximum of both bands slightly shifts toward lower wavenumbers with decreasing applied potential (see

Figure 2.3). This trend is expected for N–O stretching (ν_{NO}) in adsorbed NO species.[18]

Before interpreting the spectra in Figure 2.3, let us note that the resulting spectroscopic picture is strikingly similar to that for NO adsorption at the Pt(110)/ ultra-high vacuum (UHV) interface. Here we shall refer to a recent study by Brown and co-workers.[29] These authors analyzed in detail the effect of coverage, temperature, and surface reconstruction on the adsorption of nitric oxide on Pt(110). The spectra resulting from the adsorption of NO on Pt(110) at 300 K [(1×1) structure] at high NO exposure (saturation coverage corresponding to ca. 1 ML) present three characteristic features: a first strong broad band centered at 1796 cm^{-1}, a second band centered at 1712 cm^{-1}, and a third weak band at ca. 1613 cm^{-1}.[29] The first and third bands were attributed to N–O stretching vibration (ν_{NO}) in atop and bridge-bonded NO species, respectively, whereas the band around 1712 cm^{-1} is believed to be either due to NO adsorbed in the long bridge site (across the top layer rows) or due to NO adsorption on defect sites of the (1×1) structure.

Comparing now the UHV data with our own in situ spectra (Figure 2.3), the band between ca. 1800 and 1680 cm^{-1} must be related to atop NO, while the band at ca. 1600 cm^{-1} is assigned to ν_{NO} in bridged NO. Furthermore, the close resemblance of the infrared spectra recorded under electrochemical and UHV conditions indicates that (i) the surface structure is similar [well ordered (1×1) domains with few (1×2) defects)] and (ii) the NO saturation coverage should be similar in both cases, that is close to one. This last observation is in agreement with our voltammetric estimate of the NO saturation coverage under electrochemical conditions, ca. 1 ML for experiments in perchloric acid.[15]

The above vibrational assignments concerning NO adsorption on Pt(110) under electrochemical conditions are also in good agreement with results reported by the Alicante group. For (near) saturation coverage, Gomez et al. [13] observed a broad bipolar band at around 1740 cm^{-1}. At lower coverage they observed another weak band at around 1590 cm^{-1}. On the basis of a comparison with data from early vibrational studies under UHV conditions[30], the authors suggested that the band located at around 1740 cm^{-1} is related to atop NO, while the band at around 1590 cm^{-1} is related to bridged NO.

Brown et al.[29] also showed that at low coverages NO occupies bridge site. A further increase of the coverage is accompanied by a site switching from bridge to atop position. The site switching was explained by a larger repulsion between bridged NO than between atop NO molecules, which is believed to destabilize the bridge site in favor of the atop site at high coverages. A closer examination of the spectra, acquired in the potential region in which adsorbed NO is reduced (Figure 2.3), points to an apparent "intensity transfer" from the broad band located between

ca. 1800 and 1680 cm^{-1} (atop NO) to the band around 1600 cm^{-1} (bridged NO), thus suggesting that the site-switching scenario is valid under electrochemical conditions as well. Accordingly, in the potential region between ca. 0.45 and 0.3 V the population of atop NO species decreases, as a result of both reduction and site switching to bridge position. A significant shift of the position of the band between ca. 1800 and 1680 cm^{-1} toward lower frequencies is probably related to combined effects of (decreasing) applied potential and decreasing NO coverage, as both factors are known to cause a decrease of the N–O (ν_{NO}) stretching frequency.[18] At potentials around 0.3 V, atop NO is no longer detectable. A further decrease of the applied potential results in disappearance of the band at ca. 1600 cm^{-1} and, accordingly, reduction of bridged NO.

Similar trends with regard to the site occupation and site switching can be deduced by comparing the spectra acquired at different values of NO coverage at a potential where NO is stable. Figure 2.4 shows the potential difference spectra recorded at 0.6 V after a potential step to a given electrode potential, as indicated by the potential values in brackets. In this way, it was possible to separate the effect of the coverage from the effect of potential (at least for a given potential). A gradual decrease of NO coverage results in a gradual decrease in intensity of the band centered around 1760 cm^{-1}, accompanied by the emerging (or more likely intensification) of the band centered around 1600 cm^{-1}.

The infrared data described here demonstrate that on Pt(110) atop NO reacts in the potential region between ca. 0.45 and 0.3 V. At the same time, a low-scan rate voltammetric profile presents the reduction peak E_1^{110} in approximately the same potential window, irrespective of the supporting electrolyte (sulfate or perchlorate). Consequently, the voltammetric feature E_1^{110} may be attributed to the reductive stripping of NO molecules bonded in atop position. An analogous reasoning for the potential region between ca. 0.3 and 0.2 V implies that the voltammetric peak E_2^{110} is related mainly to the reductive stripping of NO molecules adsorbed at bridge position.

2.3.2. Pt(111)

The voltammetric profile for the reduction of a saturated NO adlayer on Pt(111) in 0.5 M sulfuric acid (Figure 2.5, the bold solid line) shows three characteristic voltammetric features: E_1^{111} at ca. 0.34 V, E_2^{111} at ca. 0.28 V, and E_3^{111} at ca. 0.15 V. The voltammetric profile is essentially the same in perchloric acid,[15] proving the absence of any significant effect of the anion (co)adsorption. From Figure 2.5 it was deduced that the charge corresponding to the three features, but not their position, is a function of the initial coverage of NO. Interestingly, the

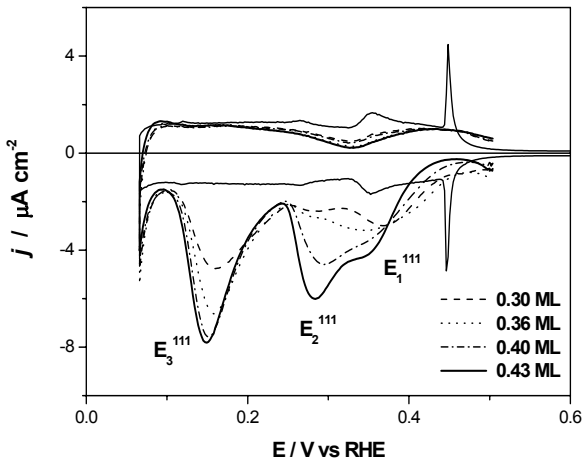

Figure 2.5. Cyclic voltammograms for the reduction of NO adlayers at different initial coverage (as indicated by the numbers in the legend) on Pt(111) in 0.5 M H_2SO_4 at 2 mV s^{-1}. The bold solid line is the voltammogram for the reduction of a saturated NO adlayer; the solid line is the Pt(111) blank voltammetry.

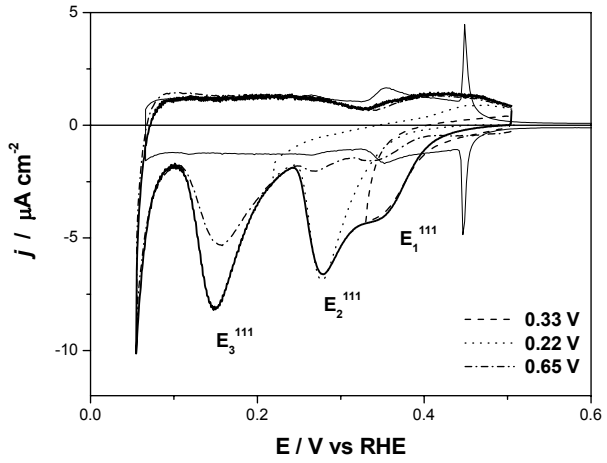

Figure 2.6. Cyclic voltammograms showing the independent removal of the voltammetric features characteristic to NO reduction on Pt(111) (see text for details). Experimental conditions: 0.5 M H_2SO_4; 2 mV s^{-1}. Numbers in the legend indicate the lower potential limit of the corresponding CVs. The bold solid line is the voltammogram for the reduction of a saturated NO adlayer; the solid (thin) line is the Pt(111) blank voltammetry.

voltammetric peak E_3^{111} is "saturated" first with increasing coverage, thus questioning a scenario, in which the three features would be due to different (consecutive) steps of NO reduction.

Figure 2.6 shows that, quite similar to reduction of NO_{ads} on Pt(110) (see Figure 2.2 and the accompanying explanations), the voltammetric features E_1^{111}, E_2^{111}, and E_3^{111} can be reduced consecutively and virtually independently. The outcome is the same for experiments performed in perchloric acid. This result strongly suggests that the three voltammetric features are determined essentially by reduction of NO molecules at different adsorption sites and not by different processes.

In contrast to NO adsorption on Pt(110), NO adsorption on Pt(111) under electrochemical conditions is documented quite well. The Alicante group has shown conclusively that stable NO adlayers can be generated on platinum, as well as on other metal electrodes, as a result of a surface decomposition of nitrous acid, either under potential control or at open-circuit potential.[8,9,13] Their in situ infrared studies of NO adlayers on Pt(111), carried out mostly in the potential region where NO is chemically stable, revealed two spectroscopic features ascribable to ν_{NO} in adsorbed NO: a bipolar (potential-dependent) band at ca. 1430 cm^{-1}, present at coverages as low as ca. 0.2 ML, and a second strong bipolar band centered at ca. 1680 cm^{-1}, present at higher coverages.[13] The higher frequency band was attributed to atop NO and the lower frequency band to bridged NO, based on early vibrational studies (see reference 13 and references therein). On the other hand, the infrared spectra, reported by Weaver et al.,[18] showed a pair of coverage-dependent bands, centered at ca. 1440 and 1665 cm^{-1} at lower coverages of NO. With increasing coverage the latter band shifts to 1680 cm^{-1} and gains in intensity, while the former band disappears toward saturation. On the basis of the UHV data available at that time, particularly those questioning earlier vibrational assignments[31], Weaver et al.[18] attributed the lower as well as the higher frequency band to NO located in the 3-fold-hollow site. However, more recent experimental and theoretical studies of NO adsorption on Pt(111), including scanning tunneling microscopy (STM) imaging,[32] dynamic low-energy electron diffraction (LEED) analysis and FTIRRAS UHV experiments,[33] density functional theory (DFT) calculations,[34] and high resolution X-ray photoelectron spectroscopy (XPS)[35] have conclusively shown that at coverages up to ca. 0.25, ML NO molecules occupy the face-centered cubic (fcc) 3-fold-hollow site, whereas at higher coverages (up to ca. 0.5 ML) the NO species in the fcc 3-fold-hollow sites coexist with NO species in atop position. Furthermore, it was suggested that at a coverage of 0.5 ML, that is the coverage close to the 0.4-0.45 ML range estimated for the NO saturation coverage under electrochemical conditions,[9,15] adsorbed nitric oxide forms a phase consisting of

one atop and one 3-fold-hollow site NO per (2×2) Pt(111) unit cell. The recent vibrational assignments[33,34] point to atop NO being responsible for the high frequency band (ca. 1715 cm^{-1}), whereas the low frequency band (ca. 1490 cm^{-1}) is attributed to NO_{ads} in the fcc 3-fold-hollow site. The maximum coverage reported under UHV conditions (0.75 ML) is unlikely to be achieved under electrochemical conditions.

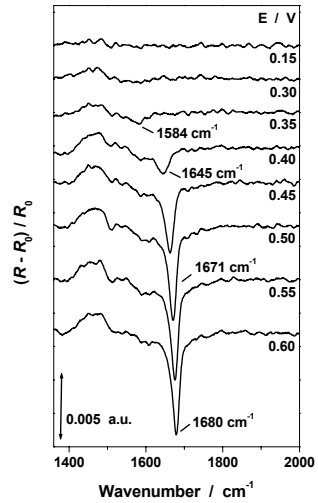

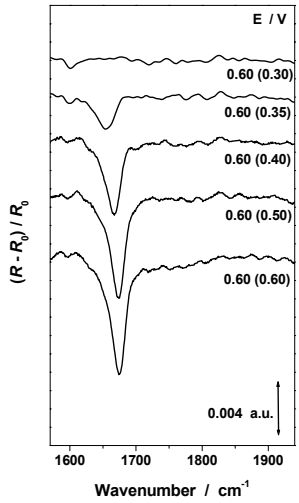

Figure 2.7. (left panel) The potential-difference infrared spectra acquired at a Pt(111) electrode covered with a preadsorbed NO adlayer. Numbers indicate the applied electrode potential on the RHE scale. Experimental conditions: 0.1 M $HClO_4$ (in D_2O), reference potential 0.1 V, p-polarized light.

Figure 2.8. (right panel) The potential-difference infrared spectra acquired at a Pt(111) electrode covered with NO adlayers at different coverages, as obtained by partial reductive stripping. All spectra were recorded at 0.60 V. Numbers in parentheses indicate the potential to which the potential was stepped prior to recording the spectrum at 0.60 V. Experimental conditions: 0.1 M $HClO_4$ (in D_2O), reference potential 0.1 V, p-polarized light.

Turning now to our own experimental infrared data, Figure 2.7 shows a set of the potential-difference spectra for a (initially) saturated NO adlayer on Pt(111) electrode. In light of the above discussion, the potential dependent band centered at ca. 1680 cm^{-1} was attributed to ν_{NO} in the atop NO species. Under the conditions of the experiment shown in Figure 2.7, it is very difficult to detect and follow the evolution of the low frequency band corresponding to 3-fold-hollow NO, as this band is strongly masked by a broad feature between ca. 1400 and 1500 cm^{-1}. This band is determined by a solution species, most probably a product of the reduction

of adsorbed NO. Accordingly, this band is still present in spectra acquired using s-polarized light and it does not show any shift with applied potential. At the same time, this band gradually loses its intensity (indicating accumulation of some species) in the potential region in which NO_{ads} is reduced.[36]

In the potential window in which NO_{ads} is stable, the peak frequency of the band located between 1700 and 1600 cm^{-1} (Figure 2.7) decreases linearly with the decreasing applied potential, with a "Stark-tuning" slope of ca. 75 cm^{-1} V^{-1}. At lower potentials, a gradual decrease of the integrated intensity, broadening, and a faster decrease of the band peak frequency with decreasing potential are observed, indicating consumption of atop NO species. At potentials around 0.3 V atop NO can no longer be detected. Nevertheless, the NO stripping voltammetry clearly shows that at this potential a significant amount of adsorbed NO (with coverage of ca. 0.2 ML) must be still present on the surface. Since no atop NO can be detected, the remaining NO molecules must be in the 3-fold-hollow sites, in accordance with the site occupation picture deduced for NO adsorption on Pt(111) under UHV and electrochemical conditions.

Figure 2.8 shows the results of an experiment similar to that described for Pt(110) (Figure 2.4), in which the potential was stepped back to the original potential of 0.6 V after a step to a given (more negative) potential. This experiment clearly indicates that in the potential window between ca. 0.45 and 0.3 V, atop NO species are stripped off the surface gradually and irreversibly, and do not exist in another (partially reduced) form.

Comparing the voltammetric and spectroscopic data on NO adsorption and reduction on Pt(111), we conclude that atop NO is reduced in the potential window between ca. 0.45 and 0.3 V, that is, the potential window in which the voltammetric peaks E_1^{111} and E_2^{111} are observed in the stripping profile. Consequently, these two features are related to the reduction of NO_{ads} in atop position. Finally, the feature E_3^{111} must be caused by the reduction of NO_{ads} in the 3-fold-hollow site. Note that two voltammetric features (E_1^{111} and E_2^{110}) seem to correspond to the reduction of a single type of adsorbed species – atop NO. A possible explanation to this observation will be given in the Discussion.

2.3.3. The product(s) of reduction of adsorbed NO

When discussing the products of NO reduction, we should make a clear distinction between continuous NO reduction and reduction of adsorbed NO. Continuous reduction of NO at polycrystalline platinum in acidic medium yields nitrous oxide (and molecular nitrogen) at moderately reductive potentials and hydroxylamine and ammonia at highly reductive potentials.[14] Importantly, the

presence of NO in solution is crucial for the production of nitrous oxide (and molecular nitrogen).[37]

In absence of any NO in solution, formation of both ammonia and hydroxylamine is possible. However recent studies on the reduction of NO adlayers on polycrystalline and single-crystal platinum electrodes point to ammonia as the main product.[9,13-15,38,39] A comparative analysis of NO adsorption on low-index single crystal platinum surfaces indicates a remarkable concordance in the vibrational frequencies of saturated NO adlayers in electrochemical and UHV environments.[18] Therefore, it would be reasonable to expect the adlayer structure and coverages to be similar on the corresponding surfaces in two cases, at least at room temperature (see also FTIR results on NO adsorption on Pt(110) in this study). Accordingly, an accurate analysis of the voltammetric charge gives coverages reasonably close to those under UHV conditions, provided that ammonia is assumed to be the product of the reductive stripping of NO_{ads}.[9,13,15,39] Finally, if any appreciable amount of hydroxylamine would be produced upon reduction of NO adlayers, unrealistically high saturation coverages would be implied (see ref 15 for a detailed discussion).

Parts A and B of Figure 2.9 show potential difference spectra for (initially) saturated NO adlayers on Pt(111) and Pt(110) surfaces, respectively, acquired with s-polarized light and in water. The broad absorption band around 1460 cm^{-1} is determined by a species in solution and is clearly related to reduction of adsorbed NO. Thus, the intensity of this band is constant in the potential region in which NO adsorbate is stable and loses in intensity (formation of a product) in the potential region in which NO_{ads} is reduced on the corresponding surfaces. Both ammonia and hydroxylamine can contribute to this spectral region.[40] However voltammetric results shown in Figures 2.1, 2.2, 2.5, and 2.6 clearly indicate the stripping of NO adlayer and virtually complete recovery of the corresponding blank CVs, thus excluding formation of a significant amount of electrochemically active species, which is hydroxylamine. Therefore, the absorption band centered around 1460 cm^{-1} can be attributed to $-(NH_3)$ (δ_s) mode in NH_4^+.[41] These results strongly suggest that ammonia is the main product of NO reduction on Pt(111) and Pt(110), presumably irrespective of the coverage.

2.3.4. Discussion

The experimental data and considerations given in the previous section point to a prominent role of the NO adsorption mode in defining the voltammetric response corresponding to the reductive stripping of nitric oxide adlayers. Accordingly, the voltammetric features observed for NO_{ads} reduction on Pt(111)

and Pt(110) (and presumably those on stepped Pt[n(111)×(111)] surfaces as well) are determined essentially by reduction of species occupying different adsorption sites and not by different (consecutive) processes (reaction steps). The linearly-bonded (atop) NO molecules seem to be more reactive than multifold-coordinated NO molecules, whatever the surface orientation. The potential windows in which linearly-bonded NO, on one hand, and multifold-coordinated NO molecules, on the other hand, react on different surfaces are very much the same: compare the positions of features E_1^{110}, E_1^{111} and E_2^{111} (atop NO) and E_2^{110} and E_3^{111} (multifold-coordinated NO), Figures 2.1 and 2.5.

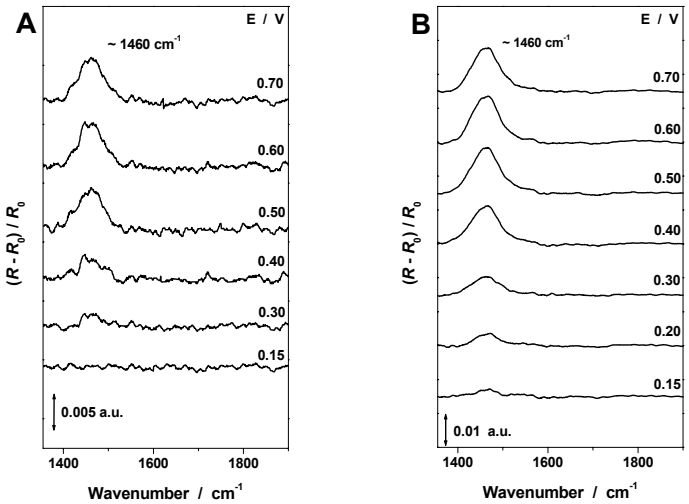

Figure 2.9. The potential-difference infrared spectra acquired at a Pt(111) (A) and Pt(110) (B) electrode covered with a preadsorbed NO adlayer in the 1350-1900 wavenumber region. Numbers indicate the applied electrode potential on the RHE scale. Experimental conditions: 0.1 M $HClO_4$ (in H_2O), reference potential 0.1 V, s-polarized light.

It is important to emphasize that these observations alone do not allow deducing the actual reaction site. The actual reaction site may be an ensemble of sites. For example, an elementary reaction step may require additional adsorption site(s), e.g. for the breaking of the N–O bond (see Chapter 3 for details).

The voltammetric features E_1^{111} and E_2^{111} (Figures 2.5 and 2.6) were both ascribed to the reductive stripping of atop NO species, on the basis of the associated evolution of the FTIR spectra (section 2.3.2). Apparently, these two spectroscopically indiscernible (atop) species show some differences in their reactivity. This response may be tentatively ascribed to different local environment

of the atop NO species within well-ordered domains of the NO adlayer (0.5 ML, 2 NO molecules per (2×2) unit cell)[32-34] and the atop NO species within somewhat disordered domains. Indeed, even under UHV conditions, the well-ordered phase corresponding to NO coverage of 0.5 ML requires special conditions (annealing of NO saturated surface at 225 K).[33] Therefore, a highly ordered NO phase corresponding to 0.5 ML is unlikely to be achieved under electrochemical conditions, in which even more interfering factors may intervene.

Interestingly, a comparison of NO reduction on Pt(111), Pt(110) and Pt[n(111)×(111)] stepped surfaces shows that NO adlayers are reduced in the same potential region between ca. 0.4 and 0.15 V, with little effect of coverage or anion adsorption. This observation, taken together with the fact that NO reduction on Pt(100) takes place in the same potential region (reduction features between ca. 0.3 and 0.2 V),[13] with little effect of coverage and anion coadsorption,[42] suggests that differences in the surface structure of platinum electrocatalyst do not result in clear-cut differences in rate (overpotential) of NO_{ads} reduction. In other words, there is little structure sensitivity with regard to the (overall) kinetics of the process.

The reduction of atop and bridged NO (features E_1^{110}, E_2^{110}, E_1^{111} and E_2^{111}) proceed in the absence of any adsorbed hydrogen or at a very low coverage of coadsorbed hydrogen, thus confirming the electrochemical hydrogenation mechanism, that is, through combined electron–proton transfer (as expressed in eqs 2.1 and 2.2)). The experimental Tafel slopes for the voltammetric features E_1^{110}, E_2^{110}, E_1^{111} and E_2^{111} (Pt(110), Pt(111), and Pt[n(111)×(111)] surfaces) are all close to 40 mV $decade^{-1}$, thus indicating the second electron transfer to be the rate-determining step (see the reaction scheme 2.1-2.3).[15] On the other hand, the reduction of NO species adsorbed at the 3-fold-hollow site of (111) terraces (E_3^{111}) is characterized by the Tafel slope of 120 mV $decade^{-1}$ and occurs in the presence of a considerable amount of coadsorbed H, thus raising the question of its role in the process. Indeed, it is not obvious that the reaction scheme (2.1-2.3) is valid in this case as well. It is noteworthy that the reductive stripping of NO adlayers on Pt(100) occurs in a potential region corresponding to high coverage of adsorbed H as well.[13] Therefore, in the presence of adsorbed hydrogen, the reduction of adsorbed NO may, in principle, follow another mechanism that could involve catalytic (Langmuir–Hinshelwood-type) hydrogenation steps. Another factor contributing to the complexity of the issue of structure sensitivity of the electrochemical reduction of NO_{ads} is the mechanism of the N–O bond breaking. At the metal–vacuum interface, the N–O bond breaking is a structure-sensitive reaction step that requires an ensemble of adsorption sites.[43] This may be the case

for NO_{ads} reduction at the metal–electrolyte interface as well (for relevant results and their discussion see Chapters 3 and 4).

Despite the apparent structure insensitivity of the NO_{ads} reduction kinetics, the detailed voltammetric profile for the reduction NO_{ads} on single-crystal platinum surfaces is sensitive to the surface structure. Figure 2.10 compares the voltammetric profiles recorded for the reductive stripping of saturated NO adlayers on the three low-index platinum surfaces – Pt(111), Pt(110), and Pt(100) – at a low scan rate. As stated above, no surface can be declared more active for NO reduction than another one, even for the case of NO stripping from stepped surfaces. Nevertheless, our results clearly indicate that the reactivity of NO_{ads} is differentiated by the (initial) site occupation, which is influenced by the coverage of NO. More specifically, linearly-bonded NO is the most active species, followed by the bridged NO, and, then, by the 3-fold-coordinated NO species. [On Pt(100), NO occupies a site close to the bridge position, at least at moderate (ca. 0.25 ML) to high (ca. 0.5 ML) coverage (Chapter 4).]

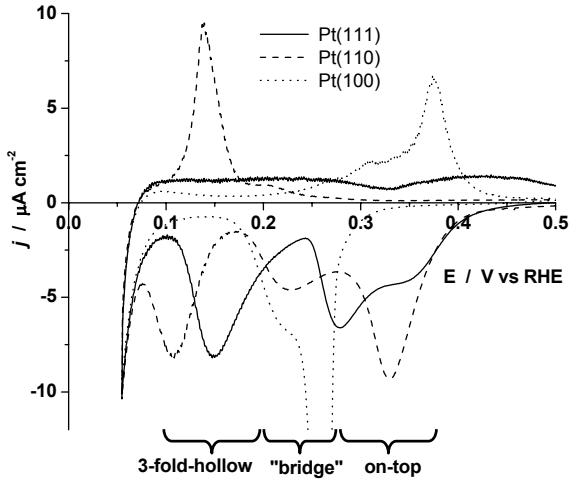

Figure 2.10. Cyclic voltammograms for the reductive stripping of saturated NO adlayers on low-index single-crystal platinum surfaces. Experimental conditions: 0.5 M H_2SO_4; starting potential 0.5 V; 2 mV s^{-1}. The terms "on-top", "bridge", and "3-fold-hollow" refer to the initial (at saturation) adsorption site of NO species, which react in the potential ranges delimited by the horizontal braces.

At this stage it would be difficult to identify the molecular-level factors causing differences in reactivity. Differences in adsorption strength would not provide a straightforward explanation (or may be even misleading) for differences in electroreduction activity of NO molecules occupying different adsorption sites.

An important observation to be taken into consideration here is that the first two steps of the process are likely to be electrochemical steps (proton/electron transfers),[15] certainly for the reduction of atop NO species on the planes examined. This could mean that the adsorbate ability to take part in an acid-base equilibrium (accompanying the electron transfer) and the stability of the resulting intermediates may determine the reactivity NO_{ads} species at different adsorption sites.

The structure sensitivity of the electrocatalytic reduction of NO_{ads} on platinum may be compared to the structure sensitivity of the extensively studied electrooxidation of carbon monoxide. Despite differences in the nature and mechanism of these processes, their structure sensitivity allows us to draw a number of interesting parallels. CO oxidation is a mechanistically structure-insensitive process. The Langmuir–Hinshelwood-type reaction between CO_{ads} and OH_{ads} is commonly perceived as the rate-determining step, which is then followed by a decay of the resulting intermediate to CO_2. In contrast to NO reduction, CO oxidation is a strongly structure-sensitive process with regard to the kinetics of the process. On Pt[n(111)×(111)] stepped surfaces, for instance, at moderately oxidative potentials, CO oxidation takes place preferentially at steps, which is related to the availability of OH_{ads} species, which are formed readily on steps.[24-26,44] Due to its high mobility on (111) terraces, CO diffuses toward and reacts exclusively at steps (or defects in general). Under certain circumstances, the voltammetric profile of CO_{ads} oxidative stripping may also exhibit several features. However, these features are not related to the oxidation of CO at specific adsorption sites.[45] In contrast to CO oxidation, reduction of NO_{ads} proceeds at (or near) the site the molecule is initially confined to, the site occupation being determined by the surface orientation and the coverage. The step sites and terrace sites are kinetically comparable. Furthermore, the site-differentiated activity in the case of NO reduction on platinum originates from the reactivity differences of linearly- and multifold-coordinated NO species (and presumably the reactivity of the reduction intermediates as well), ultimately resulting in an adsorption site - specific reaction and, consequently, an adsorption site - specific voltammetric profile.

2.5. Conclusions

The surface structure of the platinum electrocatalyst exerts a complex effect on the electrochemical reduction of nitric oxide adlayers. The process is structure sensitive in terms of coverage-dependent site occupation. On Pt(111) and Pt(110) surfaces, linearly-bonded NO species are more reactive than multifold-bonded NO

species. On the basis of voltammetric and spectroscopic evidence, it was shown that different features observed in the voltammetric profile for the reductive stripping of NO adlayers on the two surfaces are related to the reduction of NO molecules at different adsorption sites and not to different (consecutive) processes. Furthermore, as deduced from spectroscopic and electrochemical data, ammonia is the main product of the reduction of adsorbed NO on Pt(111) and Pt(110). The site occupation by NO on Pt(110) under electrochemical conditions shows a remarkable accordance with the site occupation by NO under UHV conditions. Accordingly, electrochemical reduction of the high-coverage NO adlayers (between ca. 0.5 and 1 ML) on Pt(110) is accompanied by a site switching from atop to bridge position, the bridged NO species being somewhat less reactive than atop NO species. For the electrochemical reduction of NO adlayers on Pt(111), atop NO species and the fcc 3-fold-hollow NO species coexist at high coverages (between ca. 0.25 and 0.5 ML) and may be reduced consecutively and independently.

References

(1) Horold, S.; Vorlop, K.-D.; Tacke, T.; Sell, M. *Cat. Today* **1993**, *17*, 21.
(2) Ritz, J.; Fuchs, H.; Perryman, H. G. Hydroxylamine. In *Ulmann's Encyclopedia of Industrial Chemistry*, 6th ed.; Wiley: Chichester, 2000.
(3) van de Moesdijk, C. G. M. The catalytic reduction of nitrite and nitric oxide to hydroxylamine: kinetics and mechanism. Ph.D. Thesis, Eindhoven University of Technology, 1979.
(4) Allen, B. W.; Piantadosi, C. A.; Coury, L. A., Jr. *Nitric Oxide* **2000**, *4*, 75.
(5) Ye, S.; Hattori, H.; Kita, H. *Ber. Bunsen-Ges. Phys. Chem.* **1992**, *73*, 1884.
(6) Ye, S.; Kita, H. *J. Electroanal. Chem.* **1993**, *346*, 489.
(7) Rodes, A.; Gomez, R.; Orts, J. M.; Feliu, J. M.; Perez, A.; Aldaz, A. *J. Electroanal. Chem.* **1993**, *359*, 315.
(8) Rodes, A.; Gomez, R.; Orts, J. M.; Feliu, J. M.; Perez, A.; Aldaz, A. *Langmuir* **1995**, *11*, 3549.
(9) Rodes, A.; Gomez, R.; Perez, A.; Feliu, J. M.; Aldaz, A. *Electrochim. Acta* **1996**, *41*, 729.
(10) Momoi, K.; Song, M. B.; Ito, M. *J. Electroanal. Chem.* **1999**, *473*, 43.
(11) Zang, Z.-H.; Wu, Z.-L.; Yau, S.-L. *J. Phys. Chem. B* **1999**, *103*, 9624.
(12) Casero, E.; Alonso, C.; Martin-Gago, J. A.; Bogatti, F.; Felici, R.; Renner, R.; Lee, T.; Zegenhagen, J. *Surf. Sci.* **2002**, *507-510*.
(13) Gomez, R.; Rodes, A.; Orts, J. M.; Feliu, J. M.; Perez, J. M. *Surf. Sci.* **1995**, *342*, L1104.
(14) de Vooys, A. C. A.; Beltramo, G. L.; van Riet, B.; van Veen, J. A. R.; Koper, M. T. M. *Electrochim. Acta* **2004**, *49*, 1307.
(15) Beltramo, G. L.; Koper, M. T. M. *Langmuir* **2003**, *19*, 8907.
(16) Iwasita, T.; Nart, F. C. *Prog. Surf. Sci.* **1997**, *55*, 271.
(17) Villegas, I.; Gomez, R.; Weaver, M. J. *J. Phys. Chem.* **1995**, *99*, 14832.
(18) Weaver, M. J.; Zou, S.; Tang, C. *J. Chem. Phys.* **1999**, *111*, 368.
(19) Zou, S.; Gomez, R.; Weaver, M. J. *J. Electroanal. Chem.* **1999**, *474*, 155.
(20) Clavilier, J.; Armand, D.; Sun, S. G.; Petit, M. *J. Electroanal. Chem.* **1986**, *205*, 267.
(21) Markovic, N. M.; Grgur, B. N.; Lucas, C. A.; Ross, P. N. *Surf. Sci.* **1997**, *384*, L805.

(22) Feliu, J. M.; Orts, J. M.; Fernandez-Vega, A.; Aldaz, A.; Clavilier, J. *J. Electroanal. Chem.* **1990**, *296*, 191.
(23) Iwasita, T.; Nart, F. C.; Vielstich, W. *Ber. Bunsen-Ges. Phys. Chem.* **1990**, *94*, 1030.
(24) Lebedeva, N. P.; Koper, M. T. M.; Herrero, E.; Feliu, J. M.; van Santen, R. A. *J. Electroanal. Chem.* **2000**, *487*, 37.
(25) Lebedeva, N. P.; Rodes, A.; Feliu, J. M.; Koper, M. T. M.; van Santen, R. A. *J. Phys. Chem. B* **2002**, *106*, 9863.
(26) Lebedeva, N. P.; Koper, M. T. M.; Feliu, J. M.; van Santen, R. A. *J. Phys. Chem. B* **2002**, *106*, 12938.
(27) Gomez, R.; Clavilier, J. *J. Electroanal. Chem.* **1993**, *354*, 189.
(28) Kibler, L.A.; Cuesta, A.; Kleinert, M.; Kolb, D.M. *J. Electroanal. Chem.* **2000**, *484*, 73.
(29) Brown, W. A.; Sharma, R. K.; King, D. A. *J. Phys. Chem.* **1998**, *102*, 5303.
(30) Gorte, R. J.; Gland, J. L. *Surf. Sci.* **1981**, *102*, 34.
(31) Brown, W. A.; King, D. A. *J. Phys. Chem. B* **2000**, *104*, 2578.
(32) Matsumoto, M.; Fukutani, K.; Okano, T.; Miyake, K.; Shigekawa, H.; Kato, H.; Okuyama, H.; Kawai, M. *Surf. Sci.* **2000**, *454-456*, 101.
(33) Matsumoto, M.; Tatsumi, T.; Fukutani, K.; Okano, T. *Surf. Sci.* **2002**, *513*, 485.
(34) Aizawa, H.; Morikawa, Y.; Tsuneyuki, S.; Fukutani, K.; Ohno, T. *Surf. Sci.* **2002**, *514*, 394.
(35) Zhu, J. F.; Kinne, M.; Fuhrmann, T.; Denecke, R.; Steinruck, H.-P. *Surf. Sci.* **2003**, *529*, 384.
(36) Note that our in situ FTIR experiments were performed in D_2O, although in presence of a considerable concentration of protons (0.1 M $HClO_4$ or H_2SO_4). The proton content was low enough to examine the 1500-1700 cm^{-1} frequency region, though apparently high enough to result in the formation of solution species, which may contribute in the frequency region between 1400 and 1500 cm^{-1}. We identify these species as ammonium cations, containing H and D atoms in different ratios. Accordingly, theoretical calculations similar to those described elsewhere (see reference 40 for details) show that the species DNH_3^+, $D_2NH_2^+$, and D_3NH^+ contribute around 1489 cm^{-1} (–NH_3 (δ_s) mode), 1405 cm^{-1} (–NH_2D (δ_s) mode), and 1457 cm^{-1} (–NHD scissoring mode), respectively.
(37) de Vooys, A. C. A.; Koper, M. T. M.; van Santen, R. A.; van Veen, J. A. R. *Electrochim. Acta* **2001**, *46*, 923.
(38) Gootzen, J. F. E.; van Hardeveld, R. M.; Visscher, W.; van Santen, R. A.; van Veen, J. A. R. *Recl. Trav. Chim. Pays-Bas* **1996**, *115*, 480.
(39) Rodes, A.; Climent, V.; Orts, J. M.; Perez, J. M.; Aldaz, A. *Electrochim. Acta* **1998**, *44*, 1077.
(40) Rosca, V.; Beltramo, G. L.; Koper, M. T. M. *J. Phys. Chem. B* **2004**, *108*, 8294.
(41) Silverstein, R. M.; Bassler, G. C.; Morrill, T. C. *Spectrometric Identification of Organic Compounds*; John Wiley & Sons, Inc.: New York, 1991.
(42) Rosca, V.; Koper, M. T. M., *J. Phys. Chem. B* **2005**, *109*, 16750.
(43) Masel, R. I. *Catal. Rev.-Sci. Eng.* **1986**, *28*, 335.
(44) Lebedeva, N. P.; Koper, M. T. M.; Feliu, J. M.; van Santen, R. A. *J. Electroanal. Chem.* **2002**, *524-525*, 242.
(45) Markovic, N.M.; Grgur, B.N.; Lucas, C.A.; Ross, P.N. *J. Phys. Chem. B* **1999**, *103*, 487.

3

Rate laws for reductive stripping of NO adlayers at single-crystal platinum electrodes as deduced from transient experiments

Abstract

The electrochemical reduction of nitric oxide (NO) adlayers on Pt(111) and Pt(110) surfaces has been investigated using the potential step method. The observed current transients were interpreted in terms of a kinetic model for the first- and the second-order reactions in the mean-field approximation with strong lateral interactions. Under electrochemical conditions and in the limit of saturated NO coverage, considerable repulsive interactions exist between the reacting species, having a significant effect on the chronoamperometric response of the systems examined. Accordingly, the current transients for NO reduction on Pt(111) show a hyperbolic (t^{-1}) decay, which indicates (i) first order kinetics and (ii) strong lateral interactions. For NO reduction on Pt(111) surfaces, the experimentally assessed lateral interactions between two neighboring NO species varies between ca. 0.03 and 0.05 eV. The current transients for the reductive stripping of saturated NO adlayers on the Pt(110) surface (with atop NO as the reactive species) show a potential dependent maximum, occurring at high coverages, which indicates (i) second-order kinetics and (ii) considerable lateral interactions. The second order kinetics observed in the limit of high NO coverage was attributed to the necessity of having a neighboring free site required for breaking the N–O bond. For the reduction of (nearly) saturated NO adlayers on Pt(111) surface, the apparent first-order kinetics may be tentatively explained by the availability of the neighboring free site at all coverages of NO, as suggested by the much lower saturation coverage on Pt(111) (ca. 0.5 monolayers (ML)) compared to the saturation coverage on Pt(110) (ca. 1 ML).

This chapter is based on article by V. Rosca and M.T.M. Koper, published in Surface Science, 584 (2005) 258.

3.1. Introduction

Recent advances[1] in fundamental understanding of adsorption and reactions of NO on platinum under electrochemical conditions came largely from studies on single crystal surfaces, performed under well-defined chemical conditions.[2-14] Recently, Beltramo et al.[12] reported the results of a systematic voltammetric analysis of electrochemical reduction of NO adlayers on Pt(111), Pt(110) and a series of stepped Pt[n(111)×(111)] electrodes, aimed specifically at establishing the mechanism and structure sensitivity of the process. As a result, the following tentative mechanism of the reaction was proposed:

$$NO_{ads} + H^+ + e^- \leftrightarrows HNO_{ads} \qquad \text{equilibrium} \qquad (3.1)$$

$$HNO_{ads} + H^+ + e^- \rightarrow H_2NO_{ads} \qquad \text{rds} \qquad (3.2)$$

$$H_2NO_{ads} + 4H^+ + 3\ e^- \rightarrow NH_4^+ + H_2O \qquad \text{fast} \qquad (3.3)$$

In previous chapter,[15] it was shown that the multiple features (peaks) observed in the voltammetric profile for the reductive stripping of NO adlayers are due to reduction of NO molecules at different adsorption sites and not due to different (consecutive) processes. This is an example of an adsorption site – specific reaction. Ammonia was repeatedly suggested or shown to be the main product of the reduction of adsorbed NO on platinum,[6-8,12,15,16] although it is not clear whether the reaction pathway is the same for different surfaces.[15]

The mechanism expressed in reaction scheme (3.1-3.3) points to certain differences between the reduction of NO under electrochemical conditions and in ultra-high vacuum (UHV). First of all, in our electrochemical studies, we never obtained any evidence for the influence of N–O bond breaking on the overall rate, even though it must occur, because NH_4^+ is the main product in acidic media. For NO reduction on platinum under UHV conditions, N–O bond breaking is an important and often rate-determining step.[17,18] It has been suggested that NO dissociation depends on the surface structure and the number of free sites surrounding the NO adsorption site, which are required for NO molecule to lie flat and induce the N–O bond breaking. Secondly, in UHV, lateral interactions between adsorbed NO molecules have been found to be very important, especially at high coverages,[19-21] whereas, under electrochemical conditions, no evidence for lateral interaction has been provided so far.

The influence of N–O bond breaking and lateral interactions should in principle be reflected in the rate laws for the electrochemical reduction of NO_{ads}. Stripping voltammetry, frequently used in previous studies of NO_{ads} reduction, is not the most suitable technique for deducing rate laws, in particular reaction orders.

This chapter describes the results of a study, in which the potential-step technique, or chronoamperometry, is used to investigate the rate laws for NO_{ads} reduction on Pt(111) and Pt(110) electrodes in acidic media. The experimental data are examined in terms of a recently proposed model[22] and an extension thereof, which accounts for the effect of coverage and lateral interactions on the kinetics of NO_{ads} reduction under electrochemical conditions.

3.2. Experimental Section

The H_2SO_4 and $HClO_4$ working solutions were prepared from their respective concentrated acids ("Suprapur", Merck) and ultrapure water (Millipore MilliQ system, 18.2 MΩ cm, less than 3 ppb total organic carbon).

Bead-type single-crystal platinum electrodes, prepared by Clavilier's method,[23] were used. Prior to each experiment, the working electrode was flame-annealed, cooled to room temperature in a (2:1) $Ar:H_2$ gas mixture and transferred to the electrochemical cell under the protection of a droplet of deoxygenated ultrapure water. Importantly, the surface order and cleanliness of the electrodes were checked by recording the so-called blank cyclic voltammograms and their comparison to standard voltammetric profiles[24-26] (and references therein).

Electrochemical measurements were performed in a single-compartment three-electrode glass cell, using a computer-controlled potentiostat (AutoLab-PGSTAT20, Eco Chemie, Utrecht, The Netherlands). The cell contained a small movable glass spoon[27] that allowed dosing of NO at open circuit potential from a diluted $NaNO_2$ (ca. 0.1 mM) solution. The cell and the other glassware were cleaned by boiling in a 1:1 mixture of concentrated nitric and sulfuric acid, followed by repeated boiling with ultra-pure water. A coiled platinum wire served as counter electrode. In $HClO_4$ solutions, the reference electrode was an internal reversible hydrogen electrode (RHE). In H_2SO_4 solutions a $Hg/Hg_2SO_4/K_2SO_{4\,(sat)}$ electrode, connected via a Luggin capillary, was used as reference. However, all potentials are quoted versus the RHE. Before each experiment, all solutions were deoxygenated by purging with pure (N50) argon.

3.3. Kinetic model for reduction of NO_{ads}

3.3.1 First order kinetics with lateral interactions

This section introduces a simple kinetic model for NO_{ads} reduction, the predictions of which will be compared to the experimental transients presented in section 3.4.

We consider the NO_{ads} reduction to ammonia as an irreversible process:

$$NO_{ads} + 5e^- + 6H^+ \rightarrow NH_4^+ + H_2O \qquad (3.4)$$

Assuming first order kinetics and incorporating lateral interactions between the adsorbed species, in the so-called mean-field approximation (MFA, commonly referred to as the Frumkin approximation in the electrochemistry literature[28]), the corresponding rate equation is

$$d\theta / dt = - k(E)\theta \exp (z\varepsilon\theta / RT) = - k(E)\, \theta \exp (\gamma\theta) \qquad (3.5)$$

where k(E) is the potential (E) dependent heterogeneous rate constant, θ the fractional NO surface coverage referred to the maximum coverage, z the surface coordination number of an adsorption site (for instance, z = 6 for a (111) surface and 4 for a (100) surface), ε is the repulsive interaction, R and T have their usual meaning, and $\gamma = z\varepsilon/RT$. The current flowing is given by

$$j = - nF\, \Gamma_m\, k(E)\, \theta \exp (\gamma\theta) \qquad (3.6)$$

where Γ_m is the maximum number of surface species per cm^2.

In the case of chronoamperometry (a jump to a potential E_{step}), the differential equation can be solved analytically. The exact solution to equation 3.5, with $E = E_{step}$ and $\theta\,(t = 0) = \theta_0$, is given by

$$E_i (-\gamma\theta) = E_i (-\gamma\theta_0) - kt \qquad (3.7)$$

where

$$E_i (x) = \int_{-\infty}^{x} \frac{e^t}{t}\, dt \qquad (3.8)$$

is the integral exponent function, and $k = k (E_{step})$.

For strongly repulsive lateral interaction ($\gamma \rightarrow \infty$), one may assume that in equation 3.5 the exponential term changes much faster with changes in θ than the kθ term, at least for not too low coverages ($\theta > 0.01 - 0.1$). Therefore, we can rewrite equation 3.5 as follows:

$$d\theta / dt = - \bar{k} \exp (\gamma\theta) \qquad (3.9)$$

where $\bar{k} \approx \langle k\theta \rangle \approx \frac{1}{2}\, k$. Now the differential equation can be solved explicitly:

$$\exp (-\gamma\theta) = \gamma\ \bar{k}\, t + \exp (-\gamma\theta_o) \qquad (3.10)$$

For the current density, this gives:

$$j = - nF \Gamma_m \frac{\bar{k}}{\gamma \bar{k} t + \exp(-\gamma \theta_O)} \qquad (3.11)$$

For large γ and θ sufficiently smaller than the initial coverage (or, equivalently, t sufficiently larger than 0), this leads to a hyperbolic transient:

$$j = - nF \Gamma_m (\gamma t)^{-1} \qquad (3.12)$$

Figure 3.1 shows typical transients for different values of the interaction parameter γ. The inset is a log-log plot of the data for γ = 10 showing that for high γ the transient indeed is hyperbolic over a wide range of times.

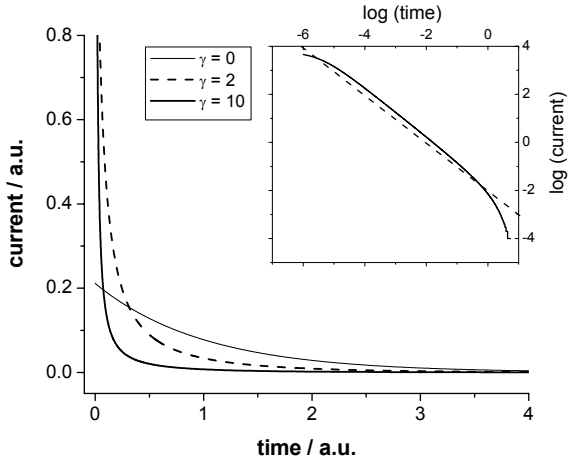

Figure 3.1. Chronoamperometric transients for the first-order reactions with lateral interactions. k = 1, θ_0 = 1, γ as indicated in the legend of the figure. The inset shows the quality of the hyperbolic approximation to the curve corresponding to γ = 10.

3.3.2. Second-order kinetics with lateral interactions

The rate law given by equation 3.5 implies that NO_{ads} reduction is first order in θ_{NO}, which seems reasonable if the N–O bond breaking occurs after the rate-determining step. However, if the N–O bond breaking is rate limiting, and we follow the notion suggested in UHV surface science that for such an elementary step a neighboring free surface site is needed, the following non-linear rate equation could be suggested:

$$d\theta / dt = - k(E)\theta (1 - \theta) \qquad (3.13)$$

where (1–θ) gives the average number of free sites on the surface. Equation 3.13 has a known analytical solution,[29] and is widely used to model CO_{ads} oxidation, where the (1 – θ) term reflects the coverage of OH_{ads} on the surface. This rate law predicts a chronoamperometric maximum at t_{max}= 1/k ln (θ_0/(1–θ_0)) at θ_{NO}=0.5. Invoking now the role of lateral interactions, we can write

$$d\theta / dt = - k(E)\theta (1 - \theta) \exp (\gamma\theta) \qquad (3.14)$$

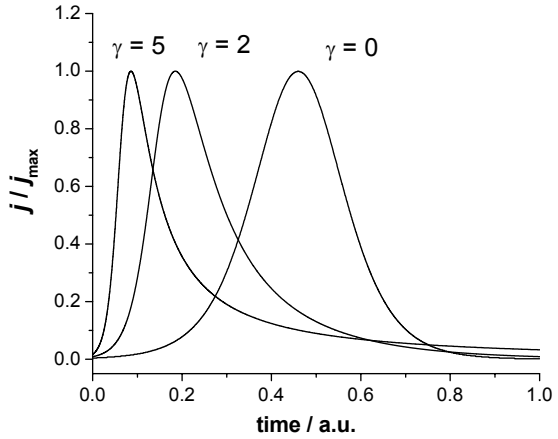

Figure 3.2. Chronoamperometric transients for the second-order reactions with lateral interactions. k = 1, θ_0 = 0.999, γ as indicated in the legend of the figure.

We have not attempted to solve this differential equation, but it is not difficult to see that it still predicts a chronoamperometric maximum, the corresponding coverage of which (θ_{max}) now depends on the parameter γ.

$$\theta_{max} = \frac{\gamma - 2 + \sqrt{4 + \gamma^2}}{2\gamma} \qquad (3.15)$$

$$= 0.5 \qquad \text{for } \gamma = 0$$

$$= \frac{1}{2}\sqrt{2} \approx 0.704 \qquad \text{for } \gamma = 2$$

$$\approx 0.838 \qquad \text{for } \gamma = 5$$

Examples of the corresponding transients (obtained numerically) are given in Figure 3.2.

From the fact that equation 3.14 can be rescaled ($t' = k(E)\, t$)

$$d\theta / dt' = -\theta (1 - \theta) \exp(\gamma\theta) \qquad (3.16)$$

which will have a solution for t'_{max}, which depends only on γ, it follows that

$$t_{max} = \frac{1}{k(E)} f(\gamma) \qquad (3.17)$$

and therefore a plot of $\log(t_{max})$ vs. E should give the Tafel slope, irrespective of γ (assuming that γ does not depend on E).

3.3.3. Validity of mean-field approximation as applied to reduction of NO_{ads} on platinum

In the above equations, we have employed the mean-field approximation, implying that the adsorbed NO species are all equally reactive, and that the effect of lateral interactions can be treated on an averaged level. The latter assumption breaks down when interactions are strong. However, as shown in a previous paper,[22] chronoamperometric hyperbolic decay (equation 3.12) is still predicted. Also, in contrast to recent discussions on the electrochemical oxidation of carbon monoxide, the surface mobility of NO_{ads} does not play a role: NO is assumed to react with a solution species (H^+), and not with another adsorbed species. The assumption that all NO_{ads} are equally reactive is in principle incorrect, as we have recently shown that NO adsorbed at different sites have a different reactivity.[15] We believe this may explain some deviations from hyperbolic decay, as will be discussed in subsection 3.4.1. A complete modeling of these effects would require a Monte–Carlo-based simulation approach.

3.4. Results and Data Analysis

3.4.1. Electrochemical reduction of nitric oxide adlayers on Pt(111)

Figure 3.3 shows the voltammetric profile for the reductive stripping of a saturated NO adlayer on Pt(111) surface in perchloric acid (bold solid line). The voltammetric profile presents three reduction features (peaks), E_1^{111}, E_2^{111} and E_3^{111}, the first two features being strongly overlapped. The voltammetric profile remains essentially the same for similar experiments in sulfuric acid, thus indicating little

effect of the anion (co)adsorption.[12] The stripping voltammetry experiments and the associated evolution of infrared spectra indicate that the voltammetric features observed are related to the reduction of NO_{ads} at different adsorption sites, and not to different (consecutive) processes (as demonstrated in chapter 2).[15] More specifically, features E_1^{111} and E_2^{111} were assigned to reduction of terminal (atop) NO species, whereas feature E_3^{111} was shown to be due to reduction of the multifold-coordinated (face-centered cubic (fcc) 3-fold-hollow site) NO species. Furthermore, features E_1^{111} and E_2^{111} can be removed selectively, leaving feature E_3^{111} intact. The saturation coverage of NO adlayers on Pt(111) under electrochemical conditions varies between ca. 0.4 and 0.5 ML.[7,12]

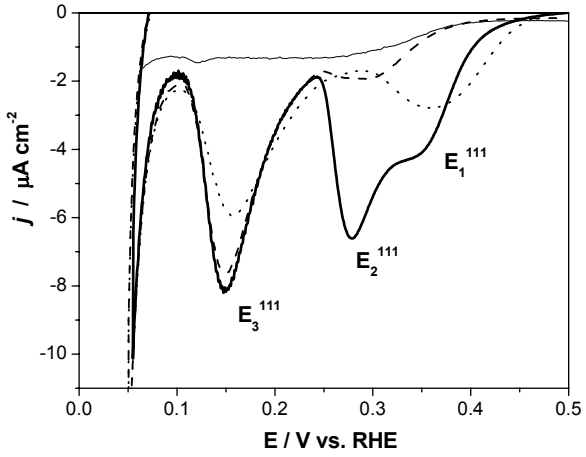

Figure 3.3. The reductive stripping of a saturated NO adlayer on Pt(111) (the bold solid line) and the blank voltammetry of Pt(111) electrode (thin solid line) in 0.5 M $HClO_4$ at 2 mV s^{-1}. The dashed line represents the voltammetric reduction of a subsaturated NO adlayer (0.26 ML), resulting from the potential step experiment in Figure 3.4. The dotted line represents the voltammetric reduction of a subsaturated NO adlayer (0.28 ML), resulting from the potential step experiment in Figure 3.5.

Figure 3.4 shows the result of a potential step experiment on Pt(111) in perchloric acid. Note that for the given step potential (E_{step}=0.25 V), only one type of species is reactive, i.e. atop NO species. Accordingly, the voltammetric profile recorded after the potential step experiment (which lasted ca. 15 seconds) indicates that feature E_1^{111} is completely removed, feature E_2^{111} is strongly reduced, whereas, feature E_3^{111} is essentially unchanged (Figure 3.3, dashed line). The log (j) – log (t) plot presents a well-defined linearity over a wide range of times (Figure 3.4B). Moreover, the slope of the least-square regression line is reasonably close to 1, that is the value predicted by the model, which suggests strong lateral interactions and

the associated hyperbolic (t^{-1}) transient (see the subsection 3.3.1 and Figure 3.1). The intercept of the line at log(t)=0 was used to calculate γ from equation 3.12 and, then, ε from the expression $\gamma = z\varepsilon/RT$. The resulting value for γ was found to be approximately 8, which corresponds to a value of 0.034 eV for ε. Note that γ =8 would indeed predict hyperbolic decay (see Figure 3.1), demonstrating the internal consistency of the modeling.

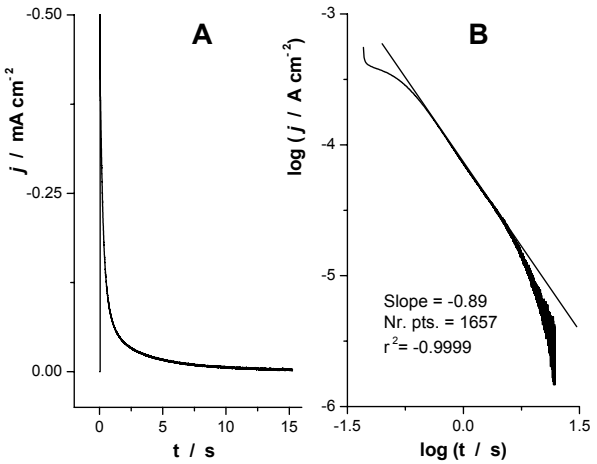

Figure 3.4. Potential step experiment for electrochemical reduction of a saturated NO adlayer on Pt(111) electrode. (A) the j – t transient; (B) the corresponding log–log plot. Experimental conditions: E_{in} = 0.5 V, E_{step}= 0.25 V, 0.5 M $HClO_4$.

As shown in Figure 3.5, a potential step to 0.1 V also results in a hyperbolic current decay, albeit in a narrower time range. Note that at such a low potential both linearly- and multifold-coordinated NO species may react. Therefore, deviations from the response predicted by the model (subsection 3.3.1) are expected. Nevertheless, hyperbolic current decay is still observed, and the slope of the log (j) – log (t) curve in the region of the hyperbolic dependence is close to the theoretical value of one. The voltammetric profile recorded after the potential step to 0.1 V (for ca. 15 seconds) shows a partial consumption of feature E_3^{111} and a virtually complete consumption of feature E_2^{111}, whereas feature E_1^{111} is still present (Figure 3.3, dotted line). The γ value, calculated from the intercept of the linear regression line in Figure 3.5B, is approximately 9.5, which corresponds to a value of 0.051 eV for the lateral interactions, which is still reasonable.

We did not notice any clear-cut effect of the hydrogen (co)adsorption on the current response. The reductive stripping of a NO adlayer on Pt(111) is

accompanied by filling of available surface sites with adsorbed hydrogen. However, the hydrogen underpotential deposition is a fast reversible process, which will not limit the system response.

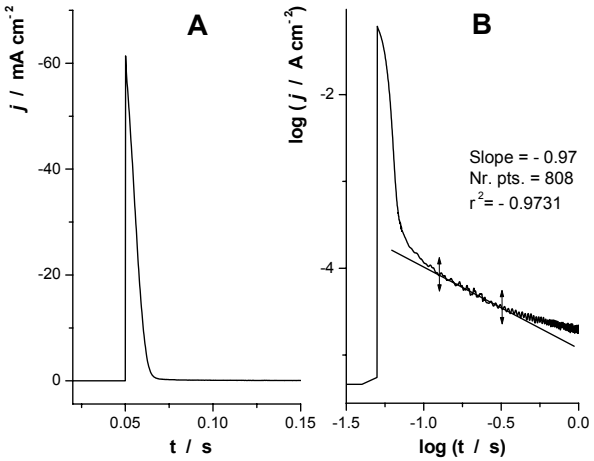

Figure 3.5. Potential step experiment for electrochemical reduction of a saturated NO adlayer on Pt(111) electrode. (A) the j – t transient; (B) the corresponding log–log plot. Experimental conditions: E_{in} = 0.5 V, E_{step}= 0.1 V, 0.5 M $HClO_4$.

Interestingly, partial stripping of the (initially) saturated NO adlayers by the potential steps to 0.25 and 0.1 V (Figures 3.4 and 3.5) results in formation of subsaturated NO adlayers having comparable coverage (ca. 0.26 ML versus ca. 0.28 ML, respectively) but, at the same time, a different adlayer structure, as deduced from the voltammetric stripping experiments (Figure 3.3, the dashed and dotted lines, respectively). The dashed line in Figure 3.3, recorded after the potential step to 0.25 V (Figure 3.4), points to an ordered NO adlayer consisting mostly of NO molecules in the fcc 3-fold-hollow site (0.25 ML, p(2×2)-NO adlayer structure [30-33]). The dotted line in Figure 3.3, recorded after the potential step to 0.1 V (Figure 3.5), points to a somewhat disordered NO adlayer, which probably consists of a mixture of p(2×2)-NO and p(2×2)-2NO disordered domains. Arguments in favor of these structural assignments were given in the previous chapter.[15] The above results indicate that the current responses in Figures 3.4 and 3.5 correspond to the reduction of NO coverage from ca. 0.5 ML to ca. 0.25 ML, i.e. the limits of high to moderate NO coverage.

The potential step to 0.1 V, performed after the atop NO species (features E_1^{111} and E_2^{111}) were selectively removed by voltammetric stripping, does not

exhibit an hyperbolic current decay, probably due to the reduced effect of lateral interactions at coverages lower than ca. 0.25 ML.

3.4.2. Electrochemical reduction of nitric oxide adlayers on Pt(110)

Figure 3.6 shows the voltammetric reduction of saturated (bold solid line) and subsaturated (dashed line) NO adlayers on Pt(110) in perchloric acid at a low potential sweep rate. The voltammetric profile for the stripping of a saturated NO adlayer in perchloric acid shows two peaks, E_1^{110} and E_2^{110}, which overlap strongly. The reductive stripping of a subsaturated NO adlayer (0.38 ML) is also shown in Figure 3.6 to indicate the position of the feature E_2^{110}. Note that the two features are better separated and better defined in sulfuric acid.[12] As shown elsewhere,[12,15] the complete stripping of NO adlayer is achieved at potentials of ca. 0.25 V in perchloric acid and at ca. 0.15 V in sulfuric acid.

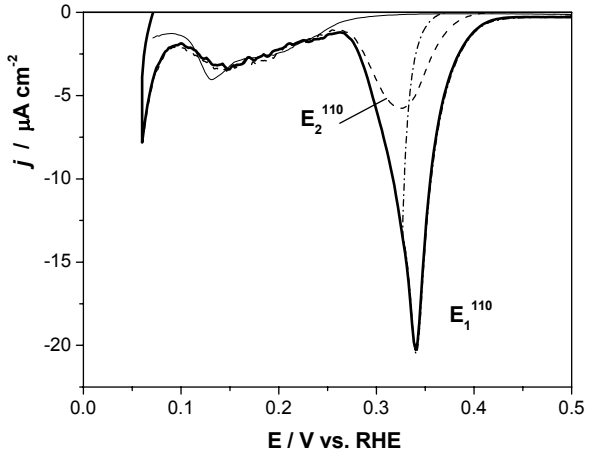

Figure 3.6. The reductive stripping of a saturated NO adlayer on Pt(110) (bold solid line) and the bare Pt(110) electrode (solid line) in 0.5 M $HClO_4$ at 2 mV s^{-1}. The dashed line represents the electrochemical reduction of a subsaturated (0.38 ML) NO adlayer on Pt(110), resulting after partial stripping of a saturated NO adlayer (dash-dotted line).

In Chapter 2, it was demonstrated that the voltammetric features E_1^{110} and E_2^{110} are not related to different (consecutive) processes.[15] On the basis of the stripping voltammetry experiments and the associated evolution of infrared spectra, these features were shown to be related to electrochemical reduction of NO species at atop site (E_1^{110}) and NO species at bridge sites (E_2^{110}), although the actual

reaction site is admittedly unknown. Importantly, the saturation coverage of NO adlayer on Pt(110) in perchloric acid, estimated from the charge analysis, was ca. 1 ML (versus ca. 0.7 ML in sulfuric acid),[12] which is close to the value deduced for a saturated NO adlayer under UHV conditions.[19] Furthermore, a good concordance between the infrared spectra recorded (in situ) under electrochemical conditions and the infrared spectra recorded under the UHV conditions (room temperature, Pt(110)-(1×1), saturation conditions) strongly suggests that the structure of NO adlayer and the coverage-dependent site occupation by NO molecules under electrochemical (in the presence of non-specifically adsorbing electrolyte species) and UHV conditions are very similar.[15] Therefore, in an electrochemical environment, the saturated NO adlayer consists exclusively of the atop NO species. During the electrochemical reduction on Pt(110), the atop NO species are consumed as a result of (i) the reductive stripping itself and (ii) site switching from atop to the bridge position,[15] which is energetically more favorable at low to moderate (< ca. 0.5 ML) coverage.[19]

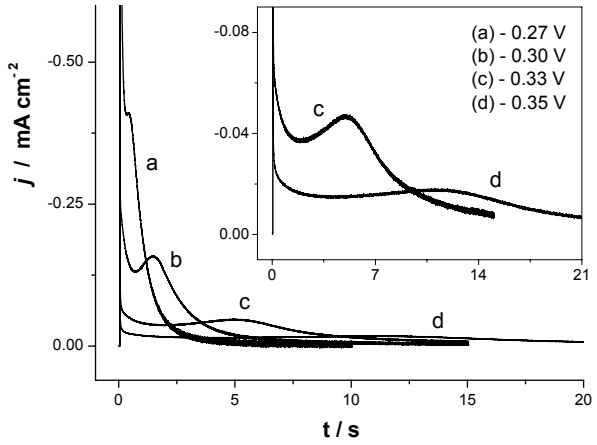

Figure 3.7. Potential step experiments for the electrochemical reduction of saturated NO adlayers on Pt(110) electrode in 0.5 M $HClO_4$. Experimental conditions: E_{in} = 0.5 V, E_{step} is indicated by the numbers in the legend (inset).

Turning now to the chronoamperometric data, Figure 3.7 shows current transients for the reduction of saturated NO adlayers for different step potentials (as shown by the numbers in the inset) in perchloric acid. Most intriguingly, the transients exhibit a maximum, which suggests a non-linear rate law. Significantly, in the time window of the experiments shown in Figure 3.7, the (initially saturated) coverage of NO was reduced to 0.82, 0.63, 0.58, and 0.56 ML for the potential

steps from 0.5 V to 0.35 V, 0.33 V, 0.30 V, and 0.27 V, respectively. This result indicates that the maximum occurs at high (> 0.5 ML) NO coverages, although admittedly the total amount of NO consumed depends on the applied potential as well. Moreover, as shown in Figure 3.8, the maximum appears exclusively for the reduction of a (nearly) saturated adlayer, in which the only species present are NO molecules in atop position.

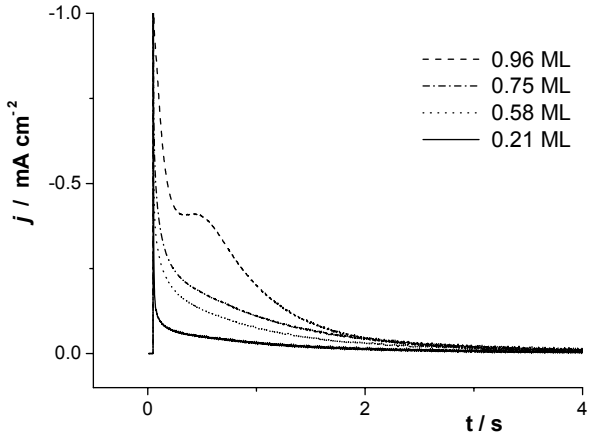

Figure 3.8. (left) Potential step experiments for the electrochemical reduction of a saturated and subsaturated NO adlayers on Pt(110) electrode in 0.5 M $HClO_4$. Numbers in the legend indicate the coverage of NO adlayers (ML). Experimental conditions: E_{in} = 0.5 V, E_{step}= 0.27 V.

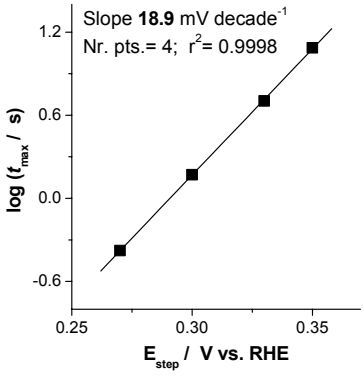

Figure 3.9. (right) The Tafel slope analysis based on the data presented in Figure 3.7. The inset shows the results of the linear regression analysis of the experimental data. Experimental conditions: as in Figure 3.7.

The maximum in the current transients for electrochemical reduction of the saturated NO adlayers on Pt(110) can be understood in terms of the model presented in the subsection 3.3.2. Accordingly, the occurrence of the chronoamperometric maximum at times corresponding to a high NO coverage (higher than 0.5 ML) can be attributed to (i) the second order kinetics of the process and (ii) the effect of considerable lateral (repulsive) interactions (equations 3.14 and 3.15). Indeed, if the lateral interactions would be negligible (equation 3.13) and the reaction would still follow the second-order kinetics, the chronoamperometric maximum would occur at half coverage, which is clearly not the case.

In subsection 3.3.2, it was shown that for the case of second-order kinetics with lateral interactions, a plot of log (t_{max}) vs. E should give the Tafel slope, irrespective of γ. Figure 3.9 presents such a plot. The slope, estimated from the least-square linear regression analysis, is ca. 19 mV decade^{-1}.

3.5. Discussion

We shall begin with discussing the data for NO_{ads} reduction on Pt(110) in perchloric acid. This electrochemical system offers a unique opportunity to look into the mechanism of NO_{ads} reduction. First, the reductive stripping of a NO adlayer is accomplished at potentials at which (i) the hydrogen adsorption is negligible and (ii) the (co)adsorption of other components of the electrolyte (perchlorate, water) should not play an important role. Second, the NO adlayer forms a densely packed layer with coverage of ca. 1 ML, thus leaving virtually no free sites in the first atomic layers. Therefore, the transient response of the system must be governed by NO reduction itself. The remarkably low value of the Tafel slope for reduction of a saturated NO adlayer on Pt(110) (19 mV dec^{-1}) indicates that the first three electron (presumably, electron/proton) transfers are at (quasi)equilibrium:

$$NO_{ads} + H^+ + e^- \leftrightarrows HNO_{ads} \quad (3.18)$$
$$HNO_{ads} + H^+ + e^- \leftrightarrows H_2NO_{ads} \quad (3.19)$$
$$H_2NO_{ads} + H^+ + e^- \leftrightarrows H_2NOH_{ads} \quad (3.20)$$

The HNO and H_2NO intermediates are suggested on the basis of the data and arguments reported elsewhere.[12,34] The value of 19 mV decade^{-1} is reasonably close to both 20 mV decade^{-1}, which would imply that the fourth step is a chemical and the rate-determining step, and 17 mV decade^{-1}, which would imply that the fourth step is an electrochemical and the rate-determining step. Note that for first- and second-order surface-confined reactions, lateral interactions do not affect the Tafel slope, obtained from either voltammetric[22] or chronoamperometric analysis (subsection 3.3.2). Regardless the nature of the forth step (chemical vs. electrochemical), it would be logical to assume that in this step the N–O bond is broken.

The observed second-order kinetics of NO_{ads} reduction on Pt(110) in the limit of high coverage can be explained by the necessity of having a neighboring free site available for breaking the N–O bond. Such a site must have a very low concentration on a well-ordered Pt(110)-(1×1) surface at the (near) saturation coverage of NO (ca. 1 ML), as all the platinum atoms of the topmost layer are

occupied by NO molecules in atop position. Therefore, the reaction would likely be initiated at defect sites. A gradual decrease of the NO coverage would result in gradual increase of the number of free sites and, hence, acceleration of the process, leading to the appearance of a chronoamperometric maximum.

Assuming the chemical rate-determining breaking of N–O bond, the reaction may take the following pathway:

$H_2NOH_{ads} + * \rightarrow H_2N_{ads} + OH_{ads}$	slow	(3.21)
$OH_{ads} + H^+ + e^- \rightarrow H_2O$	fast	(3.22)
$H_2N_{ads} + e^- + 2H^+ \rightarrow NH_4^+$	fast	(3.23)

The OH_{ads} would be unstable in the potential region corresponding to NO reduction on Pt(110) and should be reduced rapidly. Furthermore, taking into consideration that electrochemical reduction of NO adlayers on Pt(110) is accomplished in the potential region corresponding to a negligible amount of adsorbed hydrogen, reduction of the H_2N_{ads} should be an electrochemical step involving protons from solution (reaction 3.23).

Remarkably, the Tafel slope analysis based on the voltammetry measurements gives ca. 40 mV decade^{-1} for features E_1^{110} and E_2^{110} both in perchloric and sulfuric acid solutions.[12] This outcome indicates that the second, electrochemical (combined electron/proton transfer), reaction step is the rate-determining step. At the same time, it is important to recall that the voltammetric peaks occur at half coverage or even lower coverages,[22] whereas, for the system examined, the chronoamperometric maximum occurs at coverages significantly higher than 0.5 ML. Therefore, the two techniques "interrogate" the system under different conditions (coverage), thus providing complementary, and not contradictory, as it may seem, information. Indeed, the switch from second-order kinetics (and a low Tafel slope) for reduction of (nearly) saturated NO adlayer to first-order kinetics (and a higher Tafel slope) for reduction of subsaturated NO adlayers, consistently suggests (i) a change of the rate-determining step with NO coverage and (ii) necessity of a free neighboring site, required likely for breaking the N–O bond. More specifically, at near saturation coverage, N–O bond breaking is rate-determining step on Pt(110), leading to a very low Tafel slope (lower than 20 mV decade^{-1}); at coverages allowing sufficient free sites, the N–O bond breaking is fast and the second electron transfer is rate determining, leading to a Tafel slope of 40 mV decade^{-1}. Finally, note that the existence of two features observed in the voltammetric profile for NO_{ads} reduction on Pt(110) (E_1^{110} and E_2^{110}) is due to differences in reactivity of NO species at different adsorption sites

(see Chapter 2 for details), and not due to existence of different reaction sites, which would, in principle, undermine the above reasoning.

Turning now to the Pt(111) surface, the reduction of a saturated NO adlayer by stepping to 0.1 V (both atop and 3-fold NO species react, Figure 3.5) or to 0.25 V (only atop NO species react, Fig. 3.4) results in an apparent hyperbolic current decay in a wide range of times. Therefore, based on the kinetic models presented in section 3.3, it would be reasonable to invoke (i) important lateral interactions between the reacting species and (ii) (apparent) first-order kinetics in order to explain the hyperbolic current transients observed. At the same time, since ammonia is the main product of the reduction of NO adlayers, the reaction may, in principle, require an ensemble of surface sites, e.g. for breaking the N–O bond. Furthermore, although the initial steps of NO_{ads} reduction on Pt(111) surface are likely to be combined electron/proton transfers,[12] the possibility for the catalytic hydrogenation (Langmuir–Hinshelwood-type) steps occurring at later stages of the reaction cannot be ruled out. These considerations lead us to the following interpretation: because the saturation NO coverage on Pt(111) is significantly lower than on Pt(110) (0.4-0.5 ML on Pt(111) vs. 0.7-1 ML on Pt(110)),[7,12] the eventually required neighboring free site(s) is available at all coverages of NO on (111) terraces, ultimately leading to apparent first-order kinetics.

3.6. Summary and Conclusions

The potential step method was used to investigate the mechanism of the electrochemical reduction of NO adlayers on Pt(111) and Pt(110) surfaces. The experimental current transients were interpreted in terms of a kinetic model in the mean-field approximation with strong lateral interactions.

It was shown that under electrochemical conditions in the limit of high saturation of NO, strong repulsive interactions exist between the reacting species. These interactions have a clear effect on the chronoamperometric response of the systems examined. Accordingly, the current transients for NO reduction on Pt(111) show a hyperbolic (t^{-1}) decay, which indicates (i) first-order kinetics and (ii) strong lateral interactions. For NO_{ads} reduction on Pt(111) surface, the experimentally assessed lateral interaction varies between ca. 0.03 and 0.05 eV.

The apparent reaction order for the reduction of NO adlayers depends on the availability of a neighboring free site and, therefore, NO coverage. More specifically, the current transients for the reductive stripping of saturated NO adlayers on Pt(110) surface (with atop NO as the reactive species) show a potential dependent maximum, occurring at high coverages, which indicates (i) the second-order kinetics and (ii) significant lateral interactions. The second-order kinetics,

observed in the limit of high NO coverage, was attributed to the necessity of a neighboring free site required for breaking the N–O bond. For the reduction of the saturated NO adlayers on Pt(111) surface (with atop NO or/and threefold NO as the reactive species), the apparent first-order kinetics may be tentatively explained by the availability of the required reaction site (sites) at all coverages: the saturation coverage on Pt(111), ca. 0.5 ML, is much lower than that on Pt(110), ca. 1 ML.

References

(1) de Vooys, A. C. A.; Beltramo, G. L.; van Riet, B.; van Veen, J. A. R.; Koper, M. T. M. *Electrochim. Acta* **2004**, *49*, 1307.
(2) Ye, S.; Hattori, H.; Kita, H. *Ber. Bunsen-Ges. Phys. Chem.* **1992**, *73*, 1884.
(3) Ye, S.; Kita, H. *J. Electroanal. Chem.* **1993**, *346*, 489.
(4) Rodes, A.; Gomez, R.; Orts, J. M.; Feliu, J. M.; Perez, A.; Aldaz, A. *J. Electroanal. Chem.* **1993**, *359*, 315.
(5) Rodes, A.; Gomez, R.; Orts, J. M.; Feliu, J. M.; Perez, A.; Aldaz, A. *Langmuir* **1995**, *11*, 3549.
(6) Gomez, R.; Rodes, A.; Orts, J. M.; Feliu, J. M.; Perez, J. M. *Surf. Sci.* **1995**, *342*, L1104.
(7) Rodes, A.; Gomez, R.; Perez, A.; Feliu, J. M.; Aldaz, A. *Electrochim. Acta* **1996**, *41*, 729.
(8) Rodes, A.; Climent, V.; Orts, J. M.; Perez, J. M.; Aldaz, A. *Electrochim. Acta* **1998**, *44*, 1077.
(9) Momoi, K.; Song, M. B.; Ito, M. *J. Electroanal. Chem.* **1999**, *473*, 43.
(10) Zang, Z.-H.; Wu, Z.-L.; Yau, S.-L. *J. Phys. Chem. B* **1999**, *103*, 9624.
(11) Casero, E.; Alonso, C.; Martin-Gago, J. A.; Bogatti, F.; Felici, R.; Renner, R.; Lee, T.; Zegenhagen, J. *Surf. Sci.* **2002**, *507-510*.
(12) Beltramo, G. L.; Koper, M. T. M. *Langmuir* **2003**, *19*, 8907.
(13) Villegas, I.; Gomez, R.; Weaver, M. J. *J. Phys. Chem.* **1995**, *99*, 14832.
(14) Weaver, M. J.; Zou, S.; Tang, C. *J. Chem. Phys.* **1999**, *111*, 368.
(15) Rosca, V.; Beltramo, G. L.; Koper, M. T. M. *Langmuir* **2005**, *21*, 1448.
(16) Gootzen, J. F. E.; van Hardeveld, R. M.; Visscher, W.; van Santen, R. A.; van Veen, J. A. R. *Recl. Trav. Chim. Pays-Bas* **1996**, *115*, 480.
(17) Masel, R. I. *Catal. Rev. -Sci. Eng.* **1986**, *28*, 335.
(18) Egelhoff, W. R. In *The Chemical Physics and Heterogeneous Catalysis*; Woodruff, D. P., Ed.; Elsevier: New-York, 1982; Vol. 4.
(19) Brown, W. A.; Sharma, R. K.; King, D. A. *J. Phys. Chem.* **1998**, *102*, 5303.
(20) Hermse, C. G. M.; Frechard, F.; van Bavel, A. P.; Lukkien, J. J.; Niemantsverdriet, J. W.; van Santen, R. A.; Jansen, A. P. J. *J. Chem. Phys.* **2003**, *118*, 7081.
(21) van Bavel, A. P.; Hermse, C. G. M.; Hopstaken, M. J. P.; Jansen, A. P. J.; Lukkien, J. J.; Hilbers, P. A. J.; Niemantsverdriet, J. W. *Phys. Chem. Chem. Phys.* **2004**, *6*, 1830.
(22) Koper, M. T. M. *Z. Phys. Chem.* **2003**, *217*, 547.
(23) Clavilier, J.; Armand, D.; Sun, S. G.; Petit, M. *J. Electroanal. Chem.* **1986**, *205*, 267.
(24) Lebedeva, N. P.; Koper, M. T. M.; Herrero, E.; Feliu, J. M.; van Santen, R. A. *J. Electroanal. Chem.* **2000**, *487*, 37.
(25) Lebedeva, N. P.; Rodes, A.; Feliu, J. M.; Koper, M. T. M.; van Santen, R. A. *J. Phys. Chem. B* **2002**, *106*, 9863.
(26) Lebedeva, N. P.; Koper, M. T. M.; Feliu, J. M.; van Santen, R. A. *J. Phys. Chem. B* **2002**, *106*, 12938.
(27) Feliu, J. M.; Orts, J. M.; Fernandez-Vega, A.; Aldaz, A.; Clavilier, J. *J. Electroanal. Chem.* **1990**, *296*, 191.

(28) Frumkin, A. N. *Z. Phys.* **1926**, *35*, 792.
(29) Bergelin, M.; Herrero, E.; Feliu, J. M.; Wasberg, M. *J. Electroanal. Chem.* **1999**, *467*, 74.
(30) Matsumoto, M.; Fukutani, K.; Okano, T.; Miyake, K.; Shigekawa, H.; Kato, H.; Okuyama, H.; Kawai, M. *Surf. Sci.* **2000**, *454-456*, 101.
(31) Matsumoto, M.; Tatsumi, T.; Fukutani, K.; Okano, T. *Surf. Sci.* **2002**, *513*, 485.
(32) Aizawa, H.; Morikawa, Y.; Tsuneyuki, S.; Fukutani, K.; Ohno, T. *Surf. Sci.* **2002**, *514*, 394.
(33) Zhu, J. F.; Kinne, M.; Fuhrmann, T.; Denecke, R.; Steinruck, H.-P. *Surf. Sci.* **2003**, *529*, 384.
(34) Rosca, V.; Beltramo, G. L.; Koper, M. T. M. *J. Phys. Chem. B* **2004**, *108*, 8294.

4

Mechanism of electrocatalytic reduction of nitric oxide on Pt(100) surface

Abstract

The mechanism of electrocatalytic reduction of nitric oxide on Pt(100)-(1×1) in acidic media has been studied using voltammetry and in situ infrared spectroscopy and considering the effect of surface defects, NO coverage, and the nature of the supporting electrolyte (sulfate vs perchlorate). The adsorption of nitric oxide on Pt(100) results in the formation of an adlayer with a structure similar to that formed under ultra-high vacuum (UHV) conditions. Ammonia was shown to be the product of NO_{ads} reduction on Pt(100). The saturation coverage of NO adsorbate on Pt(100) was found to be around 0.5 monolayers (ML), in agreement with previous UHV and electrochemical studies. Two features observed in the voltammetric profile for the electrocatalytic reduction of saturated and subsaturated NO adlayers were tentatively ascribed to reactions of NO species having different reactivity. The Tafel slope analysis of these voltammetric features gives values of ca. 60 mV $decade^{-1}$. This value was interpreted in terms of an EC mechanism, in which the first electron/proton transfer is at equilibrium, resulting in the formation of HNO_{ads} intermediate, whereas the second reaction step is a chemical and the rate-determining step. This chemical step is assumed to involve the N–O bond breaking in the HNO_{ads} intermediate, which most probably requires a free neighboring site. From a comparison of NO_{ads} reduction on Pt(100), Pt(111), and Pt(110) it follows that (i) the reaction mechanism is structure sensitive and (ii) Pt(100) is the most active surface for breaking the N–O bond, which is in agreement with the trend observed under UHV conditions.

This chapter is based on article by V. Rosca and M.T.M. Koper, published in Journal of Physical Chemistry B, 109 (2005) 16750.

4.1. Introduction

Adsorption and reactions of nitric oxide on transition metal surfaces in an electrochemical environment are of considerable practical importance, mainly in connection with the industrial synthesis of hydroxylamine as well as with environmentally important removal of nitrate, nitrite, and nitric oxide itself. Nitric oxide adsorbs strongly on transition metals and is a key intermediate in many electrochemical transformations of inorganic nitrogen-containing compounds.[1] From a fundamental point of view, reactions of NO on single-crystal transition metal surfaces, particularly NO reduction, are attractive for carrying out model studies in heterogeneous electrocatalysis as well as for comparing reactions at the metal–gas and metal–liquid interface.

Adsorption and electrochemical transformations of NO on single-crystal platinum surfaces, as well as on other transition metal surfaces, have been intensively studied in recent years.[2-18] These studies resulted in a significant insight into the structure and reactivity of NO adlayers, as compared to earlier studies on polycrystalline platinum.[19]

In a recent detailed voltammetric study on Pt(111), Pt(110) and a series of stepped Pt[n(111)×(111)] electrodes, it was shown that the reductive stripping of NO adlayers shows little structure sensitivity, mainly manifested in differences in the voltammetric profile for NO_{ads} stripping. The conclusion regarding the apparent structure insensitivity of the reductive stripping of NO adlayers was also supported by the 40 mV decade^{-1} Tafel slopes obtained on different surfaces, which was interpreted in terms of the following EE mechanism[16] :

$NO_{ads} + H^+ + e^- \leftrightarrows HNO_{ads}$	equilibrium	(4.1)
$HNO_{ads} + H^+ + e^- \rightarrow H_2NO_{ads}$	rds	(4.2)
$H_2NO_{ads} + 4H^+ + 3\ e^- \rightarrow NH_4^+ + H_2O$	fast	(4.3)

Most importantly, the first two steps of the reaction are assumed to be combined proton-electron transfers, involving hydronium ions from solution. In agreement with the latter assumption, NO_{ads} reduction on Pt(110) (and partly on Pt(111)) occurs at potentials at which the hydrogen coverage is negligible. Additionally, the reductive stripping of NO adlayers on polycrystalline platinum shows a pH dependence that complies with the electrochemical mechanism of NO_{ads} hydrogenation.[20] Note that in mechanism (4.1-4.3), N–O bond breaking occurs after the rate-determining step.

The features observed in the voltammetric profile for NO_{ads} reduction were shown to relate to the different reactivity of NO_{ads} species with different surface

coordination (i.e., atop, bridge, 3-fold-hollow), and not to different (consecutive) steps of an overall process.[17] For more details, see Chapter 2.

Chronoamperometric analysis of NO_{ads} reduction on Pt(111) (at all coverages) and Pt(110) (at subsaturation coverages) pointed to important lateral (repulsive) interactions between reacting NO species and the apparent first-order kinetics of the overall process.[18] From chronoamperometric reduction of a (nearly) saturated NO adlayer on Pt(110) in perchloric acid (NO coverage of ca. 1 monolayer (ML)), however, we deduced second-order kinetics and a very low Tafel slope of ca. 19 mV decade^{-1} (implying that the first three electron/proton transfers are at equilibrium). The second-order kinetics was interpreted in terms of the necessity of a free neighboring site for breaking the N–O bond, which is only scarcely available at high initial coverage. For more details, see Chapter 3.

The above results make a detailed examination of the mechanism of NO reduction on Pt(100) particularly interesting. In ultra-high vacuum (UHV), NO has been reported to adsorb in only one position: a site between bridge and atop sites.[21,22] Furthermore, Pt(100) surface is known to be exceptionally active for breaking the N–O bond under UHV conditions,[23] in contrast to Pt(111) and Pt(110). One would expect these factors to be reflected in the kinetics of NO_{ads} reduction on Pt(100) in an electrochemical environment as well.

The adsorption and electrochemical reactions of NO on Pt(100) have been recently addressed in a number studies.[2,4,5,7,8,24] The NO adsorption on Pt(100) under electrochemical conditions was shown to be quite similar to NO adsorption under UHV conditions, as deduced from in situ infrared measurements.[10] Most noticeable from a mechanistic point of view is the study by Rodes et al.,[8] who investigated NO adsorption and reactivity in acidic, neutral, and alkaline media. The authors suggested ammonia as the main product of NO_{ads} reduction on Pt(100). However, a detailed mechanism for the electrocatalytic reduction of NO_{ads} on Pt(100) was not proposed. The electrooxidation of NO_{ads} was shown to give various products, depending on pH. From a charge analysis applied to the reductive voltammetry of saturated NO adlayers in acidic media, the saturation coverage of nitric oxide was estimated to be ca. 0.5 ML.

This chapter describes the results of a combined voltammetric and in situ infrared study of the electrocatalytic reduction of NO_{ads} on the Pt(100)-(1×1) surface. The aim was formulating a mechanism for NO_{ads} reduction at this surface, including the effect of anion (co)adsorption, surface defects and coverage. This chapter also provides a comparison of the electrocatalytic reduction of NO_{ads} on Pt(100) with that on the other two low-index surfaces – Pt(111) and Pt(110).

4.2. Experimental Section

The H_2SO_4 and $HClO_4$ working solutions were prepared from their respective concentrated acids ("Suprapur", Merck) and ultrapure water (Millipore MilliQ system, 18.2 MΩ cm, less than 3 ppb total organic carbon) or doubly distilled deuterium oxide ("Uvasol", Merck, deuteration degree min. 99.9%).

Two types of single-crystal platinum electrodes were used. Bead-type single-crystal platinum electrodes, prepared by Clavilier's method[25], were used for most of the electrochemical measurements. For in-situ infrared measurements, commercial platinum disk electrodes of 10 mm diameter were used (oriented within 1°, Surface Preparation Laboratory, Zaandam, The Netherlands). Before each experiment, the working electrode was flame-annealed, cooled to room temperature in an $Ar:H_2$ (3:1) gas mixture and transferred to the electrochemical cell under the protection of a droplet of deoxygenated ultrapure water.

Electrochemical measurements were performed in a single-compartment three-electrode glass cell, using a computer-controlled potentiostat (AutoLab-PGSTAT20, Eco Chemie, Utrecht, The Netherlands). The cell contained a small movable glass spoon[26], which contained a diluted $NaNO_2$ (ca. 0.1 mM in 0.1 M perchloric or sulfuric acid) solution. Immersion of the working electrode in the nitrite-containing solution results in formation of a subsaturated or a saturated (depending on the immersion time) NO adlayer.[2] This procedure allows NO dosing under an inert (argon) atmosphere at open circuit potential and, thus, avoids the use of gaseous NO. In the case of in situ infrared experiments, NO adlayers were generated in a similar way: immersion of the working electrode in a separate solution of nitrite was followed by washing of the electrode with doubly distilled deuterium oxide and subsequent transfer of the electrode to the spectroelectrochemical cell. The cell and the other glassware were cleaned by boiling in a 1:1 mixture of concentrated nitric and sulfuric acid, followed by repeated boiling with ultrapure water. A coiled platinum wire served as counter electrode. In $HClO_4$ solutions, the reference electrode was an internal reversible hydrogen electrode (RHE). In H_2SO_4 solutions a saturated mercury-mercury sulfate ($Hg|Hg_2SO_4|K_2SO_{4\,(sat)}$) electrode, connected via a Luggin capillary, was used as a reference. However, all potentials are quoted versus the RHE. Before each experiment, all solutions were deoxygenated by purging with pure (N50) argon.

The in situ Fourier transform infrared reflection-absorption spectroscopy (FTIRRAS) measurements were performed under external reflection conditions. The Fourier-transform infrared spectrometer was a Brüker IFS113V, equipped with a narrow-band MCT detector. The design of the spectroelectrochemical cell closely resembles that described elsewhere.[27] The cell featured a prismatic CaF_2 transmission window beveled at 60°. Five hundred interferograms were collected at each potential. The spectral resolution was 8 cm^{-1}. The reflectance spectra were calculated as $(R - R_0)/R_0$, where R and R_0 are the reflectance at the sample and the reference potential respectively. Therefore, the $(R - R_0)/R_0$ ratio gives negative bands for species that are formed and positive bands for species that are consumed at the sample potential, as compared to the reference potential.

The surface order and cleanliness of the working electrodes were checked before each experiment by recording the so-called blank cyclic voltammograms and their comparison to the standard voltammetric profile for the Pt(100)-(1×1) surface reported elsewhere.[28-30]

4.3. Electrocatalytic reduction of adsorbed nitric oxide

4.3.1. Stripping voltammetry of saturated NO adlayers

Figure 4.1 illustrates the electrochemical reactions of a saturated NO adlayer on Pt(100) surface in sulfuric acid. The saturated NO adlayer is electrochemically stable in a wide potential region between ca. 0.3 and 0.9 V. In this range of potentials the voltammetric profile shows very low (charging) current densities. At the same time, the hydrogen and the (bi)sulfate adsorption/desorption states in the 0.3-0.45 V region (dotted line) are essentially blocked. The voltammetric profile for the reductive stripping of a saturated NO adlayer (bold solid line) contains two characteristic features: a sharp peak E_{R3}^{100}at ca. 0.26 V and a shoulder E_{R4}^{100} at more negative potentials. In perchloric acid (Figure 4.2), the voltammetric profile for the reductive stripping of a saturated NO adlayer is virtually identical to that in sulfuric acid, thus indicating no effect of anion (co)adsorption.

The saturated NO adlayers can be oxidized reversibly (solid line, peaks E_{O2}^{100} and E_{R2}^{100}) both in sulfuric and in perchloric acid, provided the upper potential limit is not higher than 1.1 V and the potential scan rate is not lower than 5 mV s^{-1}. Although chemically reversible, the electrochemical oxidation of a saturated NO adlayer seems to be a complex process: the in situ infrared data by Rodes et al.[8] suggest that in acidic media the oxidized NO adlayer consists of a mixture of adsorbed nitrito and nitro species, while in alkaline media dissolved nitrite appears to be the main product.

4.3.2. Products of reduction of adsorbed NO

Continuous reduction of NO at polycrystalline platinum in acidic solutions yields nitrous oxide (and molecular nitrogen) at moderately reductive potentials, whereas at highly reductive potentials hydroxylamine and ammonia are the products.[19] Importantly, the presence of NO in solution is necessary for the formation of nitrous oxide (and molecular nitrogen) and, therefore, is crucial for N–N condensation.[20] As for the products of NO_{ads} reduction on Pt(100), formation of nitrous oxide may be ruled out, as the in situ infrared data on the reduction of NO_{ads} shows no sign of the formation of nitrous oxide (the N–O and N–N stretching modes at ca. 1285 cm^{-1} and ca. 2230 cm^{-1}, respectively), which is in

agreement with the above mechanism. Furthermore, the on-line mass spectrometry data presented in Chapter 5 show no formation of any gaseous products for the reductive stripping of a saturated NO adlayer (Figure 5.12). Rodes et al.[8] provided spectroscopic data, which strongly suggested ammonia as the main product of NO_{ads} reduction, although not sufficient for ruling out the formation of some hydroxylamine. These authors did not observe N_2O formation in their FTIR experiments. Furthermore, the reductive stripping of a saturated or subsaturated NO adlayer at a sufficiently low scan rate (10 mV s^{-1} or lower) results in a complete recovery of the blank voltammogram, as deduced from the subsequent positive going scan (see, for example, Figure 4.3). This excludes formation of considerable amounts of an electrochemically active product, that is, hydroxylamine. Pulling these arguments together, ammonia is indeed the main product of the reductive stripping of NO adlayers on Pt(100), similarly to NO_{ads} reduction on Pt(111) and Pt(110).[17]

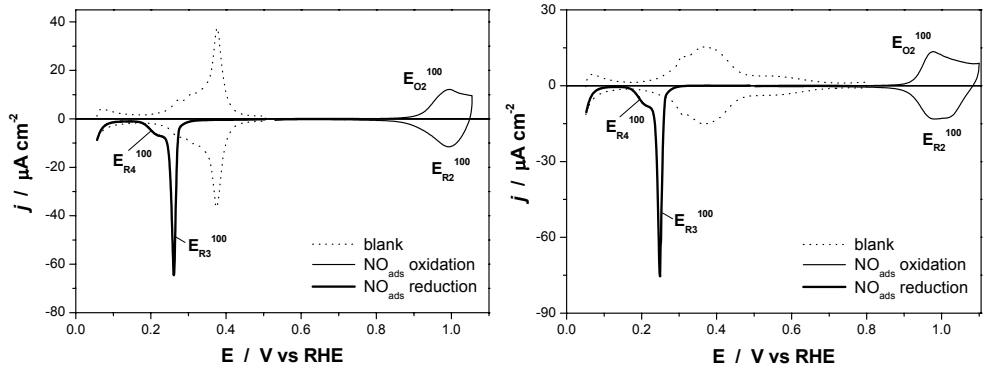

Figure 4.1. (left) Voltammetry of nitric oxide adlayers on Pt(100) in 0.5 M H_2SO_4. Bold solid line – reductive stripping of a saturated NO adlayer (at 2 mV s^{-1}). Solid line – reversible oxidation of a saturated NO adlayer (at 10 mV s^{-1}). Dotted line – Pt(100)-(1×1) blank voltammetry at 10 mV s^{-1}.

Figure 4.2. (right) Voltammetry of nitric oxide adlayers on Pt(100) in 0.5 M $HClO_4$. Bold solid line – reductive stripping of a saturated NO adlayer (at 2 mV s^{-1}). Solid line – reversible oxidation of a saturated NO adlayer (at 10 mV s^{-1}). Dotted line – Pt(100)-(1×1) blank voltammetry at 10 mV s^{-1}.

4.3.3. NO coverage and its effect on voltammetric response

The coverage of the saturated NO adlayer, estimated from a charge analysis proposed elsewhere[4] and assuming ammonia as the main product, lies between ca. 0.5 and 0.52 ML both in sulfuric and in perchloric acid. The experimental

reduction charge for the stripping of saturated NO adlayers gives values between 710 and 740 μC cm^{-2} (before correction for hydrogen adsorption) for integration between 0.5 and 0.1 V. These values of the reduction charge and the corresponding coverage values agree well with estimations by other authors.[4,7,8] The value of ca. 0.5 ML for the saturation coverage of NO under electrochemical conditions would coincide with the value for NO saturation coverage on Pt(100)-(1×1) surface under UHV conditions, as reported by different groups.[21,22,31] In more recent UHV studies, lower values for the NO saturation coverage were reported, particularly in connection with the possibility of NO dissociation even at room temperature.[32-34] The issue of NO dissociation under UHV and electrochemical conditions and the related issue of the saturation coverage and the structure of NO adlayer are addressed in some detail in the Discussion.

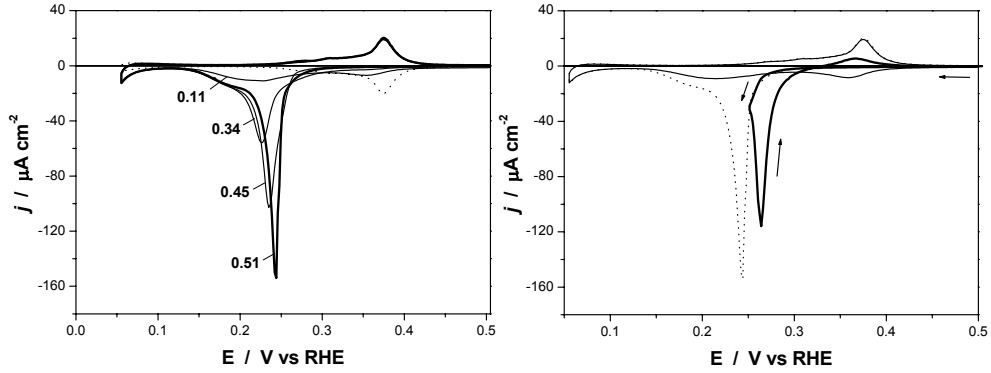

Figure 4.3. (left) The effect of NO coverage on the voltammetric profile for the reductive stripping of NO adlayers. Experimental conditions: 0.5 M H_2SO_4; starting potential 0.5 V; potential scan rate 5 mV s^{-1}. Numbers indicate the corresponding NO coverage. The dotted line represents the blank voltammetry of the Pt(100) surface.

Figure 4.4. (right) Partial stripping of a saturated NO adlayer (bold solid line) and the voltammetric profile recorded in the subsequent potential cycle (solid line). The dotted line represents the voltammetric profile for a complete stripping of a saturated NO adlayer. Experimental conditions: 0.5 M H_2SO_4; starting potential 0.5 V; potential scan rate 5 mV s^{-1}.

Figure 4.3 shows the effect of the initial NO_{ads} coverage on the voltammetric profile for the reductive stripping of nitric oxide adlayers in sulfuric acid. In perchloric acid, the effect of the initial NO coverage is quite similar (data not shown). Decrease of the initial coverage brings about a slight positive shift and attenuation of the main peak position (E_{R3}^{100}), while feature E_{R4}^{100} seems to remain unchanged at moderate to high coverages. Note that at subsaturation coverage, the

reduction of NO adsorbate seems to start slightly (ca. 50 mV) more positively. The voltammetric profile corresponding to the reductive stripping of ca. 0.1 ML of NO_{ads} exhibits only one broad feature in the potential region between ca. 0.3 and 0.15 V.

The voltammetric profile corresponding to the reductive stripping of a saturated NO adlayer can be represented reasonably well as a combination of two overlapping Voigtian peaks. The ratio of the area (charge) under the sharp peak E_{R3}^{100} and that under the broad feature E_{R4}^{100} (Q_{R3}/Q_{R4}) changes from ca. 2:1 at saturation to ca. 1:1 at ca. 0.34 ML, thus indicating an apparent attenuation of feature E_{R3}^{100} and not of feature E_{R4}^{100} with decreasing coverage in the 0.5-0.3 ML range.

The above data suggest that the reduction features E_{R3}^{100} and E_{R4}^{100} can be tentatively ascribed to the reduction of NO adsorbates having different reactivity, rather than to consecutive steps of the same reaction. We shall return to this issue again when discussing the results of the Tafel slope analysis of the two reduction features.

Figure 4.4 shows results corresponding to partial stripping of a saturated NO adlayer. In this experiment, the first, negative-going, run was reversed at ca. 0.26 V (the bold solid line). The subsequent positive-going scan shows a reduction peak at potentials ca. 50 mV more positive than it should have appeared if the potential run was not reversed (compare the bold solid line and the dotted line). First, this result seem to be in good agreement with the autocatalytic nature of NO reduction on Pt(100) known from the UHV studies.[35] Second, the strong hysteresis observed also indicates that the NO reaction on platinum is chemically irreversible at the initial stages of the reaction. Note that such a hysteresis was not observed for partial stripping of NO adlayers on Pt(111) and Pt(110).[17]

4.3.4. Effect of surface defects

To elucidate the effect of the surface defects, we have examined the reductive stripping of the saturated NO adlayers at Pt(100) electrode with different degrees of the surface order. The order of the electrode surface can be assessed from the blank voltammetry. The cyclic voltammogram corresponding to a well-ordered Pt(100)-(1×1) surface in contact with sulfuric acid is shown in Figure 4.1 (the dotted line), as deduced from combined voltammetric and LEED[30] or STM[36] studies. More specifically, the magnitude of the peak at ca. 0.38 V is a measure of the long-range order of the surface.[30,37] In our experiments, the height of this peak was typically 200 μA cm^{-2} or higher for the cyclic voltammetry measurements at 50 mV s^{-1}. The surface defects appear for an electrode cooled in air or even in

presence of traces of oxygen (see Figure 4.5. for an example),[38] or can be generated by the potentiodynamic cycling[28] (see also Figure 4.6 and its caption for details). The development of defects is reflected in a substantial current increase in the 0.05-0.25 V range, which seems to indicate increasing contribution from (111) sites, and a decrease of the adsorption state around 0.38 V. The sharp peaks at ca. 0.28 V (Figure 4.6) should relate mainly to (100)×(111) step defects.[30,37]

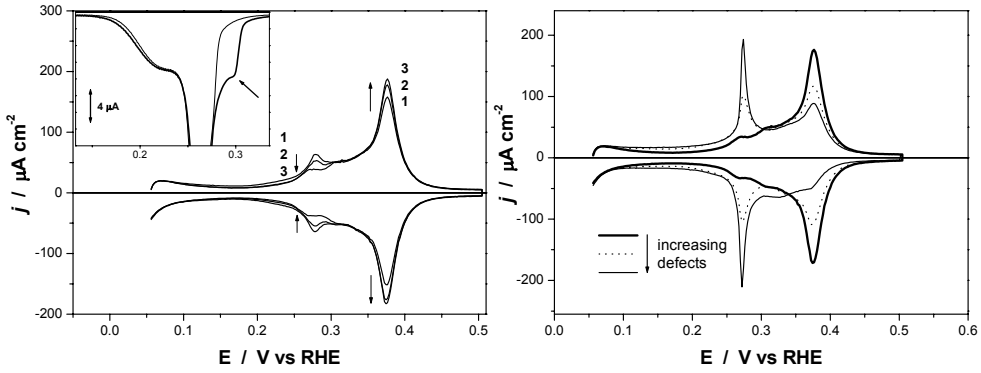

Figure 4.5. (left) The effect of repeated consecutive deposition and reductive stripping of the saturated NO adlayers on the blank voltammetry of Pt(100). Curve 1 corresponds to the initial blank voltammetry. Curves 2 and 3 correspond to the Pt(100) blank voltammogram recorded after the 1st and 3rd cycle of deposition and reductive stripping (at 2 mV s^{-1}) of saturated NO adlayers. Experimental conditions: 0.5 M H_2SO_4; potential scan rate 50 mV s^{-1}. The inset shows the voltammetry of the 1st (bold solid line) and the 3rd (solid line) NO adlayer stripping at 2 mV s^{-1}.

Figure 4.6. (right) Blank cyclic voltammetry of Pt(100)-(1×1) surface (bold solid line) as compared to disordered Pt(100) surfaces. Dotted and solid lines correspond to the cyclic voltammograms resulted from an initially well-ordered surface after 15 and 50 potential cycles, respectively, between 0.06 and 0.9 V at 20 mV s^{-1}.

Turning now to the effect of the surface defects on the reduction of NO_{ads}, the presence of a small number of the defect sites, which give rise to the pair of peaks at ca. 0.28 V (Figure 4.5), is reflected in the appearance of a pre-shoulder to the main peak of the NO_{ads} stripping (see the inset of Figure 4.5). Figure 4.6 shows the blank CVs for a well-ordered Pt(100)-(1×1) (bold solid line) as compared to Pt(100) surfaces with a different level of the surface disorder. Figure 4.7 illustrates the stripping voltammetry of saturated NO adlayers from those surfaces. Most noticeably, the sharp peak E_{R3}^{100} shifts toward positive potentials and loses its intensity with shoulders evolving at negative and positive potentials. The surface

defect sites appear to be more active sites for NO reduction, as compared to the sites on the (100) terrace, although the effect is quite moderate.

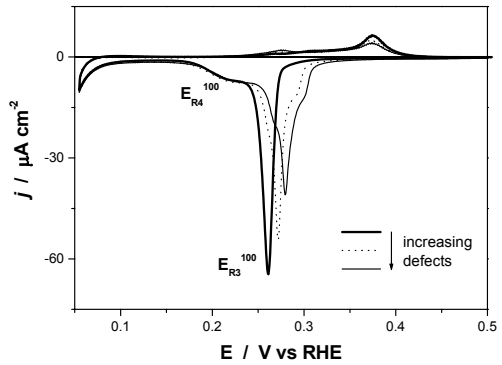

Figure 4.7. Stripping voltammetry for the electrochemical reduction of saturated nitric oxide adlayers on Pt(100) with different degree of the surface disorder. Experimental conditions: 0.5 M H_2SO_4; starting potential 0.5 V; potential scan rate 2 mV s^{-1}. The corresponding initial blank voltammetric profiles are presented in Figure 6.

Remarkably, consecutive deposition and stripping of the saturated NO adlayer result in a gradual decrease of the current contribution around 0.28 V and simultaneous increase of the intensity of the peaks at ca. 0.38 V in the blank voltammetry, which are characteristic for the adsorption/desorption processes on (100) terraces (Figure 4.5). Moreover, NO adsorption and reductive stripping bring about a considerable ordering, although not a complete recovery, of even strongly disordered Pt(100) surfaces, such as the surfaces voltammograms of which are shown in Figure 4.6. This result indicates that NO adsorption and/or NO reductive stripping can effectively extend the (100)-(1×1) domains at the expense of certain surface defects, apparently (100)×(111) step sites. This apparent smoothening of the surface can be tentatively assigned to the quasi-hexagonal reconstruction of small (1×1) domains (islands) (although, unlikely the extended (100) terraces) on the surface and the subsequent lifting of the reconstructed domains by NO adsorption, resulted in formation of more extended (1×1) domains.

4.3.5. Tafel slope analysis

Figure 4.8 shows the results of the Tafel slope analysis of the reduction features E_{R3}^{100} and E_{R4}^{100} in perchloric (A) and sulfuric acid (B), respectively. As shown elsewhere,[39,40] the peak position (E_p) versus logarithm of the scan rate (v)

graph allows determination of the Tafel slope for surface-confined processes, both for first- and for second-order kinetics. The peak position of the feature E_{R4}^{100} was obtained from deconvolution of the voltammetric profile corresponding to the reductive stripping of a saturated NO adlayer into two Voigtians. In the scan rate region between approximately 1 and 20 mV s^{-1}, the E_p – log(v) dependences for the reduction peaks E_{R3}^{100} and E_{R4}^{100} show good linearity for experiments in both sulfuric and perchloric acid, with Tafel slopes close to 60 mV $decade^{-1}$. At higher scan rates, the two features overlap even stronger and there is a clear deviation from the initial linearity of the E_p – log(v) dependence. Interestingly, for experiments in perchloric acid we could observe an apparent recovery of the linearity and the slope at higher scan rates (50-100 mV s^{-1}), although only one reduction peak is observed. As an important observation, the reduction features E_{R3}^{100} and E_{R4}^{100} show similar Tafel slopes, which would rather favor the assumption that these features are related to the reduction of adsorbed NO species having somewhat different reactivity and not to consecutive steps of an overall process.

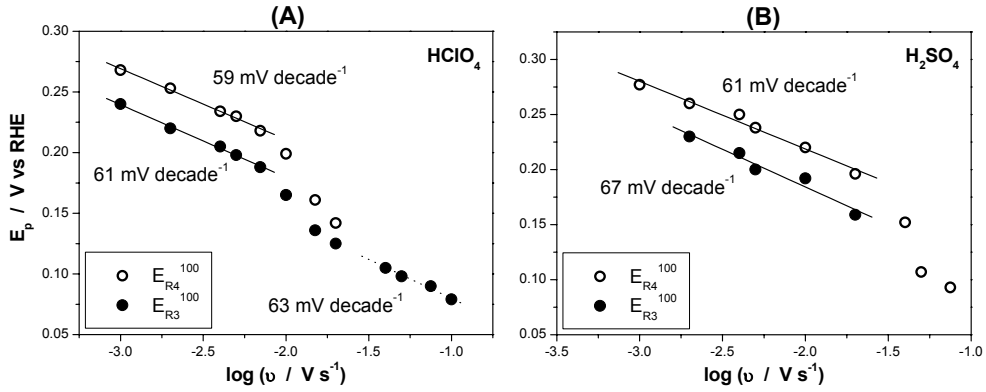

Figure 4.8. Tafel slope analysis of the voltammetric features E_{R3} and E_{R4} in perchloric (A) and sulfuric (B) acid. Experimental conditions: 0.5 M $HClO_4$ or 0.5 M H_2SO_4; saturated NO adlayer; starting potential 0.5 V. The numbers indicate the slope of the corresponding least-square linear regression lines.

4.3.6. In situ FTIR measurements

Figure 4.9 contains the potential difference spectra for the reductive stripping of a saturated NO adlayer on Pt(100). The experiment was started with a saturated NO adlayer at 0.5 V, a potential at which NO_{ads} is (electro)chemically stable. Significantly, the potential-dependent band centered between ca. 1620 and

1590 cm^{-1} (N–O stretching mode in NO_{ads} in a position between atop and bridge sites[22]) is not observed at potentials lower than ca. 0.3 V. This does not necessarily mean that there is no NO_{ads} left on the surface: some NO molecules may be still present, but either at a too low coverage to be detected or with an altered orientation, for example, by adopting a configuration similar to the theoretically predicted "side-on" configuration.[41] Note that the broad potential-independent band at ca. 1465 cm^{-1} is most probably related to a solution species – a product of NO_{ads} reduction. (We identify these species as ammonium cations, containing H and D atoms in different ratios. For details on the origin of this feature see reference 17.) Accordingly, this feature does not show any significant evolution in the potential region in which NO_{ads} is stable. In the potential region in which NO_{ads} is reduced (ca. 0.35-0.20 V), absorption around 1465 cm^{-1} increases with decreasing the potential, corresponding to accumulation of a solution species. This result also indicates that, in agreement with voltammetric results, reduction of all NO_{ads} species requires a potential as low as ca. 0.2 V.

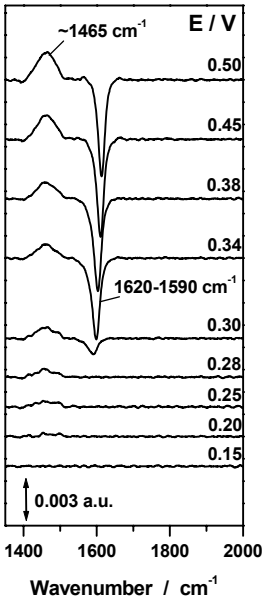

Figure 4.9. The potential-difference infrared spectra for the electrochemical reduction of a saturated NO adlayer on Pt(100). Experimental conditions: 0.1 M $HClO_4$ (in D_2O), p-polarized light, reference potential 0.1 V.

4.4. Discussion

4.4.1. Saturation coverage and structure of NO adlayer

Studies of NO adsorption on Pt(100) surface under UHV conditions are complicated by a high activity of this surface toward NO dissociation.[23] This high activity is one of the major factors determining the uncertainty in assessing the NO saturation coverage and the structure of NO adlayer on Pt(100) in UHV at room temperature. In early UHV studies of NO adsorption on Pt(100), it was generally accepted that at room temperature NO adsorbs molecularly and that the dissociation of NO takes place at temperatures well above 300 K. Although the possibility of NO dissociation on Pt(100) at room temperature was repeatedly

suggested,[32-34] this process seems to be quite sluggish (on the order of tens of minutes[42]).

The saturation coverage of 0.5 ML and a *c*(2×4) overlayer structure (Figure 4.10A) seem to account well for the LEED,[43] vibrational,[21,22] and the adsorption calorimetric[31] data for NO adsorption on Pt(100) at room temperature. A somewhat lower coverage (ca. 0.4 ML) for the saturation NO adlayer at room temperature was reported by Zemlyanov et al.[44,45] in their combined EELS and TPD studies of NO adsorption and reduction on Pt(100); the authors did not address the structure of the adlayer. More recently, in an STM study, Song et al.[33] proposed a simple *c*(2×4) overlayer structure corresponding to a coverage of 0.25 ML for the saturation NO adlayer on Pt(100) at 300 K (Figure 4.10B). Rienks et al.[34] showed in their synchrotron XPS study that in the temperature range between 250 and 325 K both molecular and dissociative adsorption of NO takes place.

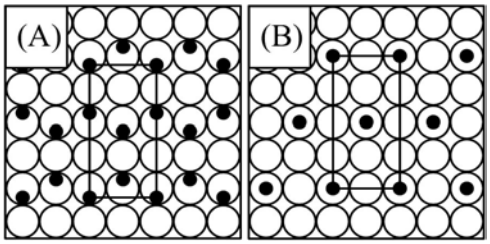

Figure 4.10. Structural models for saturated NO adlayer on Pt(100)-(1×1). Panel A shows a *c*(2×4) overlayer structure with 0.5 ML coverage, proposed by Yeo et al. (ref. 31) as a development of earlier models (refs. 43 and 22). Panel B shows a simple *c*(2×4) overlayer structure with 0.25 ML coverage, as proposed by Song et al. (ref. 33).

Turning to the coverage estimation under electrochemical conditions, the charge analysis of the stripping voltammetry of the saturated NO adlayer gives a coverage of ca. 0.5 ML, assuming ammonia as the only product of NO_{ads} reduction. This value would be consistent with the formation of a *c*(2×4) overlayer structure (or whatever the structure of the saturated adlayer is) under electrochemical conditions as well, as proposed in earlier in situ electrochemical studies.[7,8] The resemblance of the infrared spectra recorded for NO adsorbed on Pt(100) under electrochemical and UHV conditions at room temperature[10,17] supports the assumption of the structural similarity. As an indication of the stability of the molecularly adsorbed NO species, the voltammograms for Pt(100) covered with a saturated NO adlayer show very low and stable (charging) current in a wide potential region between ca. 0.9 and 0.3 V. The "direct" dissociation of NO molecules would result in the formation of adsorbed oxygen-containing species,

which would not be stable in the above potential region and would show significant faradaic currents. All together, our experimental data as well as the considerations given above confirm that in an electrochemical environment (acidic media) the NO species are adsorbed molecularly on Pt(100) and the NO saturation coverage is ca. 0.5 ML.

4.4.2. Mechanism of reduction of NO_{ads} on Pt(100)

The Tafel slope analysis of the reduction features E_{R3}^{100} and E_{R4}^{100} (Figure 4.8), corresponding to the reductive stripping of a saturated NO adlayer, gives a good linearity of the E_p–log(v) dependence. The slopes for both features are close to the theoretical value of 60 mV decade^{-1}, irrespective of the anion (sulfate vs perchlorate). This result indicates that both features correspond to an electrochemical process, in which the first electron (likely accompanied by a proton transfer) is fast (at equilibrium), while the second step is a chemical and rate-determining step. Because the reduction of NO_{ads} on Pt(100) seems to become chemically irreversible at an early stage of the process (Figure 4.4 and the corresponding discussions) and the breaking of the N–O bond is expected to be facile on Pt(100), we propose the following mechanism for NO_{ads} reduction:

$NO_{ads} + e^- + H^+ \leftrightarrows HNO_{ads}$	equilibrium	(4.4)
$HNO_{ads} + * \rightarrow HN_{ads} + O_{ads}$	slow	(4.5)
$HN_{ads} + 2\,e^- + 3H^+ \rightarrow NH_4^+ + *$	fast	(4.6)
$O_{ads} + 2e^- + 2H^+ \rightarrow H_2O + *$	fast	(4.7)

The overall reaction would then be:

$$NO_{ads} + 5e^- + 6H^+ + * \rightarrow NH_4^+ + H_2O + 2* \qquad (4.8)$$

Most importantly, we assume here that, similarly to NO reduction in UHV, breaking of the N–O bond (in HNO_{ads}) requires an adjacent free site (designated as *). The reason HNO and not NOH is suggested as the first intermediate is that gas phase HNO is about 100 kJ mol^{-1} more stable than gas phase NOH,[20] although their stability at the surface is admittedly unknown. Interestingly, Zemlyanov et al.,[46] in their combined TPR and HREELS studies, have pointed to the formation of HN_{ads} and H_2N_{ads} species during NO_{ads} reduction on Pt(100)-(1×1) at 300 K. Smirnov et al.[47] claimed the existence of chemisorbed HNO during the coadsorption of NO and H on Pt(111) from HREELS experiments. Reactions 4.6 and 4.7 are complex processes, which likely involve fast electron/proton transfers. On the other hand,

these reactions may still involve catalytic hydrogenation steps, as the electrochemical reduction of NO adlayers occurs at potentials corresponding to significant hydrogen coverage.

4.4.3. Comparison of the mechanism of NO_{ads} reduction on Pt(100), Pt(111), and Pt(110)

The voltammetric features observed in the voltammetric profile for NO_{ads} reduction on Pt(111) and Pt(110) are determined by reaction of NO_{ads} species having different coordination, as discerned from in situ infrared measurements.[17] Similar analysis is less conclusive for NO_{ads} reduction on Pt(100). Note that (HR)EELS studies[21,46] as well as FTIR[22] studies under UHV conditions (room temperature) indicate a single N–O stretching frequency of NO_{ads} on Pt(100)-(1×1) surface (1600-1640 cm^{-1} region), thus pointing to a single NO adsorption site on (100) terraces at saturation. This adsorption site is usually identified as a position between atop and bridge site, as shown in Figure 4.10A. In an electrochemical environment, adsorbed NO is also characterized by a single N–O stretching band in the 1590-1620 cm^{-1} range of frequencies, which, however, is not observed at potentials lower than ca. 0.3 V (Figure 4.9). Therefore, the two features observed in voltammetric profile for reduction of a saturated NO adlayer cannot not be straightforwardly ascribed to the reaction of NO species having different coordination, which is in contrast to NO_{ads} reduction on Pt(111) and Pt(110).

At the same time, it is important to realize that at saturation coverage a simultaneous reaction of all NO molecules on Pt(100) under UHV conditions or in an electrochemical environmental is very unlikely. This aspect is related to the necessity of a free site for breaking the N–O bond under UHV conditions and assumedly in an electrochemical environment. Therefore, we should consider the possibility of formation of a quasi-stable surface configurations formed by subsaturated NO adlayer and coadsorbed hydrogen. Existence of such a configuration would imply a different reaction environment and possibly different adsorption geometry for NO adsorbate and, thus, could give rise to a second reduction feature.

Comparing the mechanisms of the electrocatalytic reduction of NO_{ads} on Pt(111), Pt(110),[16,18] and Pt(100) (present work), the process appears to be mechanistically structure sensitive, although the main product is the same at all three surfaces – ammonia. More specifically, on Pt(110) and Pt(111), breaking of the N–O bond is preceded by two to three combined electron-proton transfers at equilibrium (Tafel slope of 40 mV $decade^{-1}$ or even lower[16,17]), while on Pt(100) the N–O bond breaking seems to occur after the first electron-proton transfer (Tafel

slope of 60 mV decade^{-1}). The more facile breaking of the N–O bond on Pt(100), as compared to the other two surfaces, is in remarkable concordance with a similar trend observed in UHV: Pt(100) is the only low-index surface at which the dissociative adsorption of NO occurs. At the same time, electrochemical hydrogenation followed by the N–O bond breaking seems to provide an energetically more favorable route for NO_{ads} reduction on Pt(100), as compared to a direct breaking of the N–O bond. Furthermore, the reaction scheme 4.4-4.7 excludes formation of hydroxylamine during NO_{ads} reduction on Pt(100).

Finally, as shown in the Results and Data Analysis section, the surface defects appear to be more active sites for NO reduction, as compared to the sites on the (100) terrace, although the effect is moderate. Lack of a considerable effect of the step density on the electrocatalyst activity was also observed for NO_{ads} reduction on Pt(111), Pt(110), and a series of Pt-[n(111)×(111)] stepped surfaces. This result is, in fact, expected, because the activity of platinum surfaces toward NO_{ads} reduction seems to be related to the coordination (linear versus multifold bonding) of NO adsorbate, and not to specific reaction sites, for example, low-coordination metal atoms.

4.5. Summary and Conclusions

We have used voltammetry and in situ infrared spectroscopy to study the mechanism of the electrocatalytic reduction of adsorbed nitric oxide on Pt(100)-(1×1). We have examined the effect of surface defects, NO coverage and the nature of the supporting electrolyte (sulfate vs perchlorate).

The voltammetric profile for the electrochemical reduction of a saturated NO adlayer exhibits two features, which were tentatively ascribed to reactions of NO species having different reactivity. Ammonia was shown to be the main product of NO_{ads} reduction on Pt(100), most probably irrespective of the coverage. The surface defects, in particular (100)×(111) steps, render the Pt(100) surface a higher activity toward NO_{ads} reduction, although the effect is moderate. The reactivity of the saturated NO adlayer on Pt(100) does not seem to be affected by the nature of the anion. There is also a small effect of the coverage of NO_{ads}: the reduction of subsaturated NO adlayers starts at more positive potentials (ca. 50 mV).

The Tafel slope analysis of the features appearing in the voltammetric profile for the reductive stripping of a saturated NO adlayer gives values of ca. 60 mV decade^{-1}, irrespective of the nature of anion. This value of the Tafel slope was interpreted in terms of an EC mechanism, in which the first electron-proton transfer is at equilibrium, whereas the second reaction step is a chemical and the rate-

determining step. This chemical step is assumed to involve the N–O bond breaking in HNO_{ads} intermediate and is postulated to require a free neighboring site.

When comparing NO_{ads} reduction on Pt(100) to NO_{ads} reduction on Pt(110) and Pt(111), breaking of the N–O bond on Pt(100) appears to occur at an earlier stage of the reaction. This result leads to the following observations. First, the mechanism of NO_{ads} reduction on platinum depends on the surface structure, although the main reaction product is still the same – ammonia. Second, despite comparable overall activities of the three surfaces toward NO_{ads} reduction, Pt(100) is still the most active in breaking the N–O bond, which is in interesting agreement with the similar trend observed under UHV conditions.

As a final remark, the mechanism proposed for the electrocatalytic reduction of NO adsorbate on Pt(100) seems to provide a framework for explaining the electrocatalytic transformations of hydroxylamine at the same surface.[48] For more details, see Chapter 5.

References

(1) Plieth, W. J. Encyclopedia of Electrochemistry of the Elements; Bard, A. J., Ed.; Marcel Dekker: New-York, 1978; pp 422.
(2) Rodes, A.; Gomez, R.; Orts, J. M.; Feliu, J. M.; Perez, A.; Aldaz, A. *J. Electroanal. Chem.* **1993**, *359*, 315.
(3) Ye, S.; Kita, H. *J. Electroanal. Chem.* **1993**, *346*, 489.
(4) Gomez, R.; Rodes, A.; Orts, J. M.; Feliu, J. M.; Perez, J. M. *Surf. Sci.* **1995**, *342*, L1104.
(5) Rodes, A.; Gomez, R.; Orts, J. M.; Feliu, J. M.; Perez, A.; Aldaz, A. *Langmuir* **1995**, *11*, 3549.
(6) Villegas, I.; Gomez, R.; Weaver, M. J. *J. Phys. Chem.* **1995**, *99*, 14832.
(7) Rodes, A.; Gomez, R.; Perez, A.; Feliu, J. M.; Aldaz, A. *Electrochim. Acta* **1996**, *41*, 729.
(8) Rodes, A.; Climent, V.; Orts, J. M.; Perez, J. M.; Aldaz, A. *Electrochim. Acta* **1998**, *44*, 1077.
(9) Momoi, K.; Song, M. B.; Ito, M. *J. Electroanal. Chem.* **1999**, *473*, 43.
(10) Weaver, M. J.; Zou, S.; Tang, C. *J. Chem. Phys.* **1999**, *111*, 368.
(11) Weaver, M. J. *Surf. Sci.* **1999**, *437*, 215.
(12) Zang, Z.-H.; Wu, Z.-L.; Yau, S.-L. *J. Phys. Chem. B* **1999**, *103*, 9624.
(13) Zou, S.; Gomez, R.; Weaver, M. J. *J. Electroanal. Chem.* **1999**, *474*, 155.
(14) Casero, E.; Alonso, C.; Martin-Gago, J. A.; Bogatti, F.; Felici, R.; Renner, R.; Lee, T.; Zegenhagen, J. *Surf. Sci.* **2002**, *507-510*.
(15) Alvarez, B.; Rodes, A.; Perez, J. M.; Feliu, J. M.; Rodriguez, J. L.; Pastor, E. *Langmuir* **2000**, *16*, 4695.
(16) Beltramo, G. L.; Koper, M. T. M. *Langmuir* **2003**, *19*, 8907.
(17) Rosca, V.; Beltramo, G. L.; Koper, M. T. M. *Langmuir* **2005**, *21*, 1448.
(18) Rosca, V.; Koper, M. T. M. *Surf. Sci.* **2005**, *584*, 258.
(19) de Vooys, A. C. A.; Beltramo, G. L.; van Riet, B.; van Veen, J. A. R.; Koper, M. T. M. *Electrochim. Acta* **2004**, *49*, 1307.
(20) de Vooys, A. C. A.; Koper, M. T. M.; van Santen, R. A.; van Veen, J. A. R. *Electrochim. Acta* **2001**, *46*, 923.
(21) Pirug, G.; Bonzel, H. P.; Hopster, H.; Ibach, H. *J. Chem. Phys.* **1979**, *71*, 593.
(22) Gardner, P.; Tueshaus, M.; Martin, R.; Bradshaw, A. M. *Surf. Sci.* **1990**, *240*, 112.

(23) Masel, R. I. *Catal. Rev. -Sci. Eng.* **1986**, *28*, 335.
(24) Tang, C.; Zou, S.; Weaver, M. J. *Surf. Sci.* **1998**, *412-413*, 344.
(25) Clavilier, J.; Armand, D.; Sun, S. G.; Petit, M. *J. Electroanal. Chem.* **1986**, *205*, 267.
(26) Feliu, J. M.; Orts, J. M.; Fernandez-Vega, A.; Aldaz, A.; Clavilier, J. *J. Electroanal. Chem.* **1990**, *296*, 191.
(27) Iwasita, T.; Nart, F. C.; Vielstich, W. *Ber. Bunsen-Ges. Phys. Chem.* **1990**, *94*, 1030.
(28) Clavilier, J.; Feliu, J. M.; Fernandez-Vega, A.; Aldaz, A. *J. Electroanal. Chem.* **1989**, *269*, 175.
(29) Rodes, A.; Clavilier, J.; Orts, J. M.; Feliu, J. M.; Aldaz, A. *J. Electroanal. Chem.* **1992**, *338*, 317.
(30) Al-Akl, A.; Attard, G. A.; Price, R.; Timothy, B. *J. Electroanal. Chem.* **1999**, *467*, 60.
(31) Yeo, Y. Y.; Vattuone, L.; King, D. A. *J. Chem. Phys.* **1996**, *104*, 3810.
(32) Sugai, S.; Takeuchi, K.; Ban, T.; Miki, H.; Kawasaki, K. *Surf. Sci.* **1993**, *282*, 67.
(33) Song, M.-B.; Momoi, K.; Ito, M. *Jpn. J. Appl. Phys.* **1997**, *36*, L1528.
(34) Rienks, E. D. L.; Bakker, J. W.; Baraldi, A.; Carabiniero, S. A. C.; Lizzit, S.; Weststrate, C. J.; Nieuwenhuys, B. E. *Surf. Sci.* **2002**, *516*, 109.
(35) Lesley, M. W.; Schmidt, L. D. *Surf. Sci.* **1985**, *155*, 215.
(36) Kibler, L. A.; Cuesta, A.; Kleinert, M.; Kolb, D. M. *J. Electroanal. Chem.* **2000**, *484*, 73.
(37) Al-Akl, A.; Attard, G. A.; Price, R.; Timothy, B. *Phys. Chem. Chem. Phys.* **2001**, *3*, 3261.
(38) Clavilier, J.; El Achi, K.; Petit, M.; Rodes, A.; Zamakhchari, M. A. *J. Electroanal. Chem.* **1990**, *295*, 333.
(39) Christiansen, P. A.; Hamnett, A. *Techniques and Mechanisms in Electrochemistry*; Blackie Academic and Proffessional: Glasgow, 1994.
(40) Koper, M. T. M.; Jansen, A. P. J.; Santen van, R. A.; Lukkien, J. J.; Hilbers, P. A. J. *J. Chem. Phys.* **1998**, *109*, 6051.
(41) Ge, Q.; Neurock, M. *J. Am. Chem. Soc.* **2004**, *126*, 1551.
(42) Fink, T.; Dath, J. P.; Bassett, M. R.; Imbihl, R.; Ertl, G. *Surf. Sci.* **1991**, *245*, 96.
(43) Bonzel, H. P.; Broden, G.; Pirug, G. *J. Catal.* **1978**, *53*, 96.
(44) Zemlyanov, D. Y.; Smirnov, M. Y.; Gorodetskii, V. V. *React. Kinet. Catal. Lett.* **1994**, *53*, 87.
(45) Zemlyanov, D. Y.; Smirnov, M. Y. *React. Kinet. Catal. Lett.* **1994**, *53*, 97.
(46) Zemlyanov, D. Y.; Smirnov, M. Y.; Gorodetskii, V. V.; Block, J. H. *Surf. Sci.* **1995**, *329*, 61.
(47) Smirnov, M. Y.; Gorodetskii, V. V.; Block, J. H. *J. Mol. Catal. A: Chem.* **1996**, *107*, 359.
(48) Rosca, V.; Beltramo, G. L.; Koper, M. T. M. *J. Phys. Chem. B* **2004**, *108*, 8294.

5

Electrocatalytic reactions of hydroxylamine at low-index single-crystal platinum surfaces in acidic media

Abstract
The electrochemistry of hydroxylamine at low-index single-crystal platinum electrodes (Pt(111), Pt(110), and Pt(100)) in acidic media has been studied using voltammetry, in situ infrared spectroscopy, and on-line mass spectrometry. The reactivity of hydroxylamine (HAM) at platinum surfaces is largely controlled by interaction of the other components of the solution or products of the HAM partial oxidation with the electrode surface. Reduction of HAM is a structure sensitive reaction, at least through the structure sensitivity of the hydrogen adsorption on platinum. No formation of gaseous products was detected in the potential region corresponding to the H_{upd} region at all the surfaces examined. Voltammetric and spectroscopic data point to adsorbed nitric oxide (NO_{ads}) as the main stable intermediate of the HAM oxidation. Being electrochemically stable in a wide potential region between ca. 0.5 and 0.8 V, adsorbed NO acts as a poison in further oxidation of HAM. The HAM oxidation to NO_{ads} appears to be a structure-insensitive process, though the adsorption of NO seems affected by anion coadsorption. The mechanism of the HAM oxidation to NO_{ads} proposed here is consistent with the mechanism of the NO_{ads} reduction proposed elsewhere. Voltammetric data for all three low-index surfaces indicates the possibility of the HAM reduction and oxidation to occur simultaneously at moderate potentials. This fact may be tentatively explained by the existence of an intermediate, which appears both in the reduction and oxidation process. Accordingly, the reduction of HAM would be activated by a dehydrogenation step. The H_2NO_{ads} or HNO_{ads} species were indicated as candidates. The formation of N_2O at moderately oxidative potentials (below ca. 0.9 V) was observed for HAM oxidation at Pt(111) and Pt(110), but not at Pt(100).

This chapter is based on article by V. Rosca, G.L. Beltramo, and M.T.M. Koper, published in Journal of Physical Chemistry B, 108 (2004) 8294.

5.1. Introduction

Electrochemical reactions of hydroxylamine (HAM) are of great technological importance as well as of significant scientific interest. In industry, HAM is obtained by the liquid-phase catalytic hydrogenation of nitric oxide (NO) or nitrate at carbon-supported platinum or palladium catalysts.[1,2] The relevance of the electrochemical studies on similar catalysts, as well as on model systems, for understanding the processes practiced in industry is well accepted.[3-6] From a scientific point of view, HAM electrochemistry is important for a fundamental understanding of the redox chemistry of inorganic nitrogen compounds. Furthermore, the electrochemical transformations of hydroxylamine could be attractive for studying fundamental aspects of the complex electrode processes involving multiple electron and proton transfer.

The mechanisms of HAM oxidation and reduction on platinum are complex,[7] and only a limited number of detailed mechanistic studies have been reported so far.[8-14] The mechanism of HAM oxidation on platinum is commonly viewed in terms of stepwise dehydrogenation and further transformation of the intermediates. The intermediates of the first two electron-proton transfers in HAM oxidation (HNOH and NOH) are considered responsible for N_2O formation, either by their interaction on the surface or by their reaction with HAM in solution.[11-13] However, explicit evidence for these intermediates remains to be established. Other factors contributing to the complexity of the subject are (i) the adsorption of intermediates, products and components of the electrolyte (anions, for example) on the electrode surface and (ii) the complex homogeneous chemistry of inorganic nitrogen containing compounds.

Recently we have studied in detail the electrochemistry of HAM at polycrystalline platinum in acidic media, combining voltammetry, on-line mass spectrometry, and in situ infrared spectroscopy.[13] An important conclusion was that the HAM electrochemical activity is masked by adsorption of other species, such as hydrogen, products of HAM oxidation (NO), anions ((bi)-sulfate) and other species. Under these circumstances, the investigation of the electrochemistry of HAM on platinum single-crystal electrodes is a logical next step, as the adsorption of these species on single-crystal surfaces is much better defined. Studies on low-index single crystals may provide information on the structure sensitivity of the processes under investigation and help in resolving the effect of adsorption phenomena on the HAM reactivity.

This chapter describes the results of a combined voltammetric, in situ infrared spectroscopic, and on-line mass spectrometry study of HAM electrochemistry at low-index single-crystal platinum electrodes in acidic media. Our aim was to characterize the reactivity of HAM on platinum and the effect of

surface structure on the reactions of HAM. The in situ Fourier transform infrared absorption-reflection spectroscopy (FTIRRAS) and the on-line electrochemical mass spectrometry (OLEMS) were used to detect two important products of HAM oxidation – nitric oxide (NO) and nitrous oxide (N_2O), as well as to identify the potential limits within which they are formed. We discuss the mechanistic aspects of HAM oxidation to NO and N_2O, as well as HAM reduction to ammonia. The mechanistic results are further discussed in light of the recent findings on the mechanism of the reduction of adsorbed NO (NO_{ads}) on polycrystalline platinum[15] and on single-crystal platinum surfaces.[16-18]

5.2. Experimental Section

The H_2SO_4 and $HClO_4$ working solutions were prepared from their respective concentrated acids ("Suprapur", Merck) and ultrapure water (Millipore MilliQ system, 18.2 MΩ cm, 2 ppb total organic carbon). The infrared experiments aimed at detection of nitric oxide were performed in a H_2SO_4 solution prepared with deuterium oxide (Merck, deuteration degree min. 99.8%). Hydroxylamine solutions were prepared by dissolving hydroxylammonium sulfate (Merck, "Pro Analysi") in ultrapure water or deuterium oxide. Prior to each experiment, all solutions were deoxygenated by purging with pure (N50) argon.

Bead-type single-crystal platinum electrodes, prepared by Clavilier's method,[19] were used for most of the electrochemical measurements. For the in situ FTIR measurements, commercial platinum disc electrodes of 10 mm in diameter were used (Surface Preparation Laboratory, Zaandam, The Netherlands). Prior to each experiment, the working electrode was flame-annealed, cooled to room temperature in an $Ar:H_2$ (3:1) atmosphere and transferred to the electrochemical cell under the protection of a droplet of deoxygenated ultrapure water.

Electrochemical measurements were performed in a conventional single-compartment three-electrode glass cell, using a computer-controlled potentiostat (AutoLab-PGSTAT20, Eco Chemie, Utrecht, The Netherlands). The cell and the other glassware were cleaned by boiling in a 1:1 mixture of concentrated nitric and sulfuric acid, followed by repeated boiling with ultrapure water. A coiled platinum wire served as counter electrode. In $HClO_4$ solutions, the reference electrode was an internal Reversible Hydrogen Electrode (RHE). In H_2SO_4 solutions, a saturated mercury-mercury sulfate ($Hg/Hg_2SO_4/K_2SO_4$) electrode, connected via a Luggin capillary, was used as reference. However, all potentials are quoted versus the RHE.

The in situ FTIRRAS measurements were performed under external reflection conditions. The spectrometer used was a Brüker IFS113V, equipped with a narrow-band MCT detector. The spectroelectrochemical cell[20] featured a prismatic CaF_2 window bevelled at 60°. Five huundred interferograms were collected at each potential. The resolution was 8 cm^{-1}. The reflectance spectra were calculated as $(R- R_0)/R_0$, where R and R_0 are the reflectance at the sample and the reference potential respectively. Consequently,

the $\Delta R/R$ ratio gives negative bands for species that are formed and positive bands for species consumed at the sample potential, as compared to the reference potential.

The on-line electrochemical mass spectrometry (OLEMS) measurements were performed using a Balzers Quadrupole (QMS 200) mass spectrometer. A Leybold turbo molecular pump together with a Leybold trivac D4B pre-pump assured a pressure lower than 5×10^{-6} mbar. The connection between the mass spectrometer and the cell was established through a steel capillary connected to a glass tube onto which a polyetheretherketon (PEEK, San Diego Plastics, Inc., National City, CA) holder was attached. The inlet of the PEEK holder (ca. 0.6 mm diameter) contained a porous Teflon membrane (pore size 10 μm, Mupor Limited, Scotland, UK). This tip inlet can be placed at 10-20 μm from the electrode surface using a specially designed positioning system. Owing to a small surface area of the inlet and, therefore, the small amount of volatile products and solvent entering the tip, differential pumping during measurement is not necessary, thus resulting in a better sensitivity. Before each experiment the tip (holder + membrane) and the glass tube, which supports the tip, where cleaned by immersion in concentrated chromic acid for ca. 1 hour, followed by a thorough rinsing with ultrapure water and then boiling in ultrapure water for ca. 20 minutes. The proximity of the tip does not affect the cleanliness of the electrode surface, as deduced from the blank voltammetry. A detailed description of the setup is published elsewhere.[21]

The system cleanliness was checked by recording the blank cyclic voltammogram (CV) before the experiment. The criteria for assessing the surface order and cleanliness of the electrode surface applied to electrodes used for in situ IR measurements were identical to those practiced in this laboratory for purely electrochemical measurements.[22,23]

5.3. Results and Data Analysis

5.3.1. Pt (111)

Figure 5.1A shows cyclic voltammograms (CVs) recorded at a Pt(111) electrode in contact with a HAM-containing sulfuric acid solution. In order to avoid any interference from the products of HAM oxidation, all potential sweep experiments were started in the hydrogen underpotential deposition (H_{upd}) region at about 0.06 V (unless otherwise stated) and subsequently ran in the positive direction. As can be seen from the figure, HAM shows no noticeable activity in the H_{upd} region up to ca. 0.2 V. However, above this potential, a prominent reduction peak occurs at ca. 0.3 V (E_{R4}^{111}), followed by the oxidation peak E_{O1}^{111} at ca. 0.45 V. The E_{R4}^{111} and E_{O1}^{111} features seem to partially overlap, thus indicating that the corresponding processes are not completely separated on the potential scale. In contrast, the oxidation feature E_{O1}^{111} is well separated from the oxidation feature E_{O2}^{111} (at ca. 0.95 V) by a wide potential region of low positive current. If the positive-going potential sweep is reversed at 1 V, the only important voltammetric

features observed in the negative-going sweep are the reduction peaks E_{R2}^{111} and E_{R3}^{111}. The situation is qualitatively similar in a perchloric acid solution (Figure 5.1B), except for the higher current densities recorded in the positive-going sweep in the potential region between ca. 0.2 and 1 V for the latter electrolyte. This finding demonstrates the qualitative effect of anion adsorption, in spite of introducing small amounts of sulfate by using hydroxylammonium sulfate as the source of HAM.

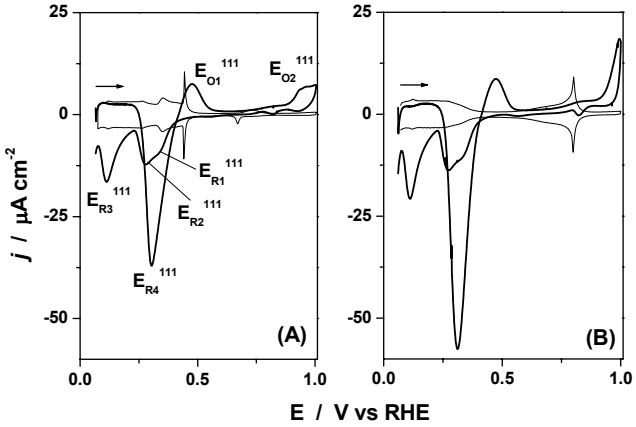

Figure 5.1. Cyclic voltammograms recorded at Pt(111) electrodes in 0.5 M sulfuric (A) and 0.5 M perchloric (B) acid solutions in absence (solid line) and presence (bold solid line) of NH_2OH. Exp. conditions: 2.5×10^{-3} M NH_2OH; potential sweep rate 5 mV s^{-1}; starting potential 0.06 V.

The positive-going scan of the CV, presented in Figure 5.1A (or B), differs significantly from the negative-going one, presumably due to the formation, the blocking effect, and the reduction of some product(s) of HAM oxidation. Continuous potential cycling, combined with a gradual increase of the upper potential limit of the CV, allowed us to follow the appearance and evolution of the reduction features E_{R2}^{111} and E_{R3}^{111} in the negative-going scan (see Figure 5.2). If a sufficiently low potential sweep rate is applied (5 mV s^{-1} or lower), the positive-going sweep has always the same shape, while the negative-going voltammetric profile changes as a function of the vertex potential. As shown in Figure 5.2A, the reduction features E_{R2}^{111} and E_{R3}^{111}, as well as (shoulder-like) feature E_{R1}^{111}, appear and develop in the negative-going sweep with the increasing upper potential limit of the corresponding CVs. Significantly, if the upper potential limit coincides with or is lower than the peak potential of the feature E_{R4}^{111}, no signs of the feature

E_{R3}^{111} can be found in the negative-going scan. Therefore, in the potential region between ca. 0.2 and 0.3 V only HAM electroreduction should occur.

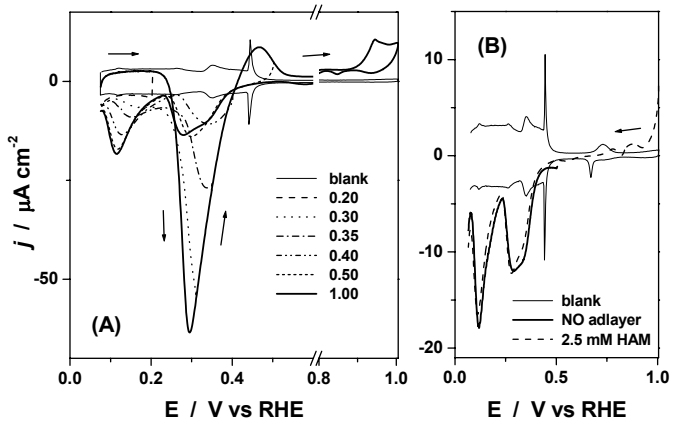

Figure 5.2. Cyclic voltammograms recorded at Pt(111) electrode in 0.5 M sulfuric (A). Numbers in the legend indicate the upper potential limit (vertex potential) of the corresponding CVs. Experimental conditions: 5×10^{-3} M NH_2OH; potential sweep rate 5 mV s^{-1}. Starting potential 0.06 V. In panel (B) the negative-going voltammetric profile recorded in the hydroxylamine-containing solution is compared to the reductive stripping of a saturated NO adlayer (in the absence of NH_2OH).

The CV profile observed can be understood in terms of (i) HAM reduction to ammonia (E_{R4}^{111}), which is the only possible reduction product, and (ii) HAM oxidation to nitric oxide (E_{O1}^{111}). The assumption of NO formation is based on a good match between both position and shape of the reduction features E_{R2}^{111} and E_{R3}^{111} with those observed for the reductive stripping of an NO adlayer under the same experimental conditions,[16] though in the absence of HAM (Figure 5.2B). Furthermore, the Tafel slope analysis of the features E_{R2}^{111} and E_{R3}^{111}, carried out in E_p - log(v) coordinates,[24,25] gives slopes of 41 mV $decade^{-1}$ and 142 mV $decade^{-1}$, respectively. These values are quite similar to those observed for the reductive stripping of saturated NO adlayers, that is 42 mV $decade^{-1}$ and 126 mV $decade^{-1}$.[16] Due to the presence and stability of the NO adlayer, HAM oxidation is essentially blocked between ca. 0.5 and 0.9 V. However, as will be argued below, in this potential region a slow (continuous) oxidation of HAM still takes place.

From the effect of the potential sweep rate on the peak height, it was deduced that features E_{R2}^{111}, E_{R3}^{111}, and E_{O1}^{111} are all surface-confined processes. Their peak current densities show a linear increase with the potential sweep rate (in log(j) – log (v) coordinates) in a wide window up to 1 V s^{-1}. The values of

corresponding slopes were close to 1 (within 10% error). The linear regression analysis was applied to 6 to 10 experimental points; the square of the correlation coefficient (r^2) was at least 0.999 in all cases. The E_{R4}^{111} feature shows the same behavior (5 experimental points, slope 0.89, $r^2 = 0.997$), although in a narrow range of sweep rates (2-20 mV s^{-1}), probably due to a stronger overlap with feature E_{O1}^{111} at higher scan rate. An additional argument in favour of a surface reaction is the applicability of the Langmuir adsorption isotherm to the corresponding process (see below).

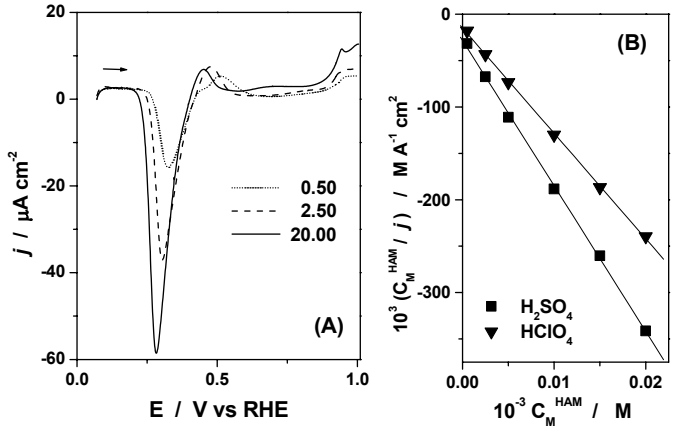

Figure 5.3. Effect of NH_2OH concentration on the positive-going voltammetric profile recorded at Pt(111) electrode (A) and the linearized Langmuir adsorption isotherm (B) (see text for details). Experimental conditions: 0.5 M H_2SO_4; potential sweep rate 5 mV s^{-1}; starting potential 0.06 V.

The effect of the HAM concentration is analyzed on the basis of Figures 5.3A and 5.3B. We studied only moderate HAM concentrations (up to 50 mM), because in this range of concentrations the effect of anion adsorption could be easily followed. Figure 5.3A shows that (i) the reduction process corresponding to the feature E_{R4}^{111} is of positive order in HAM concentration and (ii) the oxidation process corresponding to feature E_{O1}^{111} is zero order in HAM concentration. Additionally, an increase of HAM concentration results in an increase, although moderate, of the current density in the potential region between ca. 0.6 and 1 V, including the process corresponding to the feature E_{O2}^{111}. This observation supports the occurrence of the above-mentioned slow (continuous) HAM oxidation in this region in presence of adsorbed NO, whereas feature E_{O2}^{111} must be related to the

oxidation of the NO adlayer to adsorbed HNO_2 [26,27] and possibly a reaction between the nitrite formed and HAM.

As mentioned above, the log(j) – log (v) analysis of the feature E_{R4}[111] suggests that the corresponding process of HAM reduction is a surface-confined process. Consequently, the current density (j) at a given potential should be proportional to the surface coverage of HAM (θ_{HAM}). Under these circumstances one can apply the Langmuir adsorption isotherm to test the hypothesis of adsorption. Here we followed a simple formalism[28] that allows the linear form of the Langmuir adsorption isotherm to be used as a criterion for the adsorption, although the procedure is of little use for estimating the HAM coverage. The final expression used was

$$(C_{HAM} / j) = 1 / (k \beta_{HAM}) + (1 / k) \times C_{HAM} \qquad (5.1)$$

where j is the observed current density (A cm^{-2}); C_{HAM} is the concentration of HAM (mol l^{-1}); k is the proportionality constant between the observed current density and the coverage of HAM[28] (A cm^{-2}) ; β_{HAM} is the adsorption parameter which also includes the activity coefficient (mol^{-1} l). Figure 5.3B shows the results of a graphic analysis based on relation 5.1. From the figure it can be seen that a good linearity was observed for experiments in both sulfuric and perchloric acid. The different values of the slopes reflect the effect of the specific adsorption of (bi)sulfate.

So far, we have examined HAM electrochemistry at Pt(111) on the basis of the voltammetric results. These results allowed us to identify adsorbed NO as the intermediate of HAM oxidation. However, voltammetry is of little use for detection of another important product of HAM oxidation, that is, nitrous oxide (N_2O), which was, in fact, observed by other authors[12] as well as in this laboratory[13] in studies with polycrystalline platinum.

Figure 5.4 shows the potential-difference IR spectra collected in experiments with a Pt(111) electrode. Bulk N_2O can be recognized by the asymmetric stretch (ν_1) band, centered at 2231 cm^{-1}.[29] Spectra in Figure 5.4A contains a band at ca. 2230 cm^{-1}, which proves the formation of N_2O. As deduced from the change of the integrated area under this band with the applied potential, formation of N_2O begins at ca. 0.3 V. The concentration of N_2O in the thin layer appears to increase up to ca. 0.5 V and then decreases with a tendency to level at around 0.7 V. The diffusion of N_2O out of the thin layer, in combination with a decrease of its formation rate between ca. 0.5 and 0.7 V, could account for the decrease of the integrated area of the corresponding band in this potential region. Note that the potential region of increasing N_2O content (0.3-0.7 V) overlaps with the region where the processes

corresponding to the voltammetric features E_{R4}^{111} and E_{O1}^{111} are observed (see Figure 5.2A).

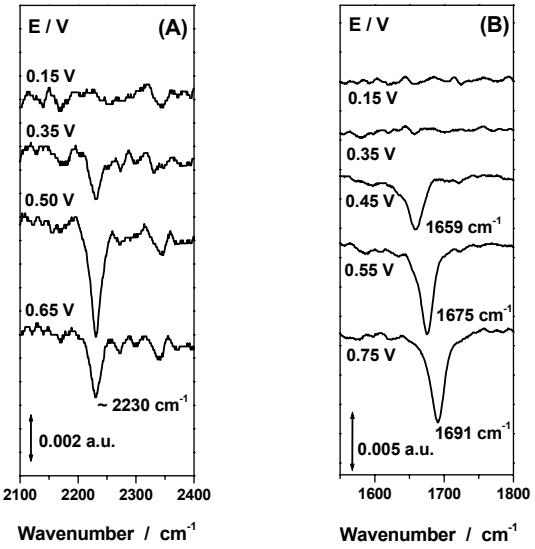

Figure 5.4. The potential-difference infrared spectra collected at Pt(111) electrode at selected values of the applied potential (as indicated). Reference potential 0.1 V. Experimental conditions: 0.1 M H_2SO_4 + 1.5×10^{-2} M NH_2OH; in H_2O (A) and in D_2O (B); p – polarized light.

The assignment of the vibrational modes of adsorbed NO must be carried out with care, as the N–O stretching mode will be displayed in a wide range of frequencies, depending on the surface orientation, NO coverage, and the applied potential. The potential-dependent negative band displayed in the 1600-1700 cm^{-1} frequency range (Figure 5.4B) can be assigned to NO adsorbed in atop position (for details, see Chapter 2, section 2.3.2). This assignment is in good agreement with previous studies of NO adsorption on Pt(111) under similar experimental conditions.[30,31] Furthermore, the experimental value of the 'Stark-tuning' slope ($d\nu_{NO}/dE$) of 72(±4) cm^{-1} V^{-1} lies in the range between 62 cm^{-1} V^{-1} and 85 cm^{-1} V^{-1}, reported by Weaver et al.[31] for the saturated (0.4-0.5 ML) and subsaturated (0.3 ML) NO adlayers, respectively. As deduced from the integrated area under the peak assigned to adsorbed NO, there is a sharp increase of NO coverage at potentials between ca. 0.4 and 0.5 V; then, a well-defined constancy of the value of the integrated area is observed in the potential region between ca. 0.5 and 0.9 V. This is in good agreement with the CV data, which points to the formation of a

(nearly) saturated NO adlayer at above ca. 0.5 V. Finally, in our infrared measurements, we did not observed NO accumulation in solution.

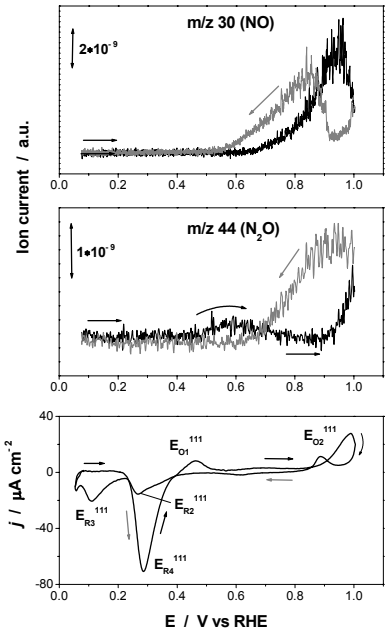

Figure 5.5. Results of the on-line electrochemical mass spectrometry measurements for the electrochemical reactions of hydroxylamine at Pt(111) surface. Experimental conditions: 0.5 M $HClO_4$; 20×10^{-3} M NH_2OH ; starting potential 0.06 V; potential scan rate 5 mV s^{-1}. Black line – positive-going scan; gray line – subsequent negative-going scan.

Figure 5.5 shows the so-called mass spectrometric cyclic voltammograms (MSCV) for selected m/z ratios, measured in perchloric acid. In good accordance with the infrared experiments, the formation of N_2O (m/z 44) is observed during the positive-going scan in the potential region between ca. 0.45 and 0.85 V. The formation of N_2O, possibly a result of the slow continuous process deduced from voltammetry, can be tentatively explained by a surface reaction, possibly between NO_{ads} and HAM or, alternatively, between NO_{ads} and products of partial dehydrogenation of HAM. Further increase of the mass signal at more positive potentials and, subsequently, during the negative-going scan coincides with the anodic peak E_{O2}^{111}, thus indicating a second source of N_2O formation. This second source is probably a reaction between nitrite formed and HAM.

The fragmentation-corrected signal for m/z 30 (NO) clearly indicates the production of a significant amount of NO in solution at potentials as low as ca. 0.6

V with a maximum at ca. 0.85 V. The negative-going scan (reversed at ca. 1V) shows a similar (peak-like) feature, though with a positive shift of ca. 100 mV. The detection of NO in solution may be tentatively assigned to (i) partial desorption of NO adlayer and (ii) (homogeneous) decomposition of nitrite to NO. We did not observe the formation of N_2. Interestingly, we did not observe N_2O formation in experiments in sulfuric acid. At the same time, we did observe some NO, though in much smaller amount than in perchloric acid.

5.3.2. Pt (110)

As shown in Figure 5.6A, the CV profile recorded at Pt(110) surface in contact with a HAM-containing sulfuric acid solution is quite different from that recorded at Pt(111) under the same experimental conditions. Most significantly, the reduction peak at ca. 0.3 V observed at Pt(111), is not present. Furthermore, in contrast to Pt(111), the Pt(110) surface is active for HAM reduction even at potentials corresponding to the saturation coverage of hydrogen (Figure 5.6A). On the other hand, similar to Pt(111), a HAM oxidation wave in the potential region between ca. 0.4 and 0.6 V can be readily deduced from the CV data. A gradual increase of the upper potential limit during continuous potential cycling brings about the appearance and development of the voltammetric features E_{R1}^{110} and E_{R2}^{110} in the subsequent negative-going sweep (Figure 5.6A). The increase of the upper potential limit from 0.4 to 0.6 V results in fully developed E_{R1}^{110} and E_{R2}^{110} peaks. This finding demonstrates the formation and the reductive stripping of adsorbed NO, and shows that the HAM reduction and oxidation processes occur simultaneously at potentials around 0.4 V. The negative-going part of the voltammetric profile recorded in the presence of HAM compares well with the one observed for the reductive stripping of the saturated NO adlayer (Figure 5.6B). However, in the presence of HAM the peak E_{R1}^{110} is less pronounced, probably due to a lower NO coverage resulting from HAM oxidation. The Tafel slope analysis of peaks E_{R1}^{110} and E_{R2}^{110} gave values of 39 mV decade^{-1} and 29 mV decade^{-1}, respectively. These values may be compared with 44 mV decade^{-1} and 42 mV decade^{-1}, respectively, obtained for the same features in the case of reductive stripping of NO adlayer.[16] The significant difference of the Tafel slope values in the case of the E_{R2}^{110} feature is probably related to the presence of HAM.

The effect of the HAM concentration was examined from the positive-going linear sweep voltammograms started in the H_{upd} region at ca. 0.06 V. As shown in Figures 5.7A and 5.7B, the reduction process(es) involving HAM in the potential region between ca. 0.06 and 0.4 V is (are) of positive order in HAM concentration, while the oxidation process corresponding to the feature E_{O1}^{110} is zero order in HAM concentration. Furthermore, as can be deduced from a comparison of the

data presented in Figures 5.7A and 5.7B, the reduction process(es) in the potential region between ca. 0.06 and 0.4 V are significantly affected by the specific coadsorption of (bi)sulfate, as expected for Pt(110). Additionally, the effect of the HAM concentration on the reduction process(es) under examination appears to be complex. At low concentrations (around 0.5 mM HAM) the positive-going potential sweep shows a minimum around 0.3 V (Figures 5.7A and 5.7B, dashed lines), while further increase of the HAM concentration brings about a faster increase of the reduction current in the potential region below ca. 0.1 V. This complex trend is particularly well defined in the case of experiments in perchloric acid, where a prominent reduction minimum can be observed at ca. 0.12 V. This potential value corresponds to a nearly saturated hydrogen coverage on Pt(110).

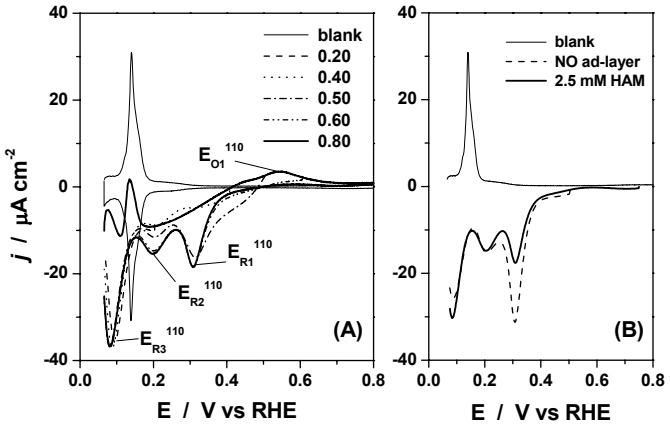

Figure 5.6. Cyclic voltammograms recorded at Pt(110) electrode in 0.5 M sulfuric (A). Numbers in the legend indicate the upper potential limit (vertex potential) of the corresponding CV. Experimental conditions: 5×10^{-3} M NH_2OH; potential sweep rate 5 mV s^{-1}. Starting potential 0.06 V. In panel (B) the negative-going voltammetric profile recorded at Pt(110) in a NH_2OH-containing solution is compared to the reductive stripping of a saturated NO adlayer (in the absence of NH_2OH), as indicated in the legend.

It is logical to assume that HAM reduction to ammonia is the process responsible for the negative current in the potential region up to 0.4 V: ammonia is the only possible reduction product. At the same time, the effect of HAM concentration suggests that the reduction processes involving HAM could be more complex. Previously, we have reported on a possible catalytic effect of HAM toward the hydrogen evolution reaction (HER),[13] as suggested from earlier mechanistic studies on HAM reduction on mercury electrodes.[32] By using on-line

differential electrochemical mass spectrometry we could observe a very small, though statistically significant, continuous increase of the m/z 2 (H_2) mass with increasing HAM concentration on polycrystalline platinum in 0.5 M H_2SO_4 solution. As the sites of the (110) plane are the dominant ones on polycrystalline platinum, the above-mentioned effect may occur on a well-oriented Pt(110) surface as well.

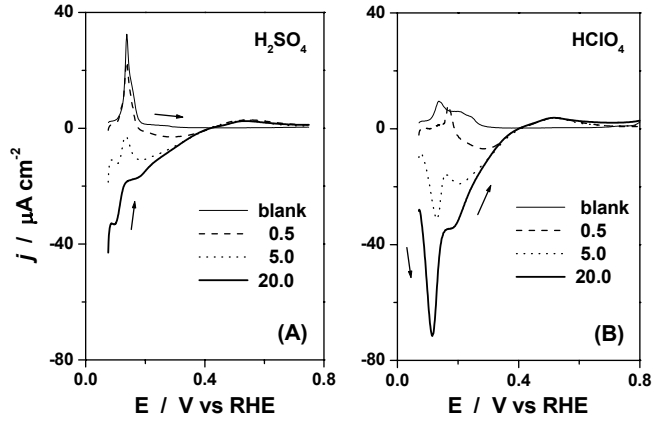

Figure 5.7. Effect of the NH_2OH concentration on the positive-going voltammetric profile recorded at Pt(110) electrode in sulfuric acid (A) and perchloric acid (B). Numbers in legends indicate the NH_2OH concentration (in mM). Experimental conditions: 0.5 M H_2SO_4; potential sweep rate 5 mV s^{-1}; starting potential 0.06 V.

Turning to the spectroscopic data on the HAM reactions at Pt(110), Figure 5.8A shows N_2O formation that begins at ca. 0.4 V (band at ca. 2230 cm^{-1}). The integrated area under this peak reaches its maximum at ca. 0.5 V and then gradually decreases. Voltammetry showed that in the potential region between ca. 0.4 and 0.6 V, the HAM oxidation to NO_{ads} takes place. Therefore, N_2O formation seems to occur simultaneously with the formation of NO adlayer. Furthermore, N_2O formation seems to be suppressed at potentials corresponding to high NO coverage (0.6 V and more positive).

Figure 5.8B shows a series of spectra in the frequency range where the N–O stretching in the adsorbed NO species is to be expected. The negative-going band centered at around 1584 cm^{-1} could be assigned to bridge-bonded NO (low NO coverage), while a broad composite band between ca. 1660 and 1780 cm^{-1} probably arises from N–O stretching in NO_{ads} in the atop position (intermediate to high NO coverage).[33] The following considerations support this assignment. Firstly, the

experiments with s-polarized light showed the absence of any spectroscopic features in the 1600-1800 cm^{-1} region. Secondly, from the experiments with NO adlayers on Pt(110) we could see a picture similar to that observed for HAM oxidation, i.e. a broad (composite) negative going band in the frequency region between ca. 1650 and 1800 cm^{-1} and a lower frequency band centered at ca. 1580 cm^{-1}.[17] Additionally, this assignment is in agreement with previous results. Gomez et al.[30] observed (i) a broad bipolar band at around 1740 cm^{-1} at near-saturation NO coverage and (ii) a weak bipolar band at ca. 1590 cm^{-1} at lower NO coverage in 0.1 M perchloric acid. All together, the spectroscopic data presented above provide sufficient evidence for the formation of an NO adlayer at potentials around 0.5 V and its increasing coverage at higher potentials as a result of HAM oxidation.

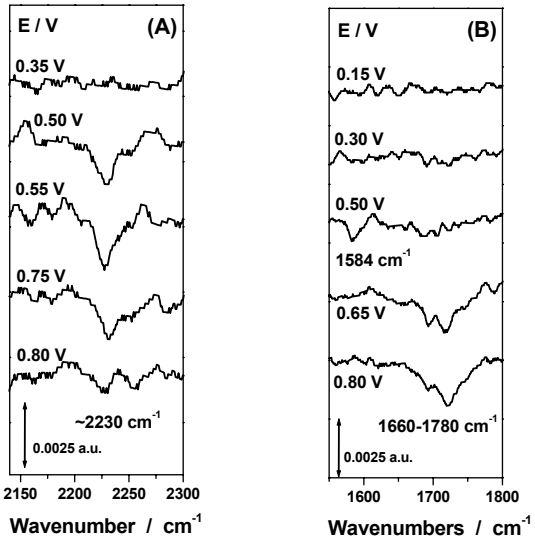

Figure 5.8. The potential-difference infrared spectra collected at Pt(110) electrodes at selected values of the applied potential (as indicated). Reference potential 0.1 V. Experimental conditions: 0.1 M H_2SO_4 + 1.5×10^{-2} M NH_2OH; in H_2O (A) and in D_2O (B); p – polarized light.

5.3.3. Pt (100)

We shall start the presentation of the results for Pt(100) with examining the effect of HAM concentration. As shown in Figure 5.9A, the positive-going voltammogram recorded for Pt(100) surface in sulfuric acid is quite similar to that for Pt(111). Firstly, Pt(100) does not show a significant activity towards HAM reduction in the potential region corresponding to a high coverage of hydrogen

(0.06 – 0.25 V). Secondly, a prominent, concentration-dependent, reduction peak (E_{R1}^{100}) is observed at potentials corresponding to subsaturated coverages of hydrogen. Thirdly, the oxidation feature E_{O1}^{100}, corresponding to HAM oxidation to adsorbed NO, occurs at ca. 0.5 V and is zero order in HAM concentration. The formation of NO_{ads} can be deduced from the effect of HAM concentration on the negative-going sweep of the corresponding CVs (see Figure 5.9B). The height and position of peak E_{R1}^{100}, which we attribute to the reductive stripping of the NO adlayer, increase with the concentration, pointing to an increasing NO coverage achieved. The NO coverage approaches its saturation value at the highest concentration of the range examined (20×10^{-3} M HAM), as deduced from the position of the E_{R3}^{100} peak. An increase of NO coverage can be achieved by longer polarization at potentials above 0.6 V at low concentrations as well. The reduction feature E_{R1}^{100} (see the inset of Figure 5.10) corresponds to HAM reduction to ammonia. Accordingly, we did not observe the formation of any gaseous products in this region by both infrared and mass spectrometry measurements (see below). Finally, quite similar voltammetric profiles and trends were observed for similar experiments in perchloric acid.

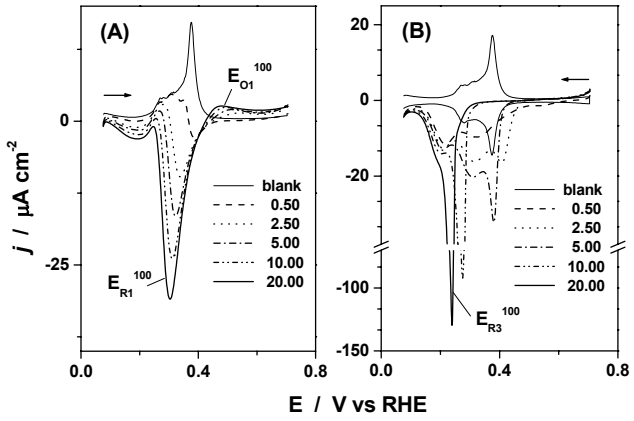

Figure 5.9. The positive-going (A) and the negative-going (B) part of the cyclic voltammograms recorded at Pt(100) electrode in 0.5 M sulfuric acid in the presence of hydroxylamine. Numbers in the legends indicate the hydroxylamine concentration. Experimental conditions: potential sweep rate 5 mV s^{-1}; starting potential 0.06 V.

Figure 5.10 shows the voltammetric reduction and oxidation of HAM in sulfuric acid. More specifically, the figure shows the effect of the upper-potential limit (vertex potential) on the negative-going voltammetric profile. In this

experiment, the potential cycle was started at ca. 0.06 V and was run in the positive-going direction first. Continuous potential cycling, combined with a gradual increase of the upper potential limit of the cyclic voltammogram, allowed us to follow the appearance and evolution of the features in the negative-going scan. If a sufficiently low potential sweep rate is applied (5 mV s^{-1} or lower), the positive-going sweep shows the same voltammetric profile (as that shown by the bold black line), while the negative-going voltammetric profile changes as a function of the vertex potential.

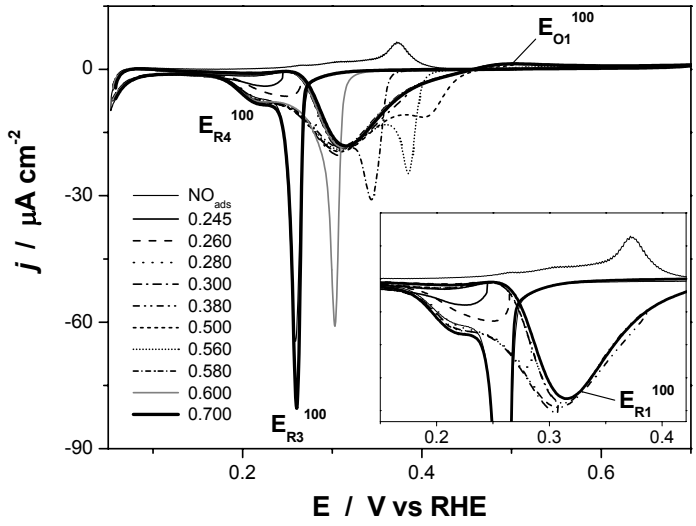

Figure 5.10. Cyclic voltammograms recorded at Pt(100) electrode in 0.5 M perchloric acid solution. Numbers in the legend indicates the upper potential limit (vertex potential) of the corresponding CV. Exp. conditions: 2.5×10^{-3} M NH_2OH; potential sweep rate 5 mV s^{-1}, starting potential 0.06 V.

As an important observation from the above experiment, reversing the potential at ca. 0.3 V (or more positive) results in the appearance of a reduction feature at ca. 0.22 V, which cannot be associated with HAM reduction, but rather with reduction of a product of the HAM partial dehydrogenation.[34] This can be concluded from the much lower currents observed in the 0.1-0.25 V region in the positive-going scan, thus indicating a low "direct" HAM reduction reactivity in this potential region. The position and the height of the reduction feature observed in the negative-going scan at ca. 0.22 V does not depend on the HAM concentration[34] or on the vertex potential (for potentials higher than ca. 0.3 V). Significantly, the

position and height of this feature appear to be identical to those of the feature E_{R4}^{100}, which is characteristic for the NO_{ads} stripping profile (Figure 5.10, the thin solid line, which strongly overlaps with the bold solid line). The above observations suggest that HAM reduction, which seems to involve initial partial dehydrogenation,[34] and the reduction of NO_{ads} proceeds through the same intermediate.

Note a sharp transition from HAM reduction to ammonia (Figure 5.10, feature E_{R1}^{100}) to HAM oxidation to NO_{ads} (Figure 5.10, feature E_{O1}^{100}). We would not exclude the possibility of simultaneous occurrence of the two processes around 0.45 V. In any case, these two processes sharing an intermediate would be a reasonable explanation for the observed voltammetric profile. We shall propose a candidate for such an intermediate in the Discussion section.

Intriguingly, Figure 5.10 indicates that the negative-going part of the CVs reversed below ca. 0.6 V show, along with features E_{R1}^{100} and E_{R4}^{100}, a sharp reduction peak, the height and position of which depend on the upper potential limit. The higher the upper potential limit the more negative the peak position and more intensive the peak is. As features E_{O1}^{100} and E_{R3}^{100} correspond to the formation and reductive stripping, respectively, of NO_{ads}, it would be logical to assume that this reduction peak corresponds to the reductive stripping of a subsaturated NO adlayer. At the same time, note that we did not observe any considerable positive shift of the E_{R3}^{100} feature with decreasing NO coverage (for NO adlayers formed by NO dosing from nitrite; see Chapter 4, Figure 4.3). Therefore, we assume that the structure and the reactivity of the (subsaturated) NO adlayer formed as a result of HAM oxidation and that formed upon NO dosing from nitrite solution differ, although their structures are identical at saturation. A definite interpretation of the evolution of the voltammetric profile described in this paragraph is difficult, because the structure of the subsaturated NO adlayer is unclear.

The above interpretation of the oxidation feature E_{O1}^{100} is confirmed by the in situ infrared data presented in Figure 5.11. This figure contains a series of potential-difference spectra, which show a potential-dependent negative band (corresponding to the accumulation of a product) centered between ca. 1586 and 1620 cm^{-1}. We assign this band to the N–O stretching mode of NO molecules adsorbed on (100) terraces, in agreement with previous in situ infrared studies by different groups. As the most important message of this figure, NO_{ads} can be detected at ca. 0.5 V or more positive potentials, which demonstrates that feature E_{O1}^{100} corresponds to HAM oxidation to NO_{ads}. Finally, in our infrared experiments we never observed the formation of nitrous oxide (the N–O and N–N stretching modes at ca. 1285 cm^{-1} and ca. 2230 cm^{-1}, respectively) at Pt(100).

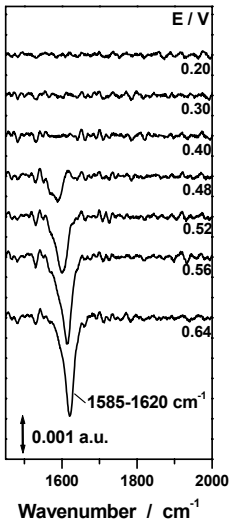

Figure 5.11. The potential-difference infrared spectra for the electrochemical oxidation of hydroxylamine at Pt(100) surface. Exp. conditions: 0.1 M $HClO_4$ + 1×10^{-3} M NH_2OH (in D_2O), p-polarized light, reference potential 0.1 V.

Figure 5.12 shows the results of the OLEMS measurements of HAM electrochemical transformations at the Pt(100) surface. No gaseous products are observed in the potential region between ca. 0.05 V and 0.9 V during the positive-going sweep (we also monitored m/z 26 (N_2) and m/z 46 (NO_2)). This result strongly suggests that the reduction feature E_{R1}^{100} corresponds to HAM reduction to ammonia and that this process, though involving a partial dehydrogenation of HAM, is not accompanied by side reactions (e.g., N–N condensation). Furthermore, no gaseous products appear to accompany HAM oxidation to NO_{ads} (the oxidation feature E_{O1}^{100} at ca. 0.5 V). In contrast, the HAM oxidation to NO_{ads} on Pt(111) and Pt(110) surfaces is accompanied by the formation of some N_2O at around 0.5 V. The (saturated) NO adlayer blocks sites for further HAM oxidation, acting as a catalyst poison. Therefore, low anodic current densities are observed in the positive-going scan (Figure 5.12, the solid black lines). The formation of N_2O and the formation of a little NO are observed in the positive-going scan starting at ca. 0.9 V (Figure 5.12, the solid black lines) and in the subsequent negative-going scan between 1 and 0.7 V (Figure 5.12, the solid gray lines). The formation of nitrous oxide at highly oxidative potentials (around 0.9 V) is most probably related to a reaction between the nitrite, resulting from NO_{ads} oxidation, and HAM. Accumulation of some NO in solution may be tentatively assigned to (i) partial desorption of NO adlayer and/or (ii) (homogeneous) decomposition of nitrite to NO.

As shown above, the oxidation of HAM in the potential window between ca. 0.45 and 0.6 V results in the formation of NO_{ads}. The negative-going scan in Figure 5.12 (the solid gray line) shows a profile virtually identical with the one recorded for the reductive stripping of a saturated NO adlayer in the absence of HAM in solution. Furthermore, no gaseous products are observed during the reductive stripping of this NO adlayer (the potentials region between ca. 0.4 and 0.05 V; Figure 5.12, the solid gray line), even in the presence of HAM. This result points again to ammonia as the product of NO_{ads} reduction on the Pt(100) surface.

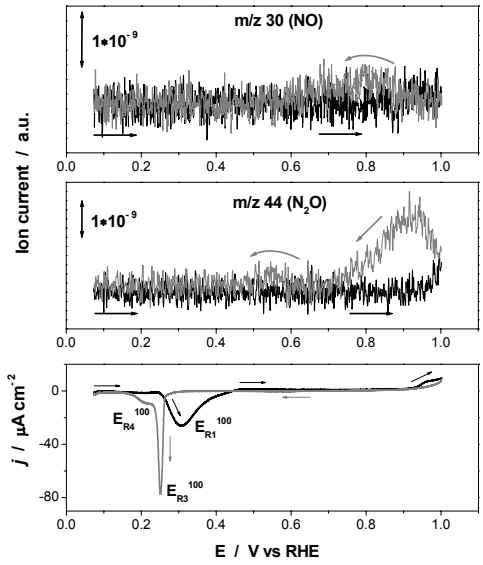

Figure 5.12. Results of the on-line electrochemical mass spectrometry measurements for the electrochemical reactions of hydroxylamine at Pt(100) surface. Experimental conditions: 0.5 M H_2SO_4 + 20×10^{-3} M NH_2OH ; starting potential 0.05 V; potential scan rate 2 mV s^{-1}. Black line – the positive-going scan; gray line – the subsequent negative-going scan.

5.3.4. Tafel slope analysis

The results of the Tafel slope analysis of HAM oxidation to NO_{ads} on Pt(111) (feature E_{O1}^{111}) and on Pt(110) (feature E_{O1}^{110}) surfaces are presented in Figure 5.13A and Figure 5.13B, respectively. The analysis was performed in the peak potential *vs.* logarithm of the sweep rate coordinates.[24,25] In the case of Pt(111), the values of the Tafel slopes were 40 mV $decade^{-1}$ and 38 mV $decade^{-1}$ in sulfuric and perchloric acid, respectively. As for the Pt(110) surface, the Tafel slope of 33 mV $decade^{-1}$ obtained in sulfuric acid is somewhat lower (though reasonably close to) than the value of 43 mV $decade^{-1}$ in perchloric acid. The Tafel slope observed for feature E_{O1}^{100} in sulfuric acid was 22 mV $decade^{-1}$ (data not shown), while in perchloric acid a poor linearity was observed.

The results of the Tafel slope analysis suggest that the second electron transfer is the rate-determining step in the process of HAM oxidation to adsorbed NO, at least on Pt(111) and Pt(110).

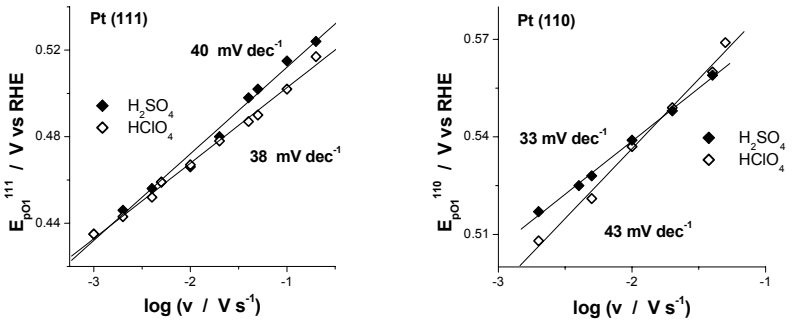

Figure 5.13. The Tafel slope analysis of the oxidation peaks E_{OI}^{111} (A) and E_{OI}^{110} (B) in 0.5 M sulfuric acid and 0.5 M perchloric acid, as indicated in the legend. Experimental conditions: 5×10^{-3} M NH_2OH; starting potential 0.06 V.

5.4. Discussion

We shall begin the Discussion section with an analysis of HAM electrooxidation. Both voltammetric and spectroscopic data point to the surface-bonded NO as the key intermediate in electrooxidation of HAM, and not the adsorbed NOH (or HNO) intermediate, as suggested in earlier studies.[12,14] Previously, this intermediate was assumed to be the main precursor in the formation of HNO_2, through a reaction with the OH_{ads} species. In our experiments, the NO formation peak is observed at around 0.5 V on all surfaces examined, which would rather exclude the above scenario. Furthermore, HAM oxidation is essentially blocked by NO adlayer, which is stable over a relatively wide potential region (up to 0.7-0.9 V), depending on the surface orientation and the nature of the supporting electrolyte (perchlorate vs. sulfate). The oxidation of the platinum surface triggers oxidation of NO_{ads} at more positive potentials and, consequently, continuous HAM oxidation. Recent studies of NO adlayers on single-crystal platinum electrodes provide sufficient (both voltammetric and spectroscopic) evidence for $HNO_{2(ads)}$ as the main product of the (reversible) oxidation of adsorbed nitric oxide in the potential region between 0.9-1.1 V.[27,30,35] Therefore, it would be reasonable to accept this scenario for the oxidation of NO adlayers on the surface in contact with a HAM-containing solution. However, no reversibility of the surface confined NO/HNO_2 is observed,[34] most probably due to an irreversible reaction between HAM and the surface HNO_2.

The Tafel slope analysis of the voltammetric peak corresponding to HAM oxidation to NO_{ads} at the Pt(111) and Pt(110) surfaces, points to the second electron transfer as the rate-limiting step. This finding confirms the tentative mechanism proposed on the basis of previous results on polycrystalline platinum:[13]

$$H_3NOH^+ \leftrightarrows H_3NOH^+_{ads} \quad (5.2)$$
$$H_3NOH^+_{ads} \leftrightarrows H_2NO_{ads} + 2H^+ + e^- \quad (5.3)$$
$$H_2NO_{ads} \rightarrow HNO_{ads} + H^+ + e^- \quad \text{rds} \quad (5.4)$$
$$HNO_{ads} \rightarrow NO_{ads} + H^+ + e^- \quad (5.5)$$

Theoretical calculations shows that in vacuum the energy of the HNO and H_2NO intermediates is lower than that of the NOH and HNOH species, respectively, albeit the stability of the surface-bonded species is not known.[16,36] Therefore the first two intermediates are indicated in reaction scheme 5.2-5.5. In acidic media, the protonated HAM molecule is commonly perceived as the reactive species.[12,14,28] However, the exact nature of the reactive species in reaction (5.3) ($H_3NOH^+_{ads}$ vs. H_2NOH_{ads}) should be considered as unknown, as the acid-base properties of HAM could be significantly affected upon interaction with the surface. Accordingly, reaction (5.3) may be split in two steps:

$$H_3NOH^+_{ads} \leftrightarrows H_2NOH_{ads} + H^+ \quad (5.3')$$
$$H_2NOH_{ads} \leftrightarrows H_2NO_{ads} + H^+ + e^- \quad (5.3'')$$

The mechanism of the HAM oxidation to NO_{ads} may be compared with a mechanism recently proposed for the reduction of NO_{ads}.[16] Briefly, the reductive stripping of the NO adlayer is perceived as a stepwise hydrogenation process, in which the formation of HNO and H_2NO intermediates is assumed:

$$NO_{ads} + H^+ + e^- \leftrightarrows HNO_{ads} \quad \text{equilibrium} \quad (5.6)$$
$$HNO_{ads} + H^+ + e^- \rightarrow H_2NO_{ads} \quad \text{rds} \quad (5.7)$$
$$H_2NO_{ads} + 4H^+ + 3e^- \rightarrow NH_4^+ + H_2O \quad \text{fast} \quad (5.8)$$

Ammonia is shown as the main product of the reduction of the adsorbed NO on platinum.[16,17,37,38] Importantly, the protons in reactions (5.6) and (5.7) seem to be transferred directly from a solution hydronium species.[16] Comparing schemes (5.2-5.5) and (5.6-5.8), reactions (5.4) and (5.7) are the forward and back reactions of the same transformation. At the same time, reactions (5.4) and (5.7) are the rate determining steps in the reaction schemes (5.2-5.5) and (5.6-5.8), respectively. Consequently, the energetic barrier for the $HNO_{ads} \leftrightarrow H_2NO_{ads}$ transformation seems to be the highest in the whole $NO_{ads} \leftrightarrow NH_2OH$ chain of transformations, whatever the direction. The implication of these intermediates in the rate-determining step may indicate their relative stability and possibly participation in side reactions, e.g. the formation of N_2O and N_2.

Another important issue to be considered is the formation of N_2O at moderately oxidative potentials. Spectroscopic data for Pt(111) and Pt(110) indicate the formation of nitrous oxide, starting at ca. 0.35 and 0.4 V, respectively. As the maximum of the N_2O formation occurs in the potential region corresponding to a subsaturated NO adlayer (ca. 0.45 V at Pt(111) and ca. 0.5 V at Pt(110), a possible explanation would be an (electro)catalytic reaction between adsorbed NO and HAM (or NO and products of HAM partial dehydrogenation), resulting in a N–N condensation process. This interpretation of the formation of N_2O (under potential control) is consistent with data on catalytic reactions between HAM and NO in acidic media at carbon-supported platinum catalysts, in which N_2O was shown as the product,[2] as well as with previous electrochemical studies of the HAM oxidation at polycrystalline platinum.[12-14] Curiously enough, we never observed N_2O formation in experiments on HAM oxidation at Pt(100).

We shall continue with a discussion of the HAM reductive activity. On Pt(111) the H_{upd} region is well separated from the (bi)sulfate adsorption region, corresponding to the unique situation of an electrode surface almost free of hydrogen and anion adsorption. At potentials around 0.3 V, the electrode surface is not covered by either hydrogen or (bi)sulfate. Therefore, the prominent reduction peak at about 0.3 V is a strong indicator of (i) a high reactivity of HAM at free platinum sites and (ii) a strong dependence of the reductive activity of HAM on the interactions of the surface with hydrogen and specifically adsorbed anions. Interestingly, the HAM reduction begins at ca. 0.20 V, corresponding to the H_{upd} coverage well below saturation (ca. 0.2 ML). This observation suggests that multiple adsorption sites (an "ensemble") are needed for HAM to be activated for reduction. The situation is quite similar for Pt(100) surface: HAM is reduced in the potential region between ca. 0.3-0.4 V, corresponding to subsaturated hydrogen and a low (bi)sulfate coverage. On Pt(110) the picture is somewhat different; HAM is reduced over the whole H_{upd} region, although affected by the nature of the anion. Furthermore, HAM is reduced even at potentials corresponding to high hydrogen coverage, suggesting that the Pt(110) surface nearly-saturated with adsorbed hydrogen still exposes sites active for the activation of HAM reduction.

Before we proceed with discussing the mechanistic implications for HAM reduction, it would be interesting to briefly recall previous mechanistic work on HAM reduction. In an early study of HAM reduction on bright platinum, Möller and Heckner interpreted their data in terms of the HAM involvement in the hydrogen evolution reaction.[8] In a later more detailed mechanistic study, the same authors assumed the breaking of the N–O bond in the first step, which was indicated as the rate-determining step (Eq. 5.10).

$$H_3NOH^+_{ads} + e^- \rightarrow (NH_3)_{ads} + OH_{ads} \qquad (5.10)$$

In two subsequent steps a fast electron transfer to and the protonation of the adsorbed OH species is postulated. A low rate of HAM reduction was explained by the blocking effect of the adsorbed NH_3 species.[28] The reduction of HAM is positive order in HAM concentration, as deduced from polycrystalline[13] as well as single crystal studies (this work), which is inconsistent with blockage by $(NH_3)_{ads}$ species.

An important clue in looking for an alternative scenario for HAM reduction on platinum may be the fact that at all surfaces examined the features corresponding to HAM reduction and oxidation partially overlap (around 0.4 V), suggesting their simultaneous occurrence. Note that this observation is in agreement with the platinum-catalyzed disproportionation of HAM, resulting in the formation of ammonia and nitrous oxide.[2] One possible explanation involves the assumption that the oxidation and reduction of HAM have a common intermediate. These considerations would lead us to the following tentative mechanism of HAM reduction:

$$H_3NOH^+ \leftrightarrows H_3NOH^+_{ads} \quad \text{equilibrium} \qquad (5.11)$$

$$H_3NOH^+_{ads} \leftrightarrows H_2NO_{ads} + 2H^+ + e^- \qquad (5.12)$$

$$H_2NO_{ads} + 4H^+ + 3e^- \rightarrow NH_4^+ + H_2O \qquad (5.13)$$

We assume that a possible way to activate reduction of HAM is partial dehydrogenation of the HAM (reaction 5.12) and formation of an adsorbed intermediate. Note that reactions (5.11) and (5.13) are identical to reactions (5.2) and (5.3), i.e. the first two steps of the scheme proposed for HAM oxidation to NO_{ads}. Therefore, we can assume that an intermediate (e.g., H_2NO_{ads}) may serve as a precursor to both NH_4^+ and NO_{ads} formation. In other words, the HAM reduction process contains an oxidative activation step – reaction (5.12). This reaction should require multiple adsorption sites, as can be inferred from the effect of the hydrogen and (bi)sulfate adsorption on HAM reduction on Pt(111) and Pt(100). In contrast to the mechanism proposed by Möller and Heckner, N–O bond is assumed to be broken at a later stage of the reaction.

Support to the reaction scheme (5.11-5.13) is provided by the voltammetric data for Pt(100). The voltammograms in Figure 5.12 show a feature at ca. 0.22 V corresponding to reduction of an (presumably) adsorbed species. The position and shape of this feature is zero order in HAM concentration (Figure 5.9B) and do not depend on the upper potential limit of the CVs (Figure 5.10), once the upper potential limit of ca 0.3 V is reached. Furthermore, the presence of the reduction feature at 0.22 V for all upper potential limits higher than 0.3 V suggests that this feature is related to the reduction of an intermediate of the NO reduction (or even

NO itself). Accordingly, the adsorbate under consideration must be a compound in which nitrogen has formal oxidation state between (+2) and (–2) but it cannot be HAM, as the positive-going scan indicates that HAM cannot be reduced at these low potentials. The possible candidates are adsorbed H_2NO (or HNOH) and HNO (or NOH) intermediates. The latter species could be preferred on Pt(100), in light of recent mechanistic studies of NO_{ads} reduction on Pt(100) (for more details, see Chapter 4, section 4.4.2). Regardless of our inability to exactly identify the nature of the species, the above considerations strongly suggest an oxidative activation scenario for the reduction of HAM.

Finally, let us comment on the structure sensitivity of the HAM reduction and oxidation in connection to its reactivity on polycrystalline platinum, as well as in connection to the structure sensitivity of the related nitrate reduction and methanol oxidation. Comparison of the reduction activity on the low-index planes to polycrystalline platinum leads to the conclusion that the reactivity of polycrystalline platinum is dominated by sites of (110) orientation. The Pt(111) and Pt(100) surfaces are more active towards HAM reduction, but only in a limited potential region, which in the case of Pt(111) is clearly related to a very low coverage of hydrogen and anions on the surface. Interestingly, both Pt(111) and Pt(100) become completely blocked for HAM reduction by hydrogen coverages that are significantly below saturation; for Pt(111) the critical coverage below which the HAM reduction starts is ca. 0.2-0.3 ML. The same observation was recently made for nitrate reduction on Pt(111),[39] suggesting that both HAM and nitrate reduction need multiple adsorption sites (an "ensemble") to adsorb and react. More generally, these results indicate that for weakly adsorbed reactants, such as HAM and nitrate, the reactive sites are those sites where the competition with coadsorbates is the least dominant. Such sites typically tend to be (111) and (100) terrace sites. The voltammetric data on HAM oxidation to NO_{ads} on the three surfaces examined point to an apparent structure insensitivity of this reaction. This is in sharp contrast with the observed structure sensitivity of a very similar reaction, namely methanol (MeOH) oxidation on platinum. Methanol oxidation is an order of magnitude faster on Pt(110) compared to Pt(111),[40] and recent chronoamperometric results indicate that methanol decomposition to adsorbed carbon monoxide takes place preferentially on the step sites of stepped platinum electrodes.[41] We assume that these differences between HAM and MeOH dehydrogenation kinetics may be traced back to their different adsorption strength.

5.5. Summary and Conclusions

This chapter has described the results of an investigation of the electrochemistry of hydroxylamine at low-index single-crystal platinum electrodes

in acidic media by voltammetry, in situ infrared spectroscopy, and on-line mass spectrometry. The study was focused particularly on the mechanistic aspects of HAM electrochemical transformations, structure sensitivity of HAM reactions, and the effect of the (co)adsorption phenomena on the HAM reactivity on platinum.

Hydroxylamine electrochemistry at platinum is largely controlled by the interaction of the other components of the solution or products of the HAM partial oxidation with the electrode surface, such as adsorbed hydrogen, sulfate and nitric oxide. Reduction of HAM seems to require multiple adsorption sites and is a structure sensitive reaction, at least through the structure sensitivity of the hydrogen adsorption on platinum. No formation of gaseous products was detected in the potential region corresponding to the H_{upd} region on Pt(111), Pt(110), and Pt(100) surfaces.

Voltammetric and spectroscopic data point to adsorbed NO as the main stable intermediate of the HAM oxidation. Being electrochemically stable in a wide potential region between ca. 0.5 and 0.8 V (dependent on the surface orientation and the nature of the supporting electrolyte), adsorbed NO acts as a poison for a further oxidation of HAM. The HAM oxidation to nitric oxide appears to be a structure-insensitive process and is somewhat affected by the anion coadsorption. The Tafel slope analysis suggests the second electron transfer to be the rate-determining step in HAM oxidation to adsorbed NO.

The mechanism of the HAM oxidation to NO_{ads} proposed here is consistent with the mechanism of the NO_{ads} reduction proposed elsewhere.[16,38] Remarkably, the energetic barrier for the $HNO_{ads} \leftrightarrow H_2NO_{ads}$ transformation seems to be the highest in the $NO_{ads} \leftrightarrow NH_2OH$ chain of transformations, whatever the direction.

Voltammetric data for all three low-index surfaces indicate the possibility of the HAM reduction and oxidation (at moderate potentials) to occur simultaneously. This observation may be tentatively explained by the existence of an intermediate (H_2NO_{ads} or HNO_{ads}), which appears both in reduction and oxidation of HAM. This observation suggests that the HAM reduction is activated by an oxidative (dehydrogenation) step. The existence of a common intermediate in the reduction and oxidation of HAM would provide a natural explanation for the platinum-catalyzed disproportionation of HAM.

References

(1) Ritz, J.; Fuchs, H.; Perryman, H. G. Hydroxylamine. In *Ulmann's Encyclopedia of Industrial Chemistry*; 6th ed.; Wiley: Chichester, 2000.
(2) Moesdijk van de, C. G. M. The catalytic reduction of nitrite and nitric oxide to hydroxylamine: kinetics and mechanism. PhD thesis, Eindhoven University of Technology, 1979.
(3) Tauszik, G. R.; Grocetta, P. *Appl. Catal.* **1985**, *17*, 1.

(4) Gootzen, J. F. E. In situ spectroscopic and electrochemical studies related to liquid-phase heterogeneous catalysis. PhD thesis, Eindhoven University of Technology, 1997.
(5) Savodnik, N. N.; Shepelin, V. A.; Zalkind, T. I. *Elektrokhimiya* **1971**, *7*, 583.
(6) Savodnik, N. N.; Shepelin, V. A.; Zalkind, T. I. *Elektrokhimiya* **1971**, *7*, 424.
(7) Plieth, W. J. Nitrogen. In *Encyclopedia of Electrochemistry of the Elements*; Bard, A. J., Ed.; Marcel Dekker: New-York, 1978; Vol. 8; pp 422.
(8) Möller, D.; Heckner, K. H. *Z. Chem.* **1971**, *11*, 157.
(9) Möller, D.; Heckner, K. H. *Z. Chem.* **1971**, *11*, 32.
(10) Möller, D.; Heckner, K. H. *Z. Chem.* **1971**, *11*, 356.
(11) Möller, D.; Heckner, K. H. *Z. Phys. Chemie* **1972**, *251*, 81.
(12) Karabinas, P.; Wolter, O.; Heitbaum, J. *Ber. Bunsen-Ges. Phys. Chem.* **1984**, *88*, 1191.
(13) Rosca, V.; Beltramo, G. L.; Koper, M. T. M. *J. Electroanal. Chem.* **2004**, *566*, 53.
(14) Piela, B.; Wrona, P. K. *J. Electrochem. Soc.* **2004**, *151*, E69.
(15) de Vooys, A. C. A.; Koper, M. T. M.; van Santen, R. A.; van Veen, J. A. R. *J. Electroanal. Chem.* **2001**, *506*, 127.
(16) Beltramo, G. L.; Koper, M. T. M. *Langmuir* **2003**, *19*, 8907.
(17) Rosca, V.; Beltramo, G. L.; Koper, M. T. M. *Langmuir* **2005**, *21*, 1448.
(18) Rosca, V.; Koper, M. T. M. *Surf. Sci.* **2005**, *584*, 258.
(19) Clavilier, J.; Armand, D.; Sun, S. G.; Petit, M. *J. Electroanal. Chem. Interfacial Electrochem.* **1986**, *205*, 267.
(20) Iwasita, T.; Nart, F. C.; Vielstich, W. *Ber. Bunsen-Ges. Phys. Chem.* **1990**, *94*, 1030.
(21) Wonders, A.; Housmans, T. H. M.; Rosca, V.; Koper, M. T. M. *J. Appl. Electrochem.*, submitted.
(22) Lebedeva, N. P.; Koper, M. T. M.; Herrero, E.; Feliu, J. M.; Santen van, R. A. *J. Electroanal. Chem.* **2000**, *487*, 37.
(23) Lebedeva, N. P.; Rodes, A.; Feliu, J. M.; Koper, M. T. M.; Santen van, R. A. *J. Phys. Chem. B* **2002**, *106*, 9863.
(24) Christiansen, P. A.; Hamnett, A. *Techniques and Mechanisms in Electrochemistry*; Blackie Academic and Proffessional: Glasgow, 1994.
(25) Koper, M. T. M.; Jansen, A. P. J.; Santen van, R. A.; Lukkien, J. J.; Hilbers, P. A. J. *J. Chem. Phys.* **1998**, *109*, 6051.
(26) Ye, S.; Kita, H. *J. Electroanal. Chem.* **1993**, *346*, 489.
(27) Zang, Z.-H.; Wu, Z.-L.; Yau, S.-L. *J. Phys. Chem. B* **1999**, *103*, 9624.
(28) Moeller, D.; Heckner, K. H. *Z. Phys. Chemie* **1974**, *255*, 33.
(29) Nakamoto, K. *Infrared and Raman Spectra of Inorganic and Coordination compounds*; John Wiley & Sons: New-York, 1986.
(30) Gomez, R.; Rodes, A.; Orts, J. M.; Feliu, J. M.; Perez, J. M. *Surf. Sci.* **1995**, *342*, L1104.
(31) Weaver, M. J.; Zou, S.; Tang, C. *J. Chem. Phys.* **1999**, *111*, 368.
(32) Heyrowsky, M.; Vavrichka, S. *Collect. Czech. Chem. Commun.* **1969**, *34*, 1204.
(33) Brown, W. A.; King, D. A. *J. Phys. Chem. B* **2000**, *104*, 2578.
(34) Rosca, V.; Beltramo, G. L.; Koper, M. T. M. *J. Phys. Chem. B* **2004**, *108*, 8294.
(35) Rodes, A.; Gomez, R.; Perez, J. M.; Feliu, J. M.; Aldaz, A. *Electrochim. Acta* **1996**, *41*, 729.
(36) de Vooys, A. C. A.; Koper, M. T. M.; van Santen, R. A.; van Veen, J. A. R. *Electrochim. Acta* **2001**, *46*, 923.
(37) Rodes, A.; Climent, V.; Orts, J. M.; Perez, J. M.; Aldaz, A. *Electrochim. Acta* **1998**, *44*, 1077.
(38) Rosca, V.; Koper, M. T. M. *J. Phys. Chem. B* **2005**, *109*, 16750.
(39) Dima, G. E.; Beltramo, G. L.; Koper, M. T. M. *Electrochim. Acta* **2003**, *554-555*, 15.
(40) Herrero, E.; Franaszczuk, K.; Wieckowski, A. *J. Phys. Chem.* **1994**, *98*, 5074.
(41) Housmans, T. H. M.; Koper, M. T. M. *J. Phys. Chem. B* **2003**, *107*, 8557.

6

Electrocatalytic oxidation of ammonia on Pt(111) and Pt(100) surfaces

Abstract
The electrocatalytic oxidation of ammonia on Pt(111) and Pt(100) has been studied using voltammetry, chronoamperometry, and in situ infrared spectroscopy. The oxidative adsorption of ammonia results in the formation of NH_x (x=0-2) adsorbates. On Pt(111), ammonia oxidation occurs in the double-layer region and results in the formation of NH and, possibly, N adsorbates. The experimental current transients show a hyperbolic decay (t^{-1}), which indicates strong lateral (repulsive) interactions between the (reacting) species. On Pt(100), the adsorbed NH_2 fragment is the stable intermediate in ammonia oxidation. Stabilization of NH (and N) and NH_2 fragments on Pt(111) and Pt(100), respectively, is in an interesting agreement with recent theoretical predictions. The Pt(111) surface shows extremely low activity in ammonia oxidation to dinitrogen, thus indicating that neither NH nor N (strongly) adsorbed species are active in dinitrogen production. Neither nitrous oxide nor nitric oxide is the product of ammonia oxidation on Pt(111) at potentials up to 0.9 V, as deduced from the in situ infrared measurements. The Pt(100) surface is highly active for dinitrogen production. This process is characterized by a Tafel slope of 30 mV $decade^{-1}$, which is explained by a rate-determining dimerization of NH_2 fragments followed by a fast decay of the surface-bound hydrazine formed to dinitrogen. Therefore, the high activity of the Pt(100) surface in ammonia oxidation to dinitrogen is likely to be related to its ability to stabilize the NH_2 adsorbate.

This chapter is to be published.

6.1. Introduction

The electrochemical oxidation of ammonia on the transition metals has been receiving considerable attention, particularly in connection with the possibility of using ammonia in the electrochemical fuel cells,[1-4] in the environmental (electro)catalysis,[5,6] and the electrochemical detection of ammonia.[7,8] From a scientific point of view, ammonia electrooxidation on platinum, as well as on other metal surfaces, is an attractive electrocatalytic model system. Achieving a molecular level understanding of the electrocatalytic reactions of ammonia obviously requires studies on single-crystal surfaces and use of the non-electrochemical molecular-level probes.

In early studies on polycrystalline platinum, ammonia oxidation in alkaline media was commonly viewed as a stepwise electrocatalytic dehydrogenation process, resulting in the formation of NH_x adsorbed species (x=0-2).[5,9,10] It was assumed that molecular nitrogen was formed by the recombination of two nitrogen adatoms.[9] In a later, more detailed, mechanistic study, Gerischer and Mauerer[11] suggested that (partially) discharged hydroxyl takes part in the dehydrogenation steps. These authors pointed to the dimerization of the NH_x (x=1,2) fragments and the subsequent dehydrogenation of the resulting dimer as the most plausible scenario for the formation of molecular nitrogen, whereas atomic nitrogen was assumed to act as a catalyst poison. The authors provided an ex situ analysis suggesting the formation of atomic nitrogen.

More recent studies provided further details on ammonia oxidation, mostly confirming and extending the Gerischer-Mauerer mechanism.[12-14] Gootzen et al.[13] identified the NH adsorbate to be the stable intermediate of ammonia oxidation to molecular nitrogen and also suggested atomic nitrogen as the catalyst poison. De Vooys et al.[14] examined the reactivity of a series of transition and coinage metals for ammonia oxidation, using voltammetry and on-line differential electrochemical mass spectrometry (DEMS). The authors pointed to the importance of the nature of the products of ammonia anodic adsorption and the overpotentials at which these adsorbates are formed. An electrode surface was active for the dinitrogen formation, provided the NH_x species were formed at sufficiently low overpotentials, whereas atomic nitrogen was indicated as the poison. In a subsequent in situ surface-enhanced Raman spectroscopy (SERS) study, de Vooys et al.[15] demonstrated the formation of atomic nitrogen on palladium, which is a poor dinitrogen formation electrocatalyst, supporting the Gerischer-Mauerer assumption that atomic nitrogen acts as a poison. In a very recent rotating ring-disk electrode (RRDE) study, Endo et al.[16] could detect in situ some weakly adsorbed intermediates, both oxidizable and reducible ones, suggesting the formation of a small amount of hydroxylamine.

There are few studies of ammonia oxidation on single-crystal platinum electrodes. Nonetheless, these studies provided important information on the structure sensitivity of ammonia oxidation. Gao et al.[17] reported mass spectrometry measurements of ammonia oxidation on Pt(100) and pointed to the high activity of this surface. These authors also observed the production of molecular nitrogen between ca. 0.6 and 0.9 V. More recently, Vidal-Iglesias et al.[18] reported a voltammetric study of ammonia oxidation on Pt(111), Pt(110) and Pt(100). The authors demonstrated a structure sensitivity of ammonia oxidation on platinum: Pt(100) was highly active for ammonia oxidation at potentials as low as 0.5 V, whereas Pt(111) and Pt(110) showed virtually no activity in the potential range up to ca. 0.9 V. In a subsequent paper, Vidal-Iglesias et al.[19] concluded that the activity toward ammonia oxidation was quite sensitive to the width of the (100) terrace and the orientation of the step. Very recently, the same authors reported results of a DEMS study of ammonia oxidation on Pt(111), Pt(110) and Pt(100), using ^{15}N labeled ammonia.[20] The Pt(100) surface showed very high activity and selectivity towards ammonia oxidation to dinitrogen; at potentials above ca. 0.7 V vs. RHE, nitrous oxide and nitric oxide become dominant products. For a cyclic voltammogram with the upper potential limit of ca. 1.5 V, a strong deactivation of the surface was observed. Pt(111) and Pt(110) were shown to be much poorer electrocatalysts for ammonia oxidation in general and to dinitrogen in particular.

This chapter describes the results of a detailed voltammetric analysis and chronoamperometry of ammonia oxidation on Pt(111) and Pt(100) surfaces, aiming particularly at understanding the initial stages of the reaction and explaining the differences in activity between these two surfaces. In situ reflection-absorption infrared spectroscopy (FTIRRAS) was employed to identify the products of ammonia oxidation on Pt(111). Taking the Gerischer-Mauerer mechanism as the starting hypothesis, we critically analyze the mechanistic aspects of ammonia electrooxidation. The Pt(100) and Pt(111) surfaces were chosen as model electrocatalysts: the former is exceptionally active and the latter is inactive towards the ammonia oxidation to dinitrogen. On the basis of our experimental results, as well as relying on the available theoretical and ultrahigh vacuum (UHV) data, we propose a more detailed mechanistic picture of ammonia oxidation on the two surfaces and, most importantly, identify the factors controlling the activity towards dinitrogen production.

6.2. Experimental Section

The 0.5 M H_2SO_4 and 0.1 M NaOH solutions were prepared from the concentrated sulfuric acid (95-98%, Suprapur, Merck) and from sodium hydroxide monohydrate (Suprapur, Merck), respectively, using ultrapure water (Millipore MilliQ system, 18.2 MΩ

cm, 3-4 ppb total organic carbon) or deuterium oxide (Uvasol, Merck, deuteration degree min. 99%) as solvents. The 0.5 M ammonia solutions were prepared from a concentrated solution (25%, Suprapur, Merck) using either ultrapure water or deuterium oxide. A corresponding volume of this solution was added to the working electrolyte to create the necessary concentration of ammonia, the resulting dilution being negligible (less than 1%).

Two types of single-crystal platinum electrodes were used. Bead-type single-crystal platinum electrodes (ca. 2 mm diameter), prepared by Clavilier's method,[21] were used for most of the electrochemical measurements. For the in situ infrared measurements, commercial disc electrode were used (10 mm diameter; oriented within 1°; Surface Preparation Laboratory, Zaandam, The Netherlands). Before each experiment, the working electrode was flame-annealed, cooled to room temperature in an $Ar:H_2$ (3:1) gas mixture and transferred to the electrochemical cell under the protection of a droplet of deoxygenated ultrapure water.

Electrochemical measurements were performed in a single-compartment three-electrode glass cell, using a computer-controlled potentiostat (AutoLab-PGSTAT20, Eco Chemie, Utrecht, The Netherlands). The cell and the other glassware were cleaned by boiling in a 1:1 mixture of the concentrated nitric and sulfuric acid, followed by repeated boiling with ultrapure water. A coiled platinum wire served as counter electrode. In NaOH solutions, the reference electrode was an internal reversible hydrogen electrode (RHE), connected via a Luggin capillary. In H_2SO_4 solutions a saturated mercury-mercury sulfate ($Hg/Hg_2SO_4/K_2SO_4(sat)$) electrode, also connected via a Luggin capillary, was used as reference. However, all potentials are quoted versus the RHE. Before each experiment, all solutions were deoxygenated by purging with pure (N50) argon for ca. 45 minutes.

The in situ Fourier transform infrared reflection-absorption spectroscopy (FTIRRAS) measurements were performed under external reflection conditions. The Fourier-transform infrared spectrometer was a Brüker IFS113V, equipped with a narrow-band MCT detector. The design of the spectroelectrochemical cell closely resembles that described elsewhere.[22] The cell featured a prismatic CaF_2 transmission window beveled at 60°. Five hundred interferograms were collected at each potential. The spectral resolution was 8 cm^{-1}. The reflectance spectra were calculated as $(R–R_0)/R_0$, where R and R_0 are the reflectance at the sample and the reference potential respectively. Therefore, the $(R–R_0)/R_0$ ratio gives negative bands for species that are formed and positive bands for species that are consumed at the sample potential, as compared to the reference potential.

The surface order and cleanliness of the working electrodes were checked before each experiment by recording the blank cyclic voltammograms in 0.5 M sulfuric acid and their comparison to the standard voltammetric profiles for the Pt(100)-(1×1) or Pt(111) surfaces.[23-27] If the CV satisfied the criteria for the surface order, the electrode was transferred to the cell containing alkaline solution.

6.3. Results and Data Analysis

6.3.1. Ammonia oxidation on Pt(111)

6.3.1.1. Cyclic voltammetry

The solid line in Figure 6.1 shows the blank voltammetric profile of a Pt(111) electrode in alkaline solution. The cyclic voltammogram (CV) presents three distinct regions: (i) the hydrogen adsorption/desorption (or hydrogen underpotential deposition, H_{upd}) region between ca. 0.05 and 0.3 V, (ii) the double layer region between ca 0.3 and 0.65 V, and (iii) the oxygen (or hydroxide) adsorption and desorption region between ca. 0.65 and 0.9 V. Note that in the present study we examine ammonia oxidation in the potential region in which the Pt(111) surface maintains its structural order (between 0.05 and 0.9 V).

The bold solid line in Figure 6.1 represents the CV recorded in the presence of ammonia in solution. Ammonia shows no activity in the H_{upd} region. Ammonia oxidation begins in the double-layer region (voltammetric peak E_{O1}^{111} at ca. 0.5 V) and continues in the OH adsorption region (peak E_{O2}^{111} at ca. 0.7 V and feature E_{O3}^{111} at potentials higher than ca. 0.8 V). The reverse negative-going scan shows three characteristic reduction features: E_{R1}^{111} at ca. 0.65 V, and peaks E_{R2}^{111} and E_{R3}^{111} between ca. 0.45 and 0.2 V. The latter two are strongly overlapped for CVs recorded at low scan rates (lower than 10 mV s^{-1}).

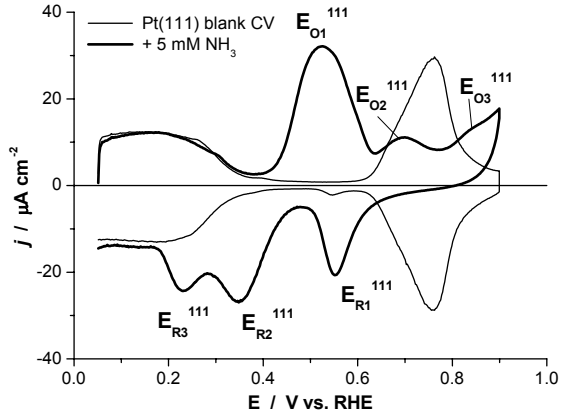

Figure 6.1. Cyclic voltammograms recorded at Pt(111) electrode in 0.1 M NaOH in the absence of ammonia (solid line) and in the presence of ammonia (bold solid line). Experimental conditions: starting potential 0.05 V; scan rate 20 mV s^{-1}; 5×10^{-3} M NH_3.

From the effect of the potential sweep rate on the peak height it was deduced that features E_{O1}^{111}, E_{R1}^{111}, E_{R2}^{111} and E_{R3}^{111} correspond to surface-confined processes. Accordingly, their peak current densities show a linear increase with the potential sweep rate (in $\log(j_p) - \log(v)$ coordinates) in a wide scan rate window. The values of corresponding slopes were close to 1 (within 10% error). The linear regression analysis was applied to 8 to 12 experimental points and the square of the correlation coefficient (r^2) was at least 0.999. The feature E_{O2} shows somewhat poorer linearity (8 experimental points, slope 0.92, $r^2 = 0.992$), which must be related to errors in reading the peak position (it is a broad peak) and increasing overlap with peak E_{O1}^{111} at scan rates higher than ca. 100 mV s^{-1}.

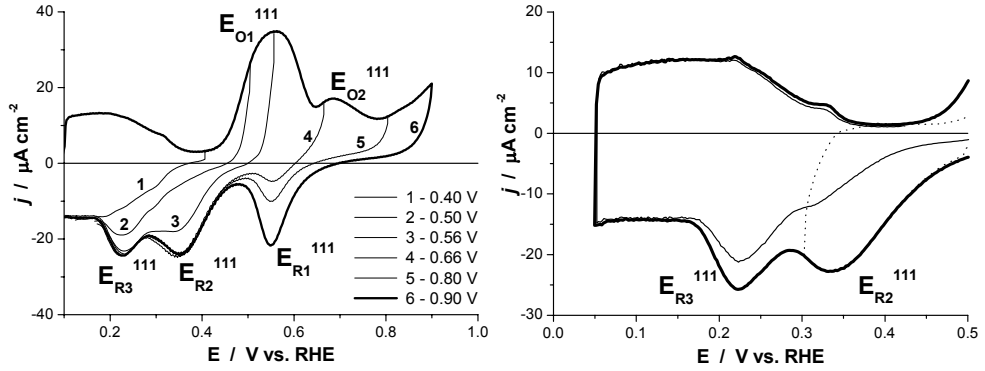

Figure 6.2. (left) Cyclic voltammograms recorded at Pt(111) electrode in 0.1 M NaOH in the presence of ammonia. The CVs differ by their upper-potential limit, as indicated in the legend of the figure. Experimental conditions: starting potential 0.05 V; scan rate 20 mV s^{-1}; 1×10^{-3} M NH_3.

Figure 6.3. (right) Cyclic voltammogram showing the independent removal of the features E_{R2} and E_{R3} (see text for details). The bold solid line shows the complete removal of features E_{R2} and E_{R3} in a single run to 0.05 V. The dotted line (CV reversed at ca. 0.3 V) and the (thin) solid line (the CV reversed at 0.05 V) were recorded consecutively. Experimental conditions: 0.1 M NaOH + 5×10^{-5} M NH_3; 20 mV s^{-1}; starting potential 0.5 V.

Figure 6.2 illustrates the effect of the value of the upper-potential limit on the negative-going part of the CV. In this experiment, the potential run was started at 0.1 V in the positive-going direction. Continuous potential cycling, combined with gradual increase of the upper potential limit of the CV, allowed us to follow the appearance of the features in the negative-going scan. First, it is obvious that the faradaic process corresponding to peak E_{O1} gives the reactants for the reduction process(es) related to peaks E_{R2}^{111} and E_{R3}^{111}. The gradual increase of the upper-potential limit brings about the appearance (in the negative-going scan) of the peak

E_{R3} first and, next, of the peak E_{R2}^{111}. The position and shape of peaks E_{R2}^{111} and E_{R3}^{111} are independent of the value of the upper-potential limit, provided the upper-potential limit of ca. 0.7 V is achieved. The charge under peak E_{O1}^{111} (Q_{O1}), corrected for the double-layer charging, corresponded to ca. 147 μC cm^{-2}. The charge under peaks E_{R2}^{111} and E_{R3}^{111} (Q_{R2+R3}), corrected for the double-layer charging and the H adsorption, is ca. 141 μC cm^{-2}. The ratio Q_{O1} / Q_{R2+R3} is, therefore, very close to one, which suggests that the ammonia oxidation in the potential region up to ca. 0.7 V is chemically reversible. We assume that ammonia is the only product of the reductive stripping corresponding to E_{R2}^{111} and E_{R3}^{111}. Second, ammonia oxidation in the OH adsorption region (between ca. 0.65 and 0.9 V), reflected in the appearance of peak E_{O2}^{111}, can be also reversed in the negative-going scan (peak E_{R1}^{111}). Feature E_{O3}^{111} probably corresponds to the OH adsorption at the available surface sites.

The experimental charge corresponding to ammonia oxidation in the double-layer region (ca. 145 μC cm^{-2}) may be compared to the charge corresponding to one electron transfer per atom of Pt(111) surface (ca. 240 μC cm^{-2}) in order to deduce the number of electrons transferred per ammonia molecule and the coverage of the adsorbed product(s). The transfer of one, two or three electrons per ammonia molecule would correspond to the formation of an adsorbate adlayer with a coverage of ca. 0.6 ML (of $NH_{2(ads)}$), 0.3 ML (of $NH_{(ads)}$) and 0.2 ML (of $N_{(ads)}$), respectively. Strong lateral interactions between the reacting species, observed for ammonia oxidation in the double-layer region (see the subsection 6.3.1.2.), would exclude low coverage values. At the same time, the Tafel slope observed for feature E_{O1}^{111} (see subsection 6.3.1.3) suggests a multiple (at least two) electron transfer, leaving NH and N adsorbates as the most likely stable intermediates of ammonia dehydrogenation on Pt(111).

Figure 6.2 also shows that peaks E_{R3}^{111} and E_{R2}^{111} appear consecutively in the negative going scan with the increasing upper-potential limit of the corresponding CVs. This result suggests that the two features do not correspond to consecutive steps of a single multistep process. Figure 6.3 gives further support to this assumption. In this experiment we have first generated an adlayer of the products of ammonia oxidation in the double-layer region (feature E_{O1}) by keeping the potential at 0.65 V for ca. two minutes. Then, the electrode potential was stepped to 0.5 V for 5 seconds, followed by a complete stripping of the formed adsorbates (Figure 6.3, the bold solid line) or by performing two consecutive potential scans; the first was reversed at ca. 0.3 V (the dotted line) and the second was reversed at ca. 0.05 V (the thin solid line). The latter potentiodynamic program revealed that peaks E_{R2}^{111} and E_{R3}^{111} could be removed consecutively and (to some extent) independently. As an interpretation of this result, the two peaks may

correspond to the reductive stripping of species having somewhat different reactivity (and, as presented in the subsection 6.3.1.3, showing different kinetics).

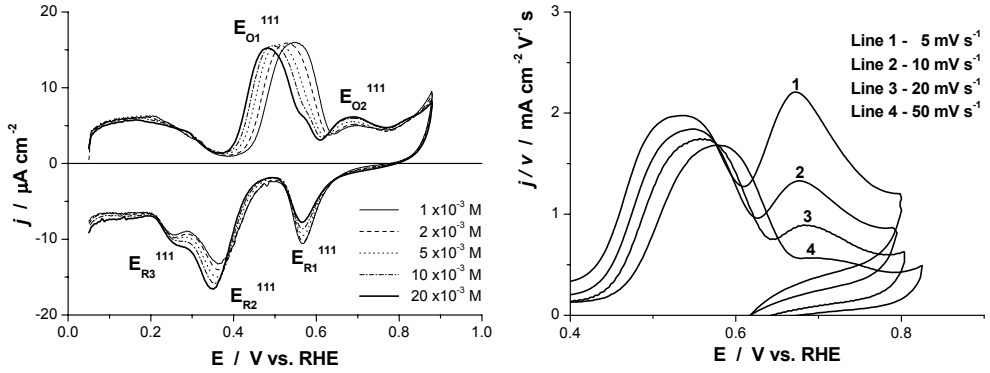

Figure 6.4. (left) Cyclic voltammograms recorded at Pt(111) electrode in 0.1 M NaOH in the presence of ammonia. Experimental conditions: starting potential 0.05 V; scan rate 10 mV s^{-1}; ammonia concentration is indicated in the legend of the figure.

Figure 6.5. (right) The scan-rate corrected cyclic voltammograms recorded at Pt(111) electrode in 0.1 M NaOH in the presence of ammonia. The CVs differ by the scan rate, as indicated by the numbers in the legend of the figure. Experimental conditions: starting potential 0.05 V; 1×10^{-3} M NH_3.

Figure 6.4 shows the effect of the ammonia concentration on the voltammetric profile recorded between 0.05 and 0.9 V. The increase of ammonia concentration does not result in a considerable increase of the current densities observed. Despite small changes, the voltammetric profile remains essentially the same. This result is in agreement with the earlier conclusion that all the voltammetric features observed in the presence of ammonia correspond to surface-confined processes. The observed changes must be related to the increasing ammonia (equilibrium) coverage with increasing concentration, as deduced from the negative shift of the peak E_{O1}^{111} position and slight increase of its charge, and, therefore, some increase of the coverage of the resulting adsorbed intermediates, as deduced form the change in the intensity of features E_{R2}^{111} and E_{R3}^{111}.

The positions of all the voltammetric features observed shift with the potential scan rate, which implies kinetic limitations. Figure 6.5 shows the voltammograms for ammonia oxidation at four different scan rates. The current density was corrected for the scan rate to facilitate the comparison of the relative intensities of the features E_{O1}^{111} and E_{O2}^{111}. An important observation here is that the relative height and the charge of peak E_{O2}^{111} (as compared to E_{O1}) increases with decreasing scan rate. This result indicates that peak E_{O2}^{111} corresponds to a

slow continuous process, which involves the adsorbed species formed from ammonia oxidation in the double-layer region (peak E_{O1}^{111}).

6.3.1.2. Chronoamperometry

We performed potential step experiments to examine the rate law(s) of ammonia oxidation as well as of the reductive stripping of the products of ammonia oxidation. Current transients provide more straightforward criteria for deducing the order of the reaction as well as for establishing the existence of (strong) lateral interactions, as compared to voltammetry. More specifically, a first-order reaction with insignificant lateral interactions between the (reacting) species would show an exponential decay, whereas a second order process would show a current transient with a maximum at half coverage.[28,29] If strong repulsive interactions exist between the (reacting) species, a first-order reaction would show a hyperbolic (t^{-1}) decay, whereas a second-order reaction would show a current transient with a maximum at coverages significantly higher than half coverage.[28,29] (See Chapter 3)

Figure 6.6 shows a current transient for the potential step from 0.4 V to 0.65 V (feature E_{O1}^{111}). The current transient shows a hyperbolic decay. The log-log plot shows a linear dependence over a wide time range with a slope very close to one. As shown elsewhere,[28] such a behavior indicates (i) (apparent) first-order kinetics and (ii) strong lateral (repulsive) interactions.

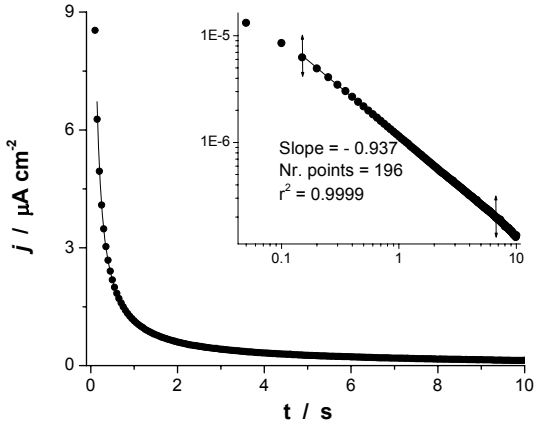

Figure 6.6. Current transients recorded at Pt(111) in 0.1 M NaOH in the presence of ammonia. The insert shows the corresponding log-log plot and the statistics of the least-square regression line. Experimental conditions: E_{in}=0.3 V, E_{step}=0.55 V; 5×10^{-3} M NH_3.

We have used chronoamperometry to investigate the processes corresponding to other features observed in the voltammetry of ammonia oxidation. Potential step experiments within the potential windows that include features E_{O2}^{111}, E_{R1}^{111}, E_{R2}^{111} and E_{R3}^{111}, showed exponential current decay only.

6.3.1.3. Tafel slope analysis

Figure 6.7 presents the results of a Tafel slope analysis. As shown elsewhere,[28,30,31] for complex surface-confined processes, such an analysis can be performed from a plot of the peak potential vs. the logarithm of the sweep rate. The observed slope was shown to be independent of the lateral interactions.[28]

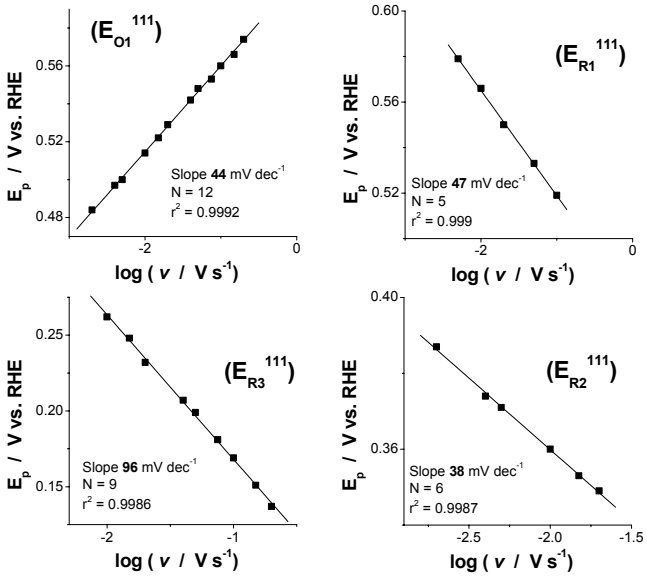

Figure 6.7. The results of the Tafel slope analysis of the voltammetric features observed in the CV recorded at Pt(111) in 0.1 M NaOH in the presence of ammonia. Exp. conditions: starting potential 0.05 V for analysis of anodic feature and 0.8 V for analysis of cathodic features; 5×10^{-3} M NH_3.

Feature E_{O1}^{111} shows a Tafel slope of 44 mV decade^{-1} (Figure 6.7) This value is reasonably close to the theoretical value of 40 mV decade^{-1}, typical for an electrochemical reaction involving at least two electron-transfer steps, the second electron transfer being the rate-determining step. Transfer of more than two electrons allows us to exclude the NH_2 adsorbate as the product of the process corresponding to feature E_{O1}^{111}. The Tafel slope values measured for the feature

E_{O2}^{111} ranged between ca. 20 mV decade^{-1} at low concentrations (1-5 mM) to almost 50 mV decade^{-1} at high concentrations (up to 20 mM), the linear regression statistics being quite poor in all cases (data not shown). The reduction features E_{R1}^{111} and E_{R2}^{111} shows the Tafel slopes of 47 and 38 mV decade^{-1}, respectively, which are still reasonably close to the value of 40 mV decade^{-1}. The Tafel slope observed for peak E_{R3}^{111} is significantly higher, close to 100 mV decade^{-1}. This result may indicate kinetic limitations related to the first electron transfer.

6.3.1.4. In situ infrared spectroscopy

The main goal of our in situ infrared spectroscopy measurements was the detection of the oxygen-containing products of ammonia oxidation in the potential region under investigation (0.05-0.9 V). Unfortunately, there is a strong overlap of the spectral regions, in which fundamentals of water and ammonia are observed.[32] Using deuterium oxide instead of water as a solvent does not result in a better separation of the fundamentals of the deuterated water and ammonia.[33] This fact, together with the exceeding water content, made it difficult to straightforwardly detect ammonia and detail on its consumption or formation with the applied potential. We have also examined the experimental data on the presence of any sign of the adsorbed NH_x (x=1-3) species, but could not isolate any clear-cut spectroscopic signatures of the above adsorbates.

Figure 6.8 shows the potential-difference spectra for ammonia oxidation, recorded with the p-polarized light and using water as solvent. As expected, the spectra show a relative increase of the water content in the thin layer with the increasing potential (Fig. 6.8A). This was deduced from a strong negative band (accumulation of species) at ca. 1650 cm^{-1}, which can be straightforwardly assigned to the water scissoring mode (δ_{HOH}). Figure 6.8B shows the spectral window between 3500 and 4000 cm^{-1}. We assign the strong positive band, corresponding to the consumption of species, at ca. 3710 cm^{-1} to the ν_{OH} mode of the solution OH^-. Accordingly, the position of this band is independent of the applied potential. Furthermore, this band was also observed in the absence of ammonia in solution. As can be deduced from the effect of the applied potential on the band intensity, moderate consumption of the hydroxyl anion in the 0.25-0.55 V region is followed by a significantly higher consumption of the hydroxyl in the 0.6-0.8 V. Such dependence was reproducibly observed in the presence of ammonia, but not in its absence, confirming that ammonia is oxidized in the entire potential region. Therefore, this dependence may reflect the trend of hydroxyl anion involvement in ammonia oxidation at different potentials. Most importantly, as is illustrated in Figure 6.8A, we never observed the presence of nitrous oxide, which

would have revealed itself by a (negative) band at ca. 2231 cm^{-1} (the asymmetric stretching mode). This result allows excluding nitrous oxide as the product of ammonia oxidation between ca. 0.05 and 0.9 V. This conclusion is in good agreement with the DEMS measurements by Vidal-Iglesias et al.[20], in which no N_2O formation was observed between 0.05 and 0.9 V.

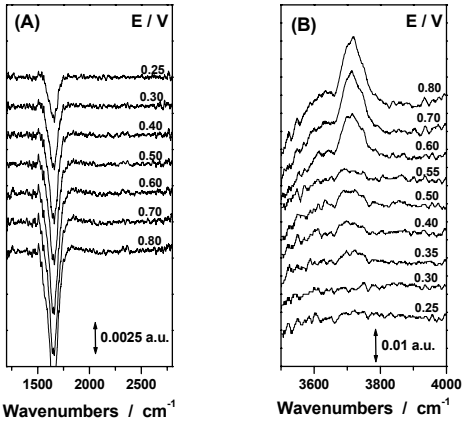

Figure 6.8. The potential difference infrared spectra for electrochemical oxidation of ammonia at Pt(111) in 0.1 M NaOH solution. Exp. conditions: 5×10^{-3} M NH_3; solvent – H_2O; the potential was increased in the positive-going direction; *p*-polarized light; E_R=0.2 V. The experiment was started at 0.2 V.

Figure 6.9 shows the potential-difference spectra for ammonia oxidation, recorded with the p-polarized light and using deuterium oxide as solvent. The deuterium oxide was used to shift the water bending mode to lower frequencies and in this way to clear the 1500-2000 cm^{-1} spectral region, in which the stretching modes of the adsorbed and solution NO species can be observed. We consider here the ν_{NO} mode between ca. 1480 and 1500 cm^{-1} of the 3-fold NO, which is observed at $\theta_{NO}\leq0.25$ ML;[34,35] then, the ν_{NO} mode between ca. 1650 and 1700 cm^{-1} of the atop NO, which is observed at $\theta_{NO}\geq0.25$ ML,[35] and the ν_{NO} mode at ca. 1870 cm^{-1} of NO in solution. No features observed in the 1500-1900 cm^{-1} spectral range could be assigned to NO species, either adsorbed or in solution. A broad negative band around 1500 cm^{-1} corresponds to a solution species (Figure 6.9A). Accordingly, its position and to a great extent its intensity do not depend on the applied position. This band was also observed in the absence of ammonia in solution. We assign this band to the δ_{HOD} mode in HOD species.[33] We have also performed experiments, in which a potential between 0.5 and 0.8 V was applied, then the electrode was pushed against the optical window, and then a series of spectra were recorded at

more negative potentials. Results of such an experiment are shown in Figure 6.9B. We never observed any spectroscopic evidence for the formation and then reductive stripping of the NO_{ads} species in these experiments, which strongly suggests that nitric oxide is not a stable intermediate (or product) of ammonia oxidation in the potential region considered. This conclusion is in agreement with the DEMS measurements by Vidal-Iglesias et al.[20], in which no NO (in solution) was detected in the 0.05-0.9 V range.

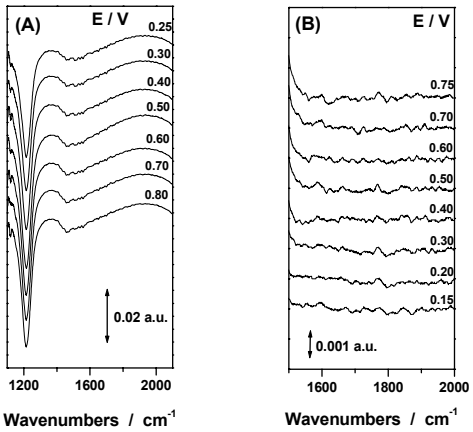

Figure 6.9. The potential-difference infrared spectra for electrochemical oxidation of ammonia at Pt(111) in 0.1 M NaOH solution. Exp. conditions: 5×10^{-3} M NH_3; solvent – D_2O; *p*-polarized light. (A) The experiment was started at 0.2 V. The potential was gradually increased; E_R=0.2 V. (B) The experiment was started at 0.8 V. The potential was gradually decreased in the negative-going direction; E_R=0.1 V.

6.3.2. Ammonia oxidation on Pt(100).

6.3.2.1 Cyclic voltammetry.

The blank CV of the Pt(100) electrode, shown in the insert of Figure 6.10, corresponds to a well-ordered Pt(100)-(1×1) surface and is stable for upper-potential limits up to 0.8 V. The CV of the Pt(100) electrode indicates that the H_{upd} region overlaps with the OH adsorption and desorption region. The local current minimum at ca. 0.43 V is taken in this work as the arbitrary boundary between the two regions. The charge obtained by integration between 0.1 and 0.7 V, and between 0.1 and 0.43 V, measured 250 μC cm^{-2} (Q_T^{100}) and 132 μC cm^{-2} (Q_H^{100}), respectively (after correction for the double-layer charging). The Q_H^{100} charge will

be used for calculating the coverage of the products of ammonia oxidation in the potential region between 0.1 and 0.43 V.

Figure 6.10 shows the voltammetry of the ammonia oxidation on Pt(100). The pair of peaks, E_{O1}^{100} at ca. 0.35 V and E_{R1}^{100} at ca. 0.32 V, observed in the H_{upd} region apparently corresponds to a surface-confined redox couple. Accordingly, the height of both peaks shows a linear increase with the potential sweep rate in a wide range of the scan rates (up to 1 V s^{-1}). The values of the corresponding slopes of the linear regression lines (in $\log(j_p) - \log(v)$ coordinates) were close to 1 (within 5% error). The linear regression analysis was applied to 15 experimental points and the square of the correlation coefficient (r^2) was at least 0.9998. The position of these peaks, but not that much the integrated charge, is slightly dependent on the ammonia concentration in solution, and independent of the upper-potential limit. The latter fact points to the formation of a stable and reproducible adlayer of the products of ammonia oxidation. The net charge under peaks E_{O1}^{100} and E_{R1}^{100} measures 63 μC cm^{-2} and 68 μC cm^{-2}, respectively, for the integration between 0.1 V and 0.43 V and after the correction for the hydrogen adsorption (Q_H^{100}). Comparing this charge with the charge corresponding to the transfer of one electron per one Pt atom of Pt(100) surface (210 μC cm^{-2}), we conclude that ammonia oxidation in the H_{upd} region involves a transfer of (approximately) one electron per three Pt atoms. Consequently, if the ammonia oxidation involves one electron transfer per molecule, the resulting coverage of the adsorbed product would be ca. 0.33 ML (of NH_2) , whereas for a two- and three-electron-transfer processes the coverage of the adsorbed products would be ca. 0.17 ML (of NH) and 0.11 ML (of N), respectively.

At potentials more positive than 0.5 V, ammonia is further oxidized in a fast continuous process (Figures 6.10). Previous studies indicated molecular nitrogen as the product of this process.[17,20] The DEMS measurements by Vidal-Iglesias et al.[20] also point to the formation of N_2O and some NO in solution, at potentials higher than ca. 0.7 V.

Our potentiodynamic measurements indicated no surface deactivation between 0.65 and 0.8 V. On the other hand, our steady-state current measurements (data not shown) indicated a slow surface deactivation in the same range of potentials, although the initial electrocatalytic activity, measured at 0.55 V, was recovered without the need of stepping to lower potentials.

6.3.2.2. Tafel slope analysis.

Figure 6.11 shows the results of the Tafel slope analysis of the peaks E_{O1}^{100} and E_{R1}^{100}. The corresponding peak potential vs. the logarithm of the sweep rate

dependences indicate a (electrochemically) quasi-reversible system, the linear relationship (the electrochemical irreversibility) being observed at scan rates higher than ca. 0.4 V s^{-1}. The values of the Tafel slope are ca. 100 mV $decade^{-1}$ and ca. 121 mV $decade^{-1}$ for E_{O1}^{100} and E_{R1}^{100}, respectively. These values suggest that the first electron transfer is the rate-determining step (theoretically 120 mV $decade^{-1}$) for both forward and back reactions. Moreover, the redox couple corresponding to peaks E_{O1}^{100} and E_{R1}^{100} seems to involve a single electron transfer (most probably combined with a proton transfer). First, we never observed any splitting of either peak with the increasing scan rate (up to 1 V s^{-1}), which would suggest complexity of the process, e.g. multiple steps. Second, if the reaction would involve more than one electron, than the coverage of the adsorbed products would be ca. 0.17 ML or lower, which seems unlikely.

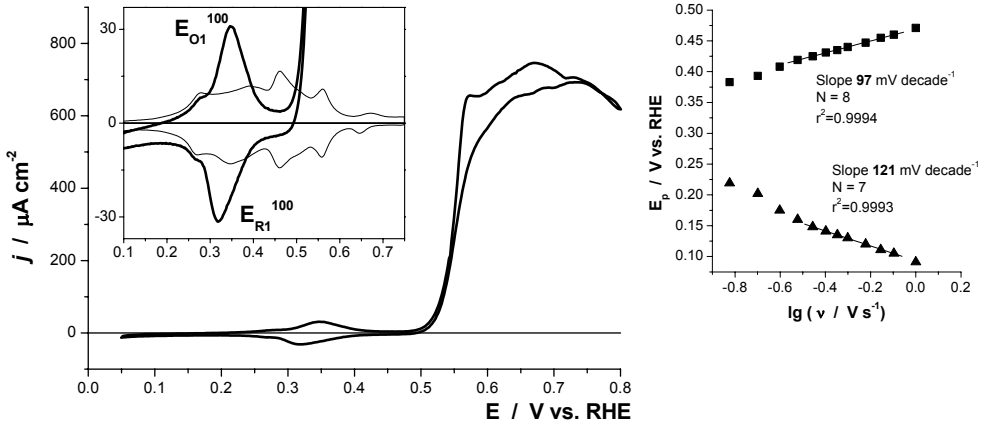

Figure 6.10. (left) Cyclic voltammograms recorded at Pt(100) electrode in 0.1 M NaOH in the absence of ammonia (solid line in the inset) and in the presence of ammonia (bold solid line). Experimental conditions: starting potential 0.05 V; scan rate 10 mV s^{-1}; 1×10^{-3} M NH_3.

Figure 6.11. (right) The results of the Tafel slope analysis of the voltammetric feature E_{O1}^{100} and E_{R1}^{100} observed in the CV recorded at Pt(100) in 0.1 M NaOH in the presence of ammonia. Experimental conditions: starting potential 0.05 V for analysis of anodic feature and 0.45 V for analysis of the cathodic feature; 5×10^{-3} M NH_3.

Figure 6.12 shows the polarization curve for ammonia oxidation at a low scan rate (2 mV s^{-1}). At such a slow scan rate the condition of (quasi-) reversibility should apply and the log (j) vs. E plot at the "foot" of the voltammetric wave should give the Tafel slope. The insert shows the result of the Tafel slope analysis at the foot of the wave. The semi-logarithmic plot is indeed linear in the potential

range between ca. 0.5 V and 0.54 V: the slope is ca. 30 mV decade^{-1} and is independent of the ammonia concentration (between 1×10^{-3} and 20×10^{-3} M NH_3) and of the scan rate (up to 10 mV s^{-1}).

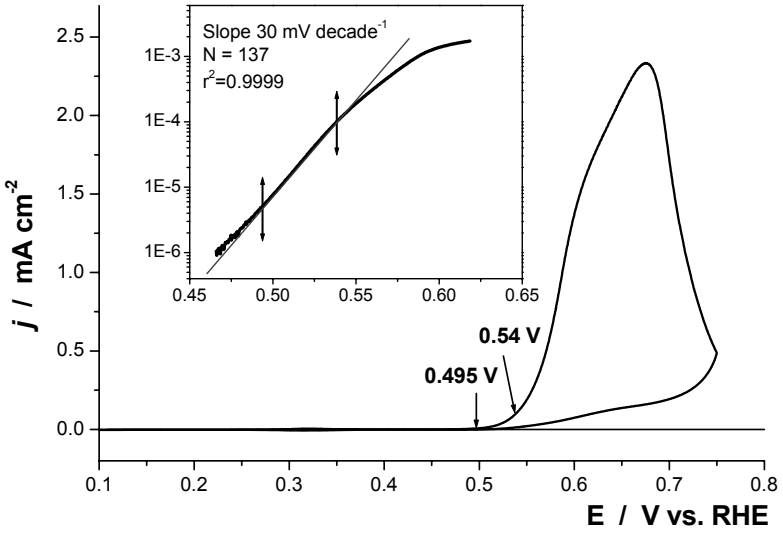

Figure 6.12. Cyclic voltammograms recorded at Pt(100) electrode in 0.1 M NaOH in the presence of ammonia. The insert shows the results of the Tafel slope analysis "at the foot" of the wave (see text for details). Experimental conditions: starting potential 0.05 V; scan rate 2 mV s^{-1}; 5×10^{-3} M NH_3.

6.3.3. Hydrazine oxidation on Pt(100).

This subsection describes the voltammetry and on-line mass spectrometry measurements of hydrazine oxidation on Pt(100) in alkaline media. It is beyond the scope of this chapter to address the electrochemical oxidation of hydrazine in detail. Instead, we shall point at several aspects of the hydrazine oxidation on Pt(100) that seem relevant for a better understanding of the mechanism of ammonia oxidation to dinitrogen on the same surface.

Figure 6.13 compares the electrochemical oxidation of ammonia and hydrazine on Pt(100) in alkaline media under the same experimental conditions. As an important observation, the hydrazine oxidation begins at ca. 0.15 V, which is ca. 400 mV more negatively than the onset of ammonia oxidation (ca. 0.5 V). The on-line electrochemical mass spectrometry measurements point to molecular nitrogen as the only product of hydrazine oxidation on Pt(100), at least under given

experimental conditions. Accordingly, the simultaneously recorded ionic current corresponding to m/z 28 (see the inset of Figure 6.13) indicates the formation of a considerable amount of molecular nitrogen. Next, we did not observe the formation of either NO, NO_2, or N_2O (m/z 30, 46, and 44, respectively) under the same experimental conditions. Finally, the electrooxidation of hydrazine on the Pt(111) surface is very similar to that on Pt(100), both with respect to the voltammetric response and the reaction products (data not shown).

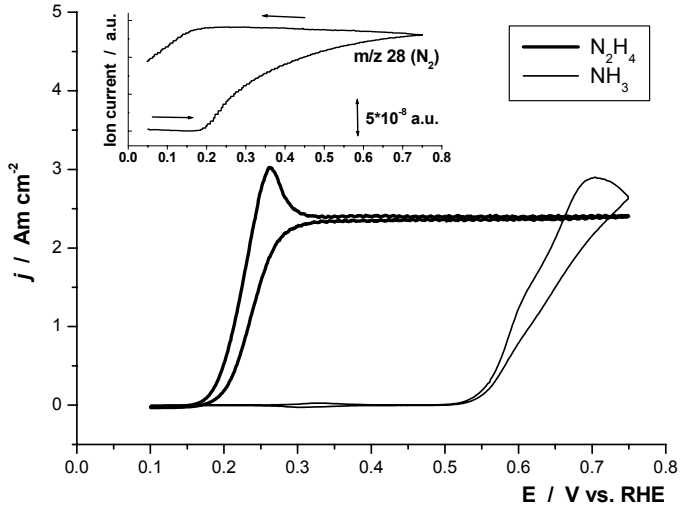

Figure 6.13. The electrochemical oxidation of ammonia (solid line) and hydrazine (bold solid line) on a Pt(100) electrode in alkaline media. Experimental conditions: 0.1 M NaOH; starting potential 0.1 V; scan rate 10 mV s^{-1}; 5×10^{-3} M NH_3 or N_2H_4. The inset shows the results of the on-line electrochemical mass spectrometry measurements for hydrazine oxidation on Pt(100) (experimental conditions – as above; for the details on the setup see section 4.2).

6.4. Discussion

Table 6.1 lists the adsorption energies and the surface configurations of NH_x fragments (x=0-2) on Pt(111), Pt(100), and Pt(110), as obtained from density functional theory (DFT) calculations.[36,37] As an interesting observation, the differences in the adsorption energy for atomic nitrogen on the three surfaces provide an explanation for a high activity of the Pt(100) surface. The energy of adsorption of the atomic nitrogen on Pt(100) is significantly lower, as compared to that on Pt(111) and Pt(110). The difference of ca. 0.3 eV (which is significant for

DFT calculations) corresponds to ca. three hundred millivolts in overpotential difference. The Gerischer-Mauerer mechanism, which found support in many recent studies on polycrystalline studies, identifies the atomic nitrogen as the catalyst poison, and not as the precursor to dinitrogen formation. Therefore, the above trend provides an explanation to the high activity of Pt(100), in the sense that Pt(100) should poison the least rapidly, and should be the most active. In the following, we will discuss how the experimental results in combination with the DFT results in Table 1 may help in identifying the key active intermediates in N_2 formation.

Table 6.1. Adsorption energies (in eV) of NH_x (x=0-2) at 0.25 ML.

Ref.	Species	**Pt (100)**	**Pt (111)**	**Pt (110)**
[36]	**NH_2**	–2.15 (on top) –3.14 (bridge)	–2.00 (on top) –2.47 (bridge)	-
	NH	–3.81 (bridge) –4.01 (hollow)	–4.24 (fcc-hollow) –3.84 (hcp-hollow)	-
	N	–4.40 (hollow)	–4.80 (fcc-hollow) –4.51 (hcp-hollow)	-
[37]	**N**	–3.95 (hollow) [a] –3.94 (bridge)	–4.32 (fcc-hollow) [a]	–4.39 (short bridge)

[a] We assume that the consistent difference of 0.45-0.5 eV between our results for N_{ads} and those from ref. 36 is related to the fact that the energy of isolated N was in our case calculated in the spin-unrestricted formalism.

6.4.1. Ammonia oxidation on Pt(111).

The experimental results for ammonia oxidation on Pt(111) allows us to draw the following picture of ammonia oxidation on Pt(111) (in the potential region between 0.05 and 0.9 V). Ammonia oxidation in the double-layer region is a surface-confined process (feature E_{O1}^{111}), resulting in the formation of an adlayer of adsorbed intermediates (NH and N). As an important indication of the mechanism of the reaction, the Tafel slope for E_{O1}^{111} (ca. 40 mV decade^{-1}) proves the involvement of a multielectron-transfer reaction. Additionally, the appreciable charge under the peak E_{O1}^{111} can be reasonably explained by the occurrence of a multielectron transfer. Therefore, we rule out the formation of (significant amounts) of the NH_2 adsorbate. On the basis of the above considerations, we propose the following mechanism for the process corresponding to peak E_{O1}^{111}:

$NH_3 + * \leftrightarrows NH_{3\,(ads)}$	equilibrium	(6.1)
$NH_{3\,(ads)} + HO^- \leftrightarrows NH_{2\,(ads)} + e^- + H_2O$	fast	(6.2)
$NH_{2\,(ads)} + HO^- \leftrightarrows NH_{(ads)} + e^- + H_2O$	rds	(6.3)
$NH_{(ads)} + HO^- \leftrightarrows N_{(ads)} + e^- + H_2O$	slow	(6.4)

The NH_2, NH, and N adsorbates were shown to be the intermediates of ammonia oxidation on Pt(111) in UHV.[38-40] These species are strongly adsorbed on Pt(111) surface, $NH_{(ads)}$ being particularly stable near room temperature (300-400 K).[38,40] The intermediates of ammonia oxidation can be stripped off reductively, complete stripping being achieved at 0.2 V or lower potentials. Ammonia oxidation on Pt(111) begins in the double-layer region (peak E_{O1}^{111}). Therefore, the oxidative adsorption of ammonia does not require coadsorbed hydroxyl, which is in disagreement with the Gerischer-Mauerer mechanism.

On the basis of the charge analysis, we conclude that the NH adsorbate is the dominant product of ammonia oxidation in the double-layer region. At the same time, the reductive stripping of the products of ammonia oxidation in this region shows a more complex picture. Features E_{R2}^{111} and E_{R3}^{111} do not seem to correspond to the consecutive steps of a single process. First, these two features can be removed consecutively and (to a great extent) independently. Second, they show different kinetics: feature E_{R2}^{111} has the Tafel slope of ca. 40 mV decade^{-1}, whereas feature E_{R3}^{111} has a significantly higher Tafel slope, ca. 100 mV decade^{-1}. These two observations can be explained by the formation and the reductive stripping of a single species (e.g., $NH_{(ads)}$) having different reactivity and kinetics. These differences can be determined by the fact that the species occupies different adsorption sites (see subsection 6.4.3). An alternative explanation is the formation and reductive stripping of two different species, e.g. coadsorbed NH and N fragments. These species are known to prefer different adsorption geometries and may, therefore, show different reactivity (see subsection 6.4.3).

In the potential region corresponding to OH adsorption (potentials more positive than 0.65 V), ammonia oxidation is strongly inhibited. The inhibition must be related to a blockage by a strongly adsorbed species, atomic nitrogen being the best candidate for that role. Therefore, we assume that the NH adsorbate could be further dehydrogenated to $N_{(ads)}$ at potentials more positive than ca. 0.65 V, e.g. according to reaction (6.4). Indeed, the progressive dehydrogenation of ammonia on Pt(111) is associated with increasing activation energy.[36,41] Therefore, the final dehydrogenation step may require high overpotentials, and possibly assistance by coadsorbed OH.

Feature E_{O2}^{111} corresponds to a continuous, although apparently very sluggish, process. The resulting adsorbate is a reducible species (feature E_{R1}^{111}).

Significantly, we have not observed the formation of any nitrous oxide in solution or nitric oxide, either in solution or adsorbed. Previous DEMS measurements on Pt(111) demonstrated the formation of small amounts of molecular nitrogen between ca. 0.7 and 0.9 V.[20] Therefore, we assume that molecular nitrogen is the product of the process corresponding to peak E_{O2}^{111}. We are not in a position to discuss details on the mechanism of this process: the results of the Tafel slope analysis of peak E_{O2} were inconclusive. Nevertheless, we can probably rule out the atomic mechanism of N_2 formation, that is, the recombination of two $N_{(ads)}$. Atomic nitrogen is strongly adsorbed in hollow sites; therefore its diffusion across the surface and reaction must be associated with high energetic barriers. On the contrary, we expect the atomic nitrogen to act as a catalyst poison. The previously proposed recombination of the NH_x surface species (x=1,2) (Gerischer-Mauerer mechanism) seem to be a more reasonable scenario, although we have no direct evidence for such a process. In some gas phase and UHV studies of ammonia oxidation at near-room temperature[38,42] (as well as nitric oxide reduction)[43] on Pt(111) at room temperature, the HNO adsorbate is suggested as an intermediate. Therefore, we would not rule out the possibility of a molecular mechanism of N_2 formation on Pt(111) involving formation of unstable oxygen-containing species. Irrespective of our inability to deduce the exact mechanism of that slow process, it seems reasonable to assume that the formation of N–O bond is very sluggish on Pt(111), even in the presence of coadsorbed OH.

6.4.2. Ammonia oxidation on Pt(100)

The oxidative adsorption of ammonia on Pt(100) electrode (peak E_{O1}^{100}) occurs at potentials corresponding to negligible OH (co)adsorption. The voltammetric data indicate a surface confined dehydrogenation step, involving the transfer of a single electron. Therefore, the reaction scheme (6.1-6.2) should apply to the first step of ammonia dehydrogenation on Pt(100) as well. The resulting NH_2 adsorbate may occupy the bridge site, by analogy with UHV and theoretical studies.[36,44] Interestingly, in a recent theoretical study it was predicted that on Pt(100) the NH_2 fragment should stabilize during ammonia reactions.[36]

The product of ammonia oxidation on Pt(100) between 0.5 and 0.65 V is molecular nitrogen.[17,20] Oxygen-containing species (NO, N_2O) are observed at more positive potentials.[20] The reaction takes place in the potential region corresponding to OH adsorption, although the exact role of the OH adsorbate is not clear. The Tafel slope measured at the foot of the wave (between ca. 0.5 and 0.55 V, Figure 6.12) is 30 mV decade^{-1}. The following tentative mechanism provides a simple explanation to the above value:

$NH_3 + * \leftrightarrows NH_{3\,(ads)}$	equilibrium	(6.5)
$NH_{3\,(ads)} + HO^- \leftrightarrows NH_{2\,(ads)} + e^- + H_2O$	fast	(6.6)
$2\,NH_{2\,(ads)} \rightarrow N_2H_{4\,(ads)}$	(rds)	(6.7)
$N_2H_{4\,(ads)} \rightarrow \ldots \rightarrow N_2 + 2*$	fast	(6.8)

We assume that the second reaction step is a chemical and the rate-determining step. This reaction scheme corresponds to the experimental Tafel slope of 30 mV decade^{-1}, as the rate-determining step is second order in the NH_2 coverage. This mechanism identifies (surface) hydrazine ($N_2H_{4\,(ads)}$) as the key precursor for dinitrogen formation, which seems to be a very plausible feature. Note, however, that a Tafel slope of 30 mV decade^{-1} in mechanism 6.3-6.8 would be obtained only if the NH_2 surface coverage follows Nernst's law. Figure 6.10 suggests that at the potential of N_2 formation, the NH_2 coverage is at saturation, and therefore, not potential dependent.

The fact that the formation of NH_2 adsorbate below ca. 0.5 V (feature E_{O1}[100]) does not result in immediate dimerization of this species may be related to an insufficient-coverage situation. If ammonia interacts non-reactively with the Pt(100) surfaces covered with NH_2 adlayer (at ca. 0.4 V), then we can assume that more positive potentials are required to activate ammonia and create the sufficient NH_2 coverage.

There have been numerous studies of the hydrazine oxidation on polycrystalline platinum, as well as on other electrode materials.[45,46] Most of the studies show that the hydrazine oxidation occurs at the N–H bond and not at the N–N bond, the dominant product being molecular nitrogen.[45] Mass spectrometry measurements using labeled hydrazine are particularly conclusive in this respect.[47,48] The mechanism of hydrazine oxidation to dinitrogen is commonly viewed as a stepwise electrocatalytic dehydrogenation process.[49,50] On polycrystalline platinum in contact with an alkaline solution, hydrazine reacts to dinitrogen at approximately 0.1 V vs. RHE,[49] that is, ca. 400 mV more negatively than ammonia oxidation to dinitrogen. The results on hydrazine oxidation presented in subsection 6.3.3 indicate that the above view is applicable to hydrazine oxidation on Pt(100) and Pt(111). As a key observation from the data on hydrazine oxidation, the decomposition of the surface-bonded hydrazine, which assumedly appears as an intermediate in ammonia oxidation to dinitrogen (reaction scheme 6.5-6.8), should not limit the overall reaction rate, thus leaving the dimerization of NH_2 species as a better candidate.

In the light of the above considerations, the surface-bonded hydrazine or, more generally, a hydrogenated N–N dimer seems to be a good candidate for being a key intermediate in the ammonia oxidation to dinitrogen.

6.4.3. Factors controlling the activity of NH_3 oxidation to N_2

In a recent detailed theoretical study, Novell-Leruth et al.[36] showed that the adsorption of ammonia (atop) and the NH_2 adsorbate (bridge) is more favorable on Pt(100) than on Pt(111), whereas the adsorption energies for NH and N fragments were quite similar (Table 6.1). The significantly lower energy of the NH_2 adsorbate on Pt(111), as compared with Pt(100), was attributed to different geometric and electronic factors associated with this adsorbate.[36] Therefore, the surface structure determines the most stable NH_x fragment: the NH_2 is stable on Pt(100) and NH is stable on Pt(111). Remarkably, the above trend, which is in reasonable agreement with the UHV data,[40,44] appears to apply to the reactions of ammonia in an electrochemical environment as well: our experimental data indicate that the NH_2 adsorbate is stabilized on Pt(100), whereas on Pt(111) the NH (and possibly $N_{(ads)}$) adsorbed species are stabilized at moderately oxidative potentials. Furthermore, we postulated the NH_2 adsorbate as the precursor for dinitrogen formation on Pt(100). The atomic nitrogen is likely to act as the catalyst poison, in accordance with the Gerischer-Mauerer formalism. Stabilization of NH adsorbate on Pt(111) does not seem to be enough to assure an appreciable activity for the production of dinitrogen.

The above findings point to the importance of an "early" stabilization of the products of ammonia dehydrogenation. Indeed, the deeper the level of dehydrogenation of ammonia, the higher the coordination (and, therefore, the adsorption energy, see Table 6.1) of the resulting species is, and the less favorable the formation of N–N bond is. Therefore, a high activity of Pt(100) surface in ammonia oxidation to molecular nitrogen could be related to the ability of this surface to stabilize the NH_2 fragment, which can dimerize to form surface-bonded hydrazine and then decay to dinitrogen in a surface reaction. Also, a relatively low affinity of Pt(100) for atomic nitrogen prevents poisoning of this surface at moderately oxidative potentials. On Pt(111), a deeper dehydrogenation of ammonia results in the formation of strongly adsorbed NH and N fragments, which seem to be unable to form dinitrogen at appreciable rates.

6.5. Summary and Conclusions

The electrocatalytic oxidation of ammonia on Pt(111) and Pt(100) electrodes was characterized by voltammetry, chronoamperometry and in situ infrared spectroscopy.

The initial stages of the electrochemical oxidation of ammonia on Pt(111) surface take place in the double-layer region, resulting in formation of NH and, possibly, N adsorbates. The initial stages of the electrochemical oxidation of

ammonia on Pt(100) surface take place in the H_{upd} region, resulting in the formation of NH_2 adsorbate. The above observations indicate that the adsorbed hydroxyl does not participate in the initial dehydrogenation steps on both surfaces examined. Stabilization of NH_2 adsorbate on Pt(100) and NH adsorbate on Pt(111) surfaces in ammonia oxidation under electrochemical conditions is an interesting similarity with ammonia oxidation in the gas phase or in UHV.

Neither nitrous oxide nor nitric oxide is the product of ammonia oxidation on Pt(111) between ca. 0.05 and 0.9 V, as deduced from the in situ infrared measurements. This result leaves N_2 as the likely product of ammonia oxidation in the OH adsorption region of potentials, that is, between ca. 0.65 and 0.9 V. At the same time, the dinitrogen formation on Pt(111) is a very sluggish process, thus indicating that neither NH nor N adsorbates can form dinitrogen at appreciable rates. A high activity of Pt(100) in ammonia oxidation to N_2 (between ca. 0.5 and 0.65 V) can be explained by the ability of this surface to stabilize the NH_2 adsorbate. In the tentative mechanism proposed here, two NH_2 fragments form surface-bonded hydrazine, which is rapidly dehydrogenated to dinitrogen.

References

(1) Wynveen, R. A. *Fuel Cells* **1963**, *2*, 153.
(2) Strickland, G. *J. Hydrogen Energy* **1984**, *9*, 759.
(3) Simons, E. L.; Cairns, E. J.; Surd, D. J. *J. Electrochem. Soc.* **1969**, *116*, 556.
(4) Vitse, F.; Cooper, M.; Botte, G. G. *J. Power Sources* **2005**, *142*, 18.
(5) Marincic, L.; Leitz, F. B. *J. Appl. Electrochem.* **1978**, *8*, 333.
(6) Feng, C.; Sugiura, N.; Shimada, S.; Maekawa, T. *J. Hazard. Mater.* **2003**, *103*, 65.
(7) Pfennig, D.-M.; Deprez, J.; Kitzelmann, D. *Ber. Bunsenges. Phys. Chem.* **1990**, *94*, 988.
(8) Lopez de Mishima, B. A.; Lescano, D.; Molina Holgado, T.; Mishima, H. T. *Electrochim. Acta* **1997**, *43*, 395.
(9) Oswin, H. G.; Salomon, M. *Can. J. Chem.* **1963**, *41*, 1686.
(10) Despic, A. R.; Drazic, D. M.; Rakin, P. M. *Electrochim. Acta* **1966**, *11*, 997.
(11) Gerischer, H.; Mauerer, A. *J. Electroanal. Chem.* **1970**, *25*, 421.
(12) Wasmus, S.; Vasini, E. J.; Krausa, M.; Mishima, H. T.; Vielstich, W. *Electrochim. Acta* **1994**, *39*, 23.
(13) Gootzen, J. F. E.; Wonders, A.; Visscher, W.; van Santen, R. A.; van Veen, J. A. R. *Electrochim. Acta* **1998**, *43*, 1851.
(14) de Vooys, A. C. A.; Koper, M. T. M.; van Santen, R. A.; van Veen, J. A. R. *J. Electroanal. Chem.* **2001**, *506*, 127.
(15) de Vooys, A. C. A.; Mrozek, M. F.; Koper, M. T. M.; Van Santen, R. A.; Van Veen, J. A. R.; Weaver, M. J. *Electrochem. Comm.* **2001**, *3*, 293.
(16) Endo, K.; Katayama, Y.; Miura, T. *Electrochim. Acta* **2005**, *50*, 2181.
(17) Gao, Y.; Kita, H.; Hattori, H. *Chem. Lett.* **1994**, *11*, 2093.
(18) Vidal-Iglesias, F. J.; Garcia-Araez, N.; Montiel, V.; Feliu, J. M.; Aldaz, A. *Electrochem. Comm.* **2003**, *5*, 22.

(19) Vidal-Iglesias, F. J.; Solla-Gullon, J.; Montiel, V.; Feliu, J. M.; Aldaz, A. *J. Phys. Chem. B* **2005**, *109*, 12914.
(20) Vidal-Iglesias, F. J. PhD thesis, Universidad de Alicante, 2005.
(21) Clavilier, J.; Armand, D.; Sun, S. G.; Petit, M. *J. Electroanal. Chem.* **1986**, *205*, 267.
(22) Iwasita, T.; Nart, F. C.; Vielstich, W. *Ber. Bunsenges. Phys. Chem.* **1990**, *94*, 1030.
(23) Clavilier, J.; Feliu, J. M.; Fernandez-Vega, A.; Aldaz, A. *J. Electroanal. Chem.* **1989**, *269*, 175.
(24) Rodes, A.; Clavilier, J.; Orts, J. M.; Feliu, J. M.; Aldaz, A. *J. Electroanal. Chem.* **1992**, *338*, 317.
(25) Al-Akl, A.; Attard, G. A.; Price, R.; Timothy, B. *J. Electroanal. Chem.* **1999**, *467*, 60.
(26) Lebedeva, N. P.; Koper, M. T. M.; Herrero, E.; Feliu, J. M.; van Santen, R. A. *J. Electroanal. Chem.* **2000**, *487*, 37.
(27) Lebedeva, N. P.; Rodes, A.; Feliu, J. M.; Koper, M. T. M.; van Santen, R. A. *J. Phys. Chem. B* **2002**, *106*, 9863.
(28) Koper, M. T. M. *Z. Phys. Chem.* **2003**, *217*, 547.
(29) Rosca, V.; Koper, M. T. M. *Surf. Sci.* **2005**, *584*, 258.
(30) Koper, M. T. M.; Jansen, A. P. J.; Santen van, R. A.; Lukkien, J. J.; Hilbers, P. A. J. *J. Chem. Phys.* **1998**, *109*, 6051.
(31) Christiansen, P. A.; Hamnett, A. *Techniques and Mechanisms in Electrochemistry*; Blackie Academic and Proffessional: Glasgow, 1994.
(32) Nakamoto, K. *Infrared and Raman Spectra of Inorganic and Coordination compounds*; John Wiley & Sons: New-York, 1986.
(33) Punchas, S.; Laulicht, I. *Infrared Spectra of Labelled Compounds*; Academic Press: London, 1971.
(34) Weaver, M. J.; Zou, S.; Tang, C. *J. Chem. Phys.* **1999**, *111*, 368.
(35) Rosca, V.; Beltramo, G. L.; Koper, M. T. M. *Langmuir* **2005**, *21*, 1448.
(36) Novell-Leruth, G.; Valcarcel, A.; Clotet, A.; Ricart, J. M.; Perez-Ramirez, J. *J. Phys. Chem. B* **2005**, *109*, 18061.
(37) Results of our own calculations. The computational details are essentially identical to those in ref. 36 (four-layers slab; 5x5x1 k-points; 400 eV energy cut-off). A (2x2) unit cell was considered with the adsorbate coverage of 1/4 ML. The important difference was that the energy of the N adsorbate was in our case calculated in the spin-unrestricted formalism.
(38) Smirnov, M. Y.; Gorodetskii, V. V.; Cholach, A. R. In *Fundamental Aspects of Heterogeneous Catalysis Studied by Particle Beams*; van Santen, R. A., Ed., 1991; pp 249.
(39) Mieher, W. D.; Ho, W. *Surf. Sci.* **1995**, *322*, 151.
(40) Sun, Y.-M.; Sloan, D.; Ihm, H.; White, J. M. *J. Vac. Sci. Technol.* **1996**, *14*, 1516.
(41) Fahmi, A.; van Santen, R. A. *Z. Phys. Chem.* **1996**, *197*, 203.
(42) Il'chenko, N. I. *Russ. Chem. Rev.* **1976**, *45*, 1119.
(43) Smirnov, M. Y.; Gorodetskii, V. V.; Block, J. H. *J. Mol. Catal. A: Chem.* **1996**, *107*, 359.
(44) Zemlyanov, D. Y.; Smirnov, M. Y.; Gorodetskii, V. V. *Surf. Sci.* **1997**, *391*, 37.
(45) Plieth, W. J. Encyclopedia of Electrochemistry of the Elements; Bard, A. J., Ed.; Marcel Dekker: New-York, 1978; Vol. 8.
(46) Fukumoto, Y.; Matsunaga, T.; Hayashi, T. *Electrochim. Acta* **1981**, *26*, 631.
(47) Schulz-Ekloff, G.; Baresel, D. *J. Electroanal. Chem.* **1972**, *35*, 73.
(48) Petek, M.; Bruckenstein, S. *J. Electroanal. Chem.* **1973**, *47*, 329.
(49) Harrison, J. A.; Khan, Z. A. *J. Electroanal. Chem.* **1970**, *26*, 1.
(50) Kodera, T.; Honda, M.; Kita, H. *Electrochim. Acta* **1985**, *30*, 669.

Summary

The mechanism and structure sensitivity of electrocatalytic reactions of nitric oxide, hydroxylamine, and ammonia on low-index single-crystal platinum electrodes were studied using electrochemical techniques, in situ Fourier transform reflection-absorption infrared spectroscopy (FTIRRAS), and on-line electrochemical mass spectrometry (OLEMS).

The main product of the reductive stripping of nitric oxide adlayers on platinum in acidic media is the ammonium cation, largely irrespective of the surface structure and the adsorbate coverage. The activity of platinum in the electrochemical reduction of adsorbed nitric oxide (NO_{ads}) is related to the coordination of NO_{ads}. As deduced from experiments on Pt(111), Pt(110), and Pt(100) surfaces, the reactivity of NO_{ads} species increases in the order NO_{atop}>NO_{bridge}>$NO_{3\text{-}fold\text{-}hollow}$. Difference in reactivity explains the appearance of multiple reduction features (peaks) in the stripping voltammetry of nitric oxide adlayers (Chapter 2).

The current transients recorded for NO_{ads} reduction on Pt(111) and Pt(110) indicate significant lateral (repulsive) interactions between the reacting species at high coverages of NO. The second-order kinetics observed for NO_{ads} reduction on Pt(110) in the limit of high coverages (ca. 1 ML) indicates the necessity of a neighboring free site, which is required most likely for breaking the N–O bond. Three fast (at equilibrium) combined electron and proton transfers precede the breaking of the N–O bond on Pt(110). The first-order kinetics was deduced from current transients recorded for NO_{ads} reduction on Pt(111) and Pt(100) at all coverages. Nevertheless, the apparent first-order kinetics can be related to a significantly lower saturation coverage of NO_{ads} on Pt(111) and Pt(100) (ca. 0.5 ML) as compared to that on Pt(110) (ca. 1 ML) and, therefore, to the availability of free sites at all coverages. A detailed mechanism of NO_{ads} reduction on Pt(110) was proposed (Chapter 3).

The reduction of NO_{ads} on Pt(100) follows an EC mechanism, in which the first electron/proton transfer is at equilibrium, resulting in the formation of HNO_{ads} intermediate, whereas the second reaction step is a chemical and the rate-determining step. This chemical step is assumed to involve the N–O bond breaking in the HNO_{ads} intermediate, which most probably requires a neighboring free site. From a comparison of NO_{ads} reduction on Pt(100), Pt(111), and Pt(110) it follows that (i) the reaction mechanism is structure sensitive and (ii) Pt(100) is the most active surface for breaking the N–O bond, which is in agreement with the trend observed under UHV conditions (Chapter 4).

The reactivity of hydroxylamine (HAM) at platinum electrodes is controlled by the interaction of the other components of the solution or products of the HAM oxidation with the electrode surface. Reduction of HAM to ammonia is a structure sensitive reaction, at least through the structure sensitivity of the hydrogen adsorption on platinum. Voltammetric data for Pt(111), Pt(110), and Pt(100) indicate the possibility of the HAM reduction and oxidation to occur simultaneously. This observation was tentatively explained by the existence of an intermediate, which appears both in the reduction and oxidation processes. Moreover, the reduction of HAM is likely to be activated by a dehydrogenation step. H_2NO_{ads} and HNO_{ads} species were suggested as candidates. Adsorbed nitric oxide (NO_{ads}) was demonstrated to be the key intermediate in the oxidation of HAM. Being electrochemically stable in a wide potential region, NO_{ads} acts as a poison in continuous oxidation of HAM. The HAM oxidation to NO_{ads} appears to be a structure-insensitive process, though somewhat affected by the anion coadsorption. The formation of N_2O at moderately oxidative potentials (below ca. 0.9 V vs. RHE) was observed for HAM oxidation at Pt(111) and Pt(110), but not at Pt(100). Mechanisms for the reduction and oxidation of HAM are proposed (Chapter 5).

The oxidative adsorption of ammonia on Pt(100) and Pt(111) in alkaline media results in the formation of NH_x (x=0-2) adsorbates. On Pt(111), ammonia oxidation occurs in the double-layer region and results in the formation of NH and, possibly, N adsorbates. On Pt(100), the NH_2 adsorbed fragment is the stable intermediate of ammonia oxidation. Interestingly, stabilization of NH and NH_2 fragments on Pt(111) and Pt(100), respectively, is in agreement with recent theoretical predictions. The Pt(111) surface shows extremely low activity for ammonia oxidation to dinitrogen, thus indicating that neither NH nor N (strongly) adsorbed species are active in dinitrogen production. Neither nitrous oxide nor nitric oxide is the product of ammonia oxidation on Pt(111) at potentials up to 0.9 V vs. RHE, as deduced from the in situ infrared measurements. The Pt(100) surface is highly active for dinitrogen production. This process is characterized by a Tafel slope of 30 mV $decade^{-1}$, which was explained by a rate-determining dimerization of NH_2 fragments followed by a fast decay of the resulted surface-bound hydrazine to molecular nitrogen. Therefore, a high activity of the Pt(100) surface in ammonia oxidation to molecular nitrogen is likely to be related to its ability to stabilize the NH_2 adsorbate (Chapter 6).

Samenvatting

Het mechanisme en de structuurgevoeligheid van de elektrokatalytische reacties van stikstofoxide, hydroxylamine en ammoniak op lage index eenkristal platina elektroden werden onderzocht m.b.v. elektrochemische technieken, in situ Fourier getransformeerde reflectie-absorptie infrarood spectroscopie (FTIRRAS) en on-line elektrochemische massa spectrometrie (OLEMS).

Het hoofdproduct van reducerend strippen van stikstofoxide adlagen op platina in zure oplossing is het ammonium kation, dat grotendeels onafhankelijk van de structuur van het oppervlak en de bedekkingsgraad van het adsorbaat gevormd wordt. De activiteit van platina in de elektrochemische reduktie van geadsorbeerd stikstofoxide (NO_{ads}) is gerelateerd aan de coördinatie van NO_{ads}. Zoals werd herleid uit experimenten aan Pt(111), Pt(110) en Pt(100) oppervlakken, neemt de reactiviteit van NO_{ads} toe in de orde van NO_{stap}>NO_{brug}>$NO_{drievoudig}$. Deze reactiviteitsdifferentiatie verklaart de verschijning van meerdere reductie-kenmerken (pieken) in de "stripping voltammetry" van stikstofoxide adlagen (Hoofdstuk 2).

De stroom-tijd curves gemeten voor de reductie van NO_{ads} aan Pt(111) en Pt(110) laten bij hoge bedekkingsgraden van NO_{ads} significante laterale (repulsive) interacties tussen de reagerende species zien. De tweede-orde reactiekinetiek, waargenomen voor NO_{ads} reductie aan Pt(110) bij hoge bedekkingsgraad (ca. 1 ML), geeft de noodzakelijkheid aan van een aangrenzende vrije site, die hoogstwaarschijnlijk nodig is voor het breken van de N–O binding. Drie snelle gecombineerde elektron- en protonoverdrachten (in evenwicht) gaan vooraf aan het breken van de N–O binding op Pt(110). De eerste-orde kinetiek werd herleid uit stroom-tijd curves gemeten voor de reductie van NO_{ads} aan Pt(111) en Pt(110) bij alle bedekkingsgraden. Desalniettemin kan de ogenschijnlijke eersteorde kinetiek gerelateerd worden aan een significant lagere maximale bedekkingsgraad van NO_{ads} op Pt(111) en Pt(100) (ca. 0.5 ML) vergeleken met die op Pt(110) (ca. 1 ML), en derhalve aan de beschikbaarheid van vrije sites bij alle bedekkingsgraden. Een gedetailleerd mechanisme van de NO_{ads} reductie aan Pt(110) werd voorgesteld (Hoofdstuk 3).

De reductie van NO_{ads} aan Pt(100) volgt een "EC" mechanisme, waarbij de eerste elektron/proton overdracht in evenwicht is, resulterend in de vorming van een HNO_{ads} intermediair, met de tweede chemische reactiestap als snelheidsbepalende stap. Bij deze chemische stap wordt het breken van de N–O binding in het HNO_{ads} intermediair verondersteld, wat waarschijnlijk een naburige vrije site nodig heeft. Uit een vergelijking van de NO_{ads} reductie aan Pt(100), Pt(111) en Pt(100) kan geconcludeerd worden dat (i) het reactiemechanisme

structuurgevoelig is en (ii) dat Pt(100) het meest actieve oppervlak is voor het breken van de N–O binding, wat in overeenstemming is met de onder ultra-hoog vacuum condities waargenomen trend (Hoofdstuk 4).

De reactiviteit van hydroxylamine (HAM) aan platina elektroden wordt bepaald door de interactie van de andere componenten van de oplossing of producten van de HAM oxidatie met het elektrodeoppervlak. Reductie van HAM naar ammoniak is een structuurgevoelige reactie, op zijn minst door de structuurgevoeligheid van de waterstof adsorptie op platina. Voltammetrische data voor Pt(111), Pt(110) en Pt(100) geeft de mogelijkheid weer van gelijktijdige HAM reductie en oxidatie. Dit waarneming werd tentatief uitgelegd door het bestaan van een intermediair, dat zowel in het reductie- als oxidatieproces een rol vervult. Bovendien wordt de reductie van HAM waarschijnlijk geactiveerd door een dehydrogenatiestap. H_2NO_{ads} en HNO_{ads} species werden gesuggereerd als kandidaten. Geadsorbeerd stikstofoxide (NO_{ads}) werd aangetoond als het belangrijkste intermediair in de oxidatie van HAM. Omdat NO_{ads} elektrochemisch stabiel is over een breed potentiaal gebied, gedraagt het zich als een gif voor de verdere oxidatie van HAM. De HAM oxidatie naar NO_{ads} lijkt een structuurongevoelig proces te zijn, ofschoon enigszins beïnvloedbaar door anion adsorptie. De vorming van N_2O bij matig oxidatieve potentialen (beneden ca. 0.9 V versus RHE) werd waargenomen tijdens de oxidatie van HAM aan Pt(111) en Pt(110), maar niet aan Pt(100). Mechanismen voor de reductie en oxidatie van HAM worden voorgesteld (Hoofdstuk 5).

De oxidatieve adsorptie van ammoniak aan Pt(100) en Pt(111) in alkalische media resulteert in de vorming van NH_x (x=0-2) adsorbaten. Aan Pt(111) vindt de ammoniak oxidatie plaats in het dubbellaag gebied en leidt tot de vorming van NH en, mogelijkerwijs, N adsorbaten. Aan Pt(100) is het NH_2 fragment een stabiel intermediair van de ammonia oxidatie. Stabilisatie van NH en NH_2 fragmenten op Pt(111) en Pt(100), respectievelijk, is, interessant genoeg, in overeenstemming met recente theoretische berekeningen. Het Pt(111) oppervlak laat een extreem lage activiteit zien voor de ammonia oxidatie naar moleculair stikstof, wat aangeeft dat de (sterk) geadsorbeerde species NH en N beide niet actief zijn in de stikstof vorming. Zowel N_2O (lachgas) als stikstofoxide worden niet waargenomen tijdens de ammoniak oxidatie aan Pt(111) bij potentialen tot 0.9 V vs. RHE, zoals herleid uit in situ infrarood metingen. Het Pt(100) oppervlak is zeer actief voor de stikstof productie. Dit proces wordt gekarakteriseerd door een Tafel helling van 30 mV $decade^{-1}$, wat wordt verklaard door een snelheidsbepalende dimerisatie van NH_2 fragmenten, gevolgd door een snel verval van de oppervlaktegebonden hydrazine tot stikstof. Derhalve is de hoge activiteit van het Pt(100) oppervlak voor de ammoniak oxidatie naar stikstof waarschijnlijk gerelateerd aan de mate waarin het oppervlak in staat is om het NH_2 adsorbaat te stabiliseren.

Rezumat

Mecanismul reacţiilor electrocatalitice ale monoxidului de azot, hidroxilaminei şi amoniacului şi dependenţa lor de structura suprafeţei au fost studiate pe suprafeţe monocristaline principale ale platinei, utilizând metode electrochimice, spectroscopia în infraroşu de reflexie-absorbţie cu trasformata Fourier (FTIRRAS) şi spectrometria de masă electrochimică (OLEMS).

Produsul de bază al stripării reductive a stratului adsorbit de monoxid de azot pe suprafeţe platinice este cationul de amoniu, indiferent de structura suprafeţei si acoperirea adsorbatului. Activitatea electrochimică a platinei în procesul de reducere a monoxidului de azot in starea adsorbită (NO_{ads}), este strâns legată de numărul de coordonare al adsorbatului. Experimentele pe suprafeţe principale – Pt(111), Pt(110) si Pt(100) – au demonstrat că reactivitatea speciilor NO_{ads} scade cu creşterea numarului de coordonare ($NO_{monocoord}$>$NO_{bicoord}$>$NO_{tricoord}$). Reactivitatea diferită explică apariţia vârfurilor succesive de reducere în voltametria de stripare a monostraturilor de NO_{ads} (Capitolul 2).

În cazul reducerii monostratului de NO_{ads} cu acoperire mare a suprafeţelor Pt(111) şi Pt(110), răspunsul cronoamperometric indică existenţa interacţiunilor laterale de repulsie între speciile adsorbite. Cinetica de ordinul doi, observată în cazul reducerii monostratului de NO_{ads} cu acoperire mare a suprafeţei Pt(110), se explică prin implicarea în scindarea legăturii N–O a unui centru liber de adsorbţie adiacent. Trei etape rapide (de echilibru) de transfer combinat de electron şi proton preced scindarea legăturii N–O pe suprafaţa Pt(110). Cinetica de ordinul unu a fost evidenţiată pentru reducerea monostratului de NO_{ads} pe suprafeţe Pt(111) şi Pt(100), indiferent de valoarea acoperirii. Totodată, acoperirea la saturaţie a NO_{ads}-ului pe suprafeţe Pt(111) (ca. 0.5 ML) şi Pt(100) (ca. 0.5 ML) este mult mai mică decât pe suprafaţa Pt(110) (ca. 1 ML). În consecinţă, acea poziţie liberă de adsorbţie necesară pentru scindarea legăturii N–O poate fi accesibil pe suprafeţele Pt(111) si Pt(100) la toate valorile acoperirii suprafeţei (Capitolul 3).

Reducerea NO_{ads} pe suprafaţa Pt(100) urmează un mecanism de reacţie de tip EC, în care prima etapă este un transfer rapid (la echilibru) de electron şi proton, din care rezultă intermediarul HNO_{ads}. Etapa a doua este o etapă chimică, fiind şi etapa determinantă de viteză. Se presupune că această etapă implică scindarea legăturii N–O în intermediarul HNO_{ads} şi probabil necesită o poziţie liberă de adsorbţie adiacentă. O comparaţie a reducerii NO_{ads} pe suprafeţele Pt(111), Pt(110) şi Pt(100) arată că (i) mecanismul de reacţie depinde de structura suprafeţei şi că (ii) suprafaţa Pt(100) este cea mai activă în scindarea legăturii N–O dintre toate

suprafețele, fapt care este în bun acord cu tendința similară observată în studii în vid înalt (Capitolul 5).

Reactivitatea hidroxilaminei pe electrozi de platină este controlată de interacțiuni ale altor componenți din soluție sau ale produşilor de oxidare a hidroxilaminei cu suprafața electrodului. Reducerea hidroxilaminei la cationul de amoniu este o reacție dependentă de structura suprafeței electrodului, cel puțin prin efectul structurii suprafeței asupra adsorbției hidrogenului. Rezultatele voltametriei indică posibilitatea unei desfăşurări simultane a reducerii şi oxidării hidroxilaminei pe cele trei suprafețe studiate – Pt(111), Pt(110) si Pt(100). Această observație poate fi explicată prin existența unui intermediar comun, care figurează atât în procesul de oxidare cât şi în cel de reducere. Specii ca H_2NO_{ads} si HNO_{ads} sunt propuse drept candidați pentru acel rol de intermediar comun. Monoxidul de azot în stare adsorbită este intermediarul stabil cheie în oxidarea hidroxilaminei pe suprafețe platinice. NO_{ads} este electrochimic stabil într-un domeniu larg de potențiale şi, în consecință, acționează drept otravă pentru catalizator. Procesul de oxidare a hidroxilaminei la NO_{ads} nu este afectat de structura suprafeței, însă este afectat de adsorbția de anioni. Oxidarea hidroxilaminei pe suprafețele Pt(111) şi Pt(110), însa nu şi pe Pt(100), este însoțită de formarea protoxidului de azot (N_2O) la potențiale moderate de oxidare (mai negativ de 0.9 V). În final, sunt propuse mecanismele reacțiilor de oxidare şi reducere a hidroxilaminei (Capitolul 5).

Prin oxidarea electrocatalitică a amoniacului pe suprafețele Pt(100) şi Pt(111) în mediu alcalin rezultă speciile adsorbite de tip NH_x (x=0-2). Oxidarea amoniacului pe suprafața Pt(111) are loc la potențiale corespunzătoare încărcării stratului dublu electric şi este soldată cu formarea speciilor adsorbite NH şi, posibil, N. Pe suprafața Pt(100) adsorbatul NH_2 este intermediarul stabil. Este interesant de menționat că stabilizarea adsorbatului NH pe suprafața Pt(111) şi adsorbatului NH_2 pe suprfața Pt(100) este în acord cu prezicerile teoretice recente. Suprafața Pt(111) este practic inactivă pentru oxidarea amoniacului la azot molecular. Astfel, atât adsorbatul NH cât şi adsorbatul N sunt inactivi în formarea azotului molecular. Măsuratori in situ de spectroscopie în infraroşu au permis excluderea atât a monoxidului de azot cât şi a protoxidului de azot din produşii de oxidare a amoniacului pe suprafața Pt(111). Suprafața Pt(100) este exceptional de activă în oxidarea amoniacului la azot molecular. Acest proces este caracterizat prin panta Tafel de 30 mV, care poate fi explicată prin desfăşurarea unui proces al carui viteză este limitată de dimerizarea speciilor NH_2 pe suprfața electrodului şi ulterioara descompunere a hidrazinei formate în azot molecular. În concluzie, activitatea de excepție a suprafeței Pt(100) în oxidarea electrocatalitică a amoniacului la azot molecular se poate atribui capacității sale de a stabiliza adsorbatul NH_2 (Capitolul 6).

Резюме

Механизм электрохимических превращений монооксида азота, гидроксиламина и аммиака на монокристаллах платины, а также влияние структуры поверхности электрода, были исследованы с помощью электрохимических методов, in situ инфракрасной спектроскопии и электрохимической масс-спектрометрии.

Основным продуктом элетрохимического восстановления адсорбированного слоя NO ($NO_{адс}$) на платине в кислой среде является катион аммония вне зависимости от структуры и степени заполнения поверхности. Активность платины в восстановлении $NO_{адс}$ напрямую зависит от координационной насыщености адсорбата. На основании экспериментальных данных полученных для монокристаллов Pt(111), Pt(110) и Pt(100) было установлено, что перенапряжение восстановления $NO_{адс}$ увеличивается в следующем порядке: $NO_{монокоорд}<NO_{бикоорд}<NO_{трикоорд}$. Это различие в реакционной способности адсорбированных молекул NO объясняет появление пиков восстановления на соответствующих вольтамперных кривых (Глава 2).

По данным хроноамперометрии, электрохимическое восстановление $NO_{адс}$ при высоком или максимальном поверхностном заполнении (до 1 ML) на кристалле Pt(110) характеризуется кинетикой второго порядка по $NO_{адс}$ и значительным отталкивающим взаимодействием между частицами адсорбата. Кинетика второго порядка объяснена участием дополнительного адсорбционного места, по всей вероятности, в разрыве связи N–O. Показано, что реакция включает три последовательные равновесные стадии переноса электрона (и протона) и последующую медленную стадию разрыва связи N–O. Восстановление $NO_{адс}$ на монокристаллах Pt(111) и Pt(100) характеризуется кинетикой первого порядка по $NO_{адс}$, независимо от степени заполнения поверхности. Кинетика первого порядка объяснена значительно более низкими значениями максимального поверхностного заполнения $NO_{адс}$ на Pt(111) (около 0.5 ML) и Pt(100) (около 0.5 ML), чем на Pt(110) (до 1 ML) и, соответственно, достаточным количеством дополнительных адсорбционных мест при любых степенях заполнения. Предложен детальный механизм электрохимического восстановления $NO_{адс}$ на монокристалле Pt(110) (Глава 3).

Электрохимическое восстановление $NO_{адс}$ на монокристалле Pt(100) включает равновесный перенос электрона (и протона) и последующую

медленную химическую стадию. Предположительно, эта химическая стадия включает разрыв связи N–O в адсорбированном интермедиате HNO (или NOH) и предусматривает участие дополнительного адсорбционного места. Сравнение механизмов восстановления $NO_{адс}$ на монокристаллах Pt(111), Pt(110) и Pt(100) позволило установить, что механизм реакции зависит от структуры поверхности. Кроме того, установлено, что плоскость (100) является наиболее активной в разрыве связи N–O, что хорошо согласуется с данными, полученными при изучении восстановления $NO_{адс}$ в высоком вакууме (Глава 4).

Электрохимические превращения гидроксиламина на платиновых электродах в значительной степени контролируются взаимодействием компонентов раствора или продуктов окисления гидроксиламина с поверхностью электрода. Восстановление гидроксиламина до аммиака является структурно-чувствительной реакцией, по крайней мере опосредовано, из-за структурно-чувствительной адсорбции водорода. На основе данных вольтамперометрии, полученных на монокристаллах Pt(111), Pt(110) и Pt(100), было установлено, что электрохимическое окисление и восстановление гидроксиламина могут протекать одновременно. Это наблюдение указывает на возможность существования интермедиата, общего для реакций окисления и восстановления. Адсорбированные частицы H_2NO и HNO предложенны в качестве кандидатов. Частичная дегидрогенизация гидроксиламина вероятно необходима для инициации его полного восстановления. Адсорбированный NO является ключевым стабильным интермедиатом окисления гидроксиламина на платине. Поскольку адсорбированные слои NO проявляют электрохимическую стабильность в широкой области потенциалов, $NO_{адс}$ представляет собой каталитический яд для последующего окисления гидроксиламина. Установлено, что окисление гидроксиламина до $NO_{адс}$ не является структурно-чувствительным процессом, хотя специфическая адсорбция анионов оказывает влияние на адсорбцию NO. Образование закиси азота (N_2O) наблюдается на монокристаллах Pt(111) и Pt(110), но не на монокристалле Pt(100). Предложен детальный механизм электрохимического окисления и восстановления гидроксиламина на платине (Глава 5).

Электрохимическое окисление аммиака в щелочной среде на монокристаллах Pt(111) и Pt(100) приводит вначале к образованию адсорбатов с общей формулой NH_x (x=1-2). Установлено, что на Pt(111) анодная адсорбция аммиака происходит в области потенциалов соответствующих заряжению двойного электрического слоя, и приводит к образованию адсорбированной частицы NH и, возможно, N. В случае

окисления аммиака на монокристалле Pt(100), адсорбированный NH_2 является стабильным интермедиатом. Стабилизация адсорбированного фрагмента NH на Pt(111) и NH_2 на Pt(100) согласуется с недавно опубликованными теоретическими данными. Монокристалл Pt(111) проявляет крайне низкую активность в окислении аммиака до молекулярного азота, что указывает на низкую реакционную способность $NH_{адс}$ и $N_{адс}$. По данным in situ ИК-спектроскопии установлено, что N_2O и NO не являются продуктами окисления аммиака на Pt(111) в области умеренных перенапряжений окисления (до 900 мВ). Монокристалл Pt(100) чрезвычайно активен в реакции окисления аммиака до молекулярного азота. Тафелевский наклон составляет 30 мВ, что вероятно объясняется наличием медленной стадии димеризации адсорбированного NH_2 и последующим быстрым распадом образовавшегося димера до молекулярного азота. В соответствии с предложенным механизмом, высокая активность монокристалла Pt(100) в образовании молекулярного азота объясняется способностью этой плоскости к стабилизации адсорбированного NH_2 (Глава 6).

List of Publications

Rosca, V.; Koper, M.T.M. Mechanism of electrocatalytic reduction of nitric oxide on Pt(100) surface. *J. Phys. Chem. B* **2005**, *109*, 16750.

Rosca, V.; Koper, M.T.M. Rate laws for reductive stripping of NO adlayers at single-crystal platinum electrodes as deduced from transient experiments. *Surf. Sci.* **2005**, *584*, 258.

Rosca, V.; Beltramo, G.L.; Koper, M.T.M. Reduction of NO adlayers on Pt(110) and Pt(111) in acidic media: evidence for adsorption site - specific reduction. *Langmuir* **2005**, *21*, 1448.

Rosca, V.; Beltramo, G.L.; Koper, M.T.M. Hydroxylamine electrochemistry at low-index single-crystal platinum electrodes in acidic media. *J. Phys. Chem. B* **2004**, *108*, 8294.

Rosca, V.; Beltramo, G.L.; Koper, M.T.M. Hydroxylamine electrochemistry at polycrystalline platinum in acidic media: a voltammetric, DEMS and FTIR study. *J. Electroanal. Chem.* **2004**, *566*, 53.

Rosca, V.; Koper, M. T. M. Electrocatalytic oxidation of ammonia on Pt(111) and Pt(100) surfaces., manuscript in preparation.

Dima, G.E.; Rosca, V.; Koper, M.T.M. Role of promoters in electrocatalysis. Nitrate reduction at Pt/Ge electrode in acidic media. *J. Electroanal. Chem.*, in press.

Wonders, A.H.; Housmans, T.H.M.; Rosca, V.; Koper, M.T.M. On-line mass spectrometry system for measurements at single-crystal electrodes in hanging meniscus configuration. *J. Appl. Electrochem.*, in press.

Rosca, V.; Popescu, I.C. Kinetic analysis of horseradish peroxidase 'wiring' in polyelectrolyte-peroxidase multilayer assemblies. *Electrochem. Comm.* **2002**, *4*, 904.

Rosca, V.; Muresan, L.; Popescu, I.C.; Cristea, C.; Silberg, I.A. Gold electrodes modified with 16H-dibenzo[c,l]-7,9-dithia-16,18-diazapentacene for electrocatalytic oxidation of NADH. *Electrochem. Comm.* **2001**, *3*, 439.

Acknowledgements

I am grateful to my supervisors, Prof. Rutger A. van Santen and Prof. Marc T.M. Koper, for giving me a unique opportunity to study and work in Eindhoven. I would like to thank Marc, my daily supervisor, for guidance, so many helpful discussions, and, importantly, criticism.

A significant part of the work presented in this thesis was done in collaboration with Dr. Guillermo L. Beltramo. Guillermo, thank you for many interesting discussions we had (and are still having) and for a very helpful introduction into the practice of in-situ spectroscopy of electrode surfaces. My special thanks to Natalia (Dr. N.P. Lebedeva) and to Guillermo for giving me the invaluable lessons in (meta)physics and (al)chemistry of single-crystal electrodes.

Several members of the technical staff supported my work. I thank Ad Wonders for making possible the mass spectrometry measurements; Jos van Wolput for assistance in my first in situ infrared measurements; both Ad Wonders and Martin Otten for help in dealing with everyday laboratory issues. I would like to acknowledge the professionalism and cooperation of the glassblower team (Frans Kuijpers et al.) and the precise instrumentation team (Jos de Laat et al.), who dealt so well with the versatility and obscurity of my orders.

I thank members of the doctorate committee for their comments and suggestions, which were helpful in improving the text of this thesis.

My complements to the members of the scientific as well as of the supporting staff of SKA for creating such a stimulating and friendly working environment. I thank all the former and current members of the department for their help, occasional corridor chat or for a friendly greeting. My special thanks to all the former and current members of the electrocatalysis group, my brothers in arms, so to say, for keeping me company at work and at leisure. Ad, Afifa, Alexander, Gabi, Guillermo, Martin, Natalia, Peter, Tom, Tanya, Thijs, I am glad we met and had such a great time together. Andrey and Evgeny, thanks for many chats and laughs we had; that was fun indeed.

I want to take this opportunity and thank Dr. Pushnyak A.N., supervisor of my diploma project, for helping me in getting to my first “Eureka!”-experiences. I thank Prof. Ionel C. Popescu and Dr. Adrian Nicoara (both of University of Cluj-Napoca, Romania) for teaching me electrochemistry.

Carina, Gabi, Guillermo, Ionel, Natalia, Sorinela, Tony and Mihaela, my friends, this four-year “quest” could be much more troublous and much less fun without you around.

Katia, I could not go so far without you by my side. Thank you for your support and understanding. I dedicate this work to you and Alex.

Curriculum Vitæ

Victor Rosca was born on the 21st of July 1976 in Chisinau, Republic of Moldova (Soviet Union, at that time). He studied chemistry and chemical technology at the State University of Moldova and received his degree in 1998. The diploma work concerned adsorption on natural and synthetic adsorbents. Same year, he was appointed as research assistant at the Department of Physical Chemistry, University of Cluj-Napoca, Romania, where he worked in the field of electroanalytical chemistry. In February 2002 he joined the electrocatalysis group, Laboratory of Inorganic Chemistry and Catalysis, Eindhoven University of Technology, The Netherlands, as research assistant and worked on the mechanistic aspects of the electrocatalytic reactions of inorganic nitrogen compounds on single-crystal platinum surfaces. The most important results of this research are described in the present thesis.